A METHOD FOR ATMOSPHERE CHARACTERIZATION USING MESOSCALE MODELS, SATELLITE DATA, AND GROUND MEASUREMENTS

Vanni Nardino
Relatore: Steven N. Shore

Corso di Dottorato in Fisica Applicata AA 2006 Università di Pisa

Acknowledgments

I wish to thank Prof. Steven N. Shore, without whom this work would not have been possible. I wish to thank him for many things which include his enormous experience, his great respect for his students, his patience, his time and his friendship.

I would next like to thank Dr. Patrice Poinsotte: his enthusiasm in meteorology and his experience in numerical models have been extremely helpful during the development of the work.

I wish to thank my external supervisor, Dr. Emilio Simeone, head of Flyby (Livorno), for providing the doctoral fellowship (through the Physics Dept., University of Pisa) and working environment in which a part of the work for this thesis was performed.

Thanks to Antonio Masi for some tips about MSG data reading and thanks to Linda Corucci for helping in debugging the IDL code.

I would finally like to thank my friends and family for their continuous support and encouragement. In particular I thank my girlfriend Shirley Harrison: she always supported me during the writing of the thesis with great patience, love and understanding.

Summary

The initial purpose of this work was to develop a tool for providing UV ground irradiance map in the generally cloudy case. The use of a meteorological model for providing the structure of a three-dimensional atmosphere was intended to be used as a prediction tool. In its actual form, this thesis describes a new procedure for computing irradiances for the Earth's atmosphere including the three-dimensional structure of the local atmosphere around the point of interest. The atmospheric structure is obtained from the MM5 meteorological model providing gridded three-dimensional constituents profiles and cloud position. Simulated data are validated using both ground sensors in UV and visible bands and Meteosat Second Generation satellite images. The effects of a variety of atmospheric constituents (i.e. aerosols and clouds) are also discussed.

Nowadays there are many tools implementing radiative transfer models used for simulating the propagation of the light in the atmosphere. In general, these models consider a plane parallel atmosphere, whose layer being characterized by optical parameters depending on the physical constituents. Although the problem of light propagation is resolved three-dimensionally, the atmosphere characterization is one-dimensional: the parameters are depending by altitude only. In a word, the adopted model is translationally invariant. When the data characterizing the radiative transfer problem are given in a three-dimensional form (i.e. a grid of constituent profiles, or a map of cloud cover at different altitude) the radiative transfer simulation for the point of interest is, in general, performed using atmospheric layers characterized by the parameters of the corresponding pixel of the grid, assuming locally constant values. Neglecting the local discontinuity of atmospheric constituents (presence of aerosol due to local condensation, fog banks, smoke), and considering the ground as "flat", in a cloudless situation such an assumption represents usually a realistic model for the real system. Although these models are in general accurate enough for ground irradiation prediction, there are in fact situations requiring the three-dimensional structure of the atmosphere to be considered, e.g. the cloud constellation with respect to the direction of the Sun.

In this thesis, two schemes are compared, a standard atmospheric radiative transfer code that is widely used in the community (UVSPEC, part of the freely distributed libRadtran package, using for the comparison with ground measurements and satellite data) and a fast algorithm for treating multilayer direct transfer with scattering. The latter is still inaccurate for precise radiative transfer calculations, but it represents an initial step in the modeling of radiative transfer in situations, characterized by irregular cloud cover, that can't be described with an on-the-vertical (one-dimensional) atmosphere model only but require the atmospheric structure to be considered also in pixels far away from the position of the observer (e.g. clouds covering the Sun with cloudless conditions around the zenith). These situations are pointed out in the thesis and their effects have been measured by ground sensors.

The libRadtran package, chosen for the comparison with the ground measurements and for the simulation of the satellite data, satisfies the need for a fast tool for atmospheric radiative transfer calculation, although it still requires a plane parallel atmosphere in input, i.e. a single, one-dimensional profile, preventing the simulation of atmospheric layers with non-constant characteristics (e.g. broken clouds, discontinuities in the atmospheric column constituents).

The possibility of a radiative transfer model simulating the light propagation in a three-dimensional atmosphere is, in fact, computationally difficult (there are, in fact, models simulating a realistic, three-dimensional environment, but the long computation time often limits their utilization in general problems and their use is not examined in this work).

The thesis focuses on the search for a method for reconstructing a profile, to be used as input for the radiative transfer model, taking into account the three-dimensional structure of the input data: a composite atmosphere model, in which a plane parallel atmosphere is built using a composite profile, obtained by cutting the profile of each pixel of the grid in the Sun-observer direction. The simulations of the model are compared with measurements by ground sensors in the bands of UV and visible - near infrared. The atmospheric profile grid is not arbitrarily constructed, it results from the mesoscale predictions of MM5 and is therefore a naturally inhomogeneous atmospheric profile that can be inserted into any radiative transfer modeling, but still there are free parameters to be tuned, i.e. cloud drop radius distribution, aerosol effects, etc.

The satellite measurements (by Meteosat Second Generation data) provide high spatial and time resolution images of the Earth around the point of interest, thus providing an alternative point of view for model verification, but a direct comparison with satellite observed data would require the tuning of an even bigger number of unknown parameters (i.e. ground albedo, terrain model, etc.). The problem is bypassed by applying a stable method for estimating the cloudiness amount independently of the others atmospheric effects by comparison with cloudless time series of images. Because the main point of interest is the correct simulation of clouds, it offers a valid comparison tool. Hence the verification of the model is performed using both ground measures (providing also the relative contributions of diffuse and direct illumination) as well as satellite observations (providing a spatial map of the cloud cover in each corresponding pixel of the input grid).

Other model parameters, i.e. the aerosol type and radial distribution of both aerosol and cloud drops (considering clouds as a type of aerosol) remain unknown. They are not provided by either the meteorological model or by direct measurements, consequently an order of magnitude estimate is required for the radiative transfer model. For this purpose, time series of aerosol size distributions based on AERONET (AErosol RObotic NETwork) are analyzed and discussed. The aerosol measurements provide a test case for which the size distribution is explored to understand the dependencies of the model on such uncertain physical assumptions as aerosol type, particle size, convection scheme, cloud formation and distribution. Because a direct measurement of aerosol properties in the point of interest is still missing, the simulations and the comparison with the acquired data are performed exploring the effects of a range of fixed cloud drop values.

In the end, this thesis is not to be intended as an exhaustive work defining a full procedure for radiative transfer calculation in a generally cloudy atmosphere. The presented model takes into account the problem of joining a three-dimensional data grid of atmospheric profiles from a meteorological model for being used in the radiative transfer code. Other unmodeled events due to broken clouds or partial cloud cover situations have been measured during the ground sensor acquisition campaign and are described in the work. These phenomena remain, due to the long computation time required for their correct treatment,

still unconsidered at the moment. The first order radiative transfer scheme introduced in the work has to be interpreted as a starting point proposal for a future modeling taking advantage not only by a composite profile on the line of sight observer-Sun but using, for each observer line of sight, a different composite profile, being able to treat these phenomena. The development of this model could, in fact, model the radiative transfer in a realistic, non-plane-parallel atmosphere.

Note

In the description of the procedures and codes, the following conventions are used:

- names of user-modified files are printed using *this font*;
- names of external program (such as the components of software packages) are printed using **this font**;
- names of IDL functions and procedures developed during this work are printed using `THIS FONT`;
- names of external freely distributed IDL functions and procedures are printed using THIS FONT.

Contents

1 Introduction

The estimate of the radiation budget reaching the ground has broad application in different fields: meteorology and climatological research, simulation and monitoring of Sun powered installations (e.g. photovoltaic devices), environment monitoring and ultraviolet (UV) exposure monitoring. UV radiation exposure interacts through different reaction with biological systems: it induces the production of vitamin D, is responsible of human skin suntanning by increasing melanin production, and, in case of prolonged exposure, brings to various harmful effects: sunburning (erythematic reactions and various skin irritation depending on individual sensibility), skin aging (by interacting with skin collagen fibers), cornea, lens and retina damage, and even skin cancer (from DNA damage). Thus, planning human outdoor activities requires a precise determination and monitoring of ground level UV radiation.

Radiation from Sun interacts with the atmosphere by scattering and absorption. The amount of radiation reaching the ground depends on the atmospheric constituents, Sun position and cloud constellation (as described in details in the work), thus, the knowledge of atmospheric optical behavior around the point of interest is a need for the calculation of the radiation at ground level.

The straightforward way to determine the ground irradiation is the direct measurement by sensors. Together with ground measurements, also remote sensing data provide a way for atmospheric monitoring by acquiring images in different bands. By the use of inversion techniques, satellite data allow the reconstruction of atmospheric components as particulate and aerosol distribution, gaseous absorbers concentration and clouds presence. Satellite images, e.g. MODIS data (Moderate Resolution Imaging Spectroradiometer, http://modis.gsfc.nasa.gov), are disseminated together with ancillary data reporting the value of various atmospheric parameters. These satellites provide high spatial resolution data, although the time resolution for a continuous monitoring of a given location is often poor.

Geostationary satellites, such as Meteosat Second Generation (whose data are amply discussed and used in this work) provide a real time monitoring of the Earth by producing images and meteorological data with a timescale of 15 minutes, although the spatial resolution is usually lower than polar orbit satellites[1].

In recent years, also ground based monitoring networks and data archives (e.g. AERONET [25] for aerosol data) provide a continuous monitoring of atmospheric optical parameters in different location in the world, maintaining a freely accessible data archive.

Cloud characterization by Meteosat satellites is at the basis of procedures, such as the Heliosat method [14, 39], for broadband ground irradiance determination, obtained by scaling the result for a cloud free atmosphere using analytical, numerical or empirical models (radiative transfer models, i.e. computer programs for modeling atmospheric propagation of radiation). In the scientific literature a widely used code is the MODTRAN (http://modtran.org),

[1] Geostationary orbit (e.g. Meteosat satellites orbit) is approximately at altitude of $35786\,km$, whereas solar orbit satellites (e.g. MODIS) orbit is located often between few hundreds of km and approximately $1000km$ of altitude ASL The proximity of polar orbit satellites allows images with a corresponding ground pixel of few hundreds of meters, the Meteosat Second Generation images resolves a ground pixel of $\sim 1\,km$ at the best resolution.

characterized by a maintained model of molecular absorption data, HITRAN (www.cfa.harvard.edu/hitran), based on DISORT (DIScrete Ordinates Radiative Transfer program for a multi layered plane parallel medium [45]) public and general code applicable to problems from the ultraviolet to the radar regions of the electromagnetic spectrum. In this work the radiative transfer code used is based on libRadtran package [32] (www.libradtran.org), made up of freely downloadable functions and programs (MODTRAN itself is based on these codes [4]) for radiative transfer calculation in the Earth's atmosphere.

The determination of radiation behavior requires the solution of the so-called *direct problem*[2]: the radiative properties are calculated, assuming an atmospheric structure, at fixed direction and coordinate, accounting for scattering and absorption. Usually the model is defined by atmospheric data derived from multi-spectral satellite observations (by inversion techniques) interpolated on the vertical of the point of interest. Each atmospheric layer is characterized by parameters depending on altitude only (thus this model of atmosphere is one-dimensional). Using the given atmospheric profile, the radiative transfer model simulates light propagation.

The approach used in this work is different: the atmospheric structure comes from a mesoscale meteorological model calculation that reconstructs the profile in each atmospheric layer on a grid. The atmosphere used in the radiative transfer model is made up of homogeneous layers, but the profile is composite, using the three-dimensional information of the grid taking the section of the profiles in the Sun direction.

The accuracy of the meteorological and atmospheric model is then verified by comparison with satellite observation in visible band and by ground measurements, carried on in Livorno, Italy at Flyby s.r.l. (that provided the instrument for ground measurements and the hardware for downloading Meteosat Second Generation data). The comparison ensures that the atmosphere is realistically described, and that the radiative transfer model calculates the amount of observed radiation using the same atmospheric profile.

The problem is described in section 2, together with the definition of the variables and the description of the new model of atmosphere. Section 3 describes the measurement campaign carried on for the purposes of the work and the other ground measured data used. Sections 4 and 5 describe the radiative transfer model and its customization, and the meteorological model providing gridded three-dimensional atmospheric profiles and cloud positions. Section 6 describes Meteosat data for cloudiness characterization used for comparison with simulated values. Section 7 shows the results obtained using our procedure and the comparison from measured and satellite estimated values.

[2]The *inverse problem* is on the contrary the determination of the atmospheric structure most consistent with the measured data.

2 The problem

2.1 Aim of the section

Determining the amount of the ground irradiation, assuming the atmospheric structure, requires a model. Usually, even if a map of atmospheric constituent profiles is provided (e.g. a grid containing, for each pixel, a profile of atmospheric constituents as a function of the altitude), the atmosphere characterization is, in general, one-dimensional: the atmosphere is represented as made up of parallel layers, that is the model assumes a single profile of the grid (the one of the pixel corresponding to the observer location) being representative of the entire part of atmosphere interested by the radiative transfer problem). Nevertheless, there are situations in which this assumption is not representative of a real atmosphere. Cloud cover requires treating the three-dimensional structure of the atmosphere. A simple example can be offered by situations in which a portion of the sky is covered by clouds, and the rest presents cloud-free conditions. In such a situation the amount of radiation reaching the ground depends primarily on the presence of clouds on the Sun-observer direction. Consequently, the atmospheric layers can't be considered horizontally constant. Unmodeled phenomena can occur in a non-plane-parallel atmosphere: for example, ground radiation amplification phenomena are expected (and the corresponding ground measurements are shown in the section) in case of clear-sky conditions along the line of sight Observer-Sun together with clouds, on the vertical of the observer, back-scattering the ascending radiation. A sensor would indeed measure a ground irradiation greater than in a fully cloudless conditions.

This section presents an overview of the plane parallel model limits in representing a real atmosphere, with a description of the phenomena occurring in broken cloud situations, together with the corresponding ground measurements. The "composite atmosphere" approach is then described, that is a procedure for providing a "composite" profile calculated, along the observer-Sun line of sight, using the information from different profiles of a spatially gridded atmospheric model obtained from a meteorological simulation and calculated for each time step. Such a composite profile (which is time dependent and computed for the corresponding Sun position) is then used as input into the plane parallel radiative transfer model.

The composite profile is not a conclusive procedure taking into account the completeness of the phenomena occurring in a real atmosphere: for this reason, a suggestion for a basic, first-order radiative transfer model is also presented. The latter model represents a "proof of concept" study, not a final model, as a first step for a future development of a computationally fast radiative transfer model taking into account the contributions to the observed radiation that are still neglected by a plane parallel atmospheric model.

2.2 The basic problem

The precise estimate of ground ultraviolet (UV, $280 - 400\,nm$) and visible - near infrared radiation ($400 - 2500\,nm$)[3] is important for the interactions of

[3]The bands actually measured and simulated in this work are: $280 - 360\,nm$ and $355 - 2200\,nm$(given by the transmission of the sensor used). They can be considered representative of UV and visible - near infrared radiation.

the sunlight with Earth surface and atmosphere (daily irradiation estimate, interactions with biological systems, etc.) and for the effects that UV radiation causes on biological systems (i.e. the human skin erythemal, skin cancer, etc.). In this work an innovative model, taking into account the realistic structure for the Earth atmosphere to be used as input for radiative transfer procedures, is presented.

In a non-scattering atmosphere the exact amount of radiation impinging at ground for the wavelength of interest is easily computable by the knowledge of absorption properties of the medium. Difficulties in this calculation come by considering both scattering and absorption events.

Scattering and absorption properties characterize the Earth atmosphere so, together with the direct propagation (directly from Sun to the observer), also the diffuse (scattered) propagation plays an important role in the radiative transfer of light, thus a precise determination of the radiation impinging on the ground is not trivial. For this reason, the determination of the exact amount of the ground radiation can be carried out only by the knowledge of the optical properties of the medium and geometry conditions of illumination (i.e. Sun position with respect to the observer).

Light scattering is influenced both by the gaseous constituents of the atmosphere (mainly oxygen and nitrogen), which are responsible for the Rayleigh or molecular scattering , as well as by aerosol (particulate, dust, condensed matter, etc.). Condensation is responsible for aerosol nucleation and cloud formation both near the ground (fog, haze) and at higher altitude [49]. Atmospheric absorption is due to gaseous constituents (i.e. ozone in the UV bands, water vapor in the near infrared bands) and aerosol. Gases and aerosol have a different behavior respect with the wavelength: gas absorption is characterized both by broad absorption bands with slow spectral variation (continuous absorption spectrum, typical of UV and visible wavelength range: $290 - 700\,nm$) and by narrow absorption lines (especially in near infrared: $700 - 1200\,nm$), aerosol absorption depends on the composition and dimensions (with respect to the wavelength) of the particles involved. Clouds are a particular type of aerosol made up by liquid and ice water drops in suspension in the atmosphere. Clouds, if present, are in general the principal cause for scattering and absorption in UV, visible and near infrared wavelength range. For these reasons, the principal difficulties in calculating the ground radiation arise because of the cloud cover. Depending on cloud position and structure, the radiation scattered or absorbed in the atmospheric column can drastically change.

A good way of mapping and estimating the cloud cover is offered by geostationary satellite data. Satellite images provide a quasi continuous cover of the Earth surface, with temporal and spatial high resolution data, thus allowing to estimating the cloud cover and the principal properties of the atmosphere integrated on the satellite line of sight. An implicit hypothesis is assumed in using cloud cover estimate by satellite: the atmospheric structure is not resolved, that is the properties "seen" by the satellite for a ground patch are the result of an integration of atmospheric properties along the line of sight.

A different approach uses station-measured data. Atmospheric soundings can provide information about the atmospheric constituents along the air column, but the data, although well resolved with respect to the vertical direction (the common resolution is approximately $1\,m$), describe realistically the atmosphere only in a single point and with a poor time resolution (timescales of many

hours). For these reasons it is technically difficult to obtain high temporal or spatial resolution data by the use of station measurements.

In this work, together with cloud cover information from satellite images, the vertical structure of the (in general cloudy) atmosphere is provided independently from satellite data and with a spatial cover unreachable by station measured data alone, by running an atmospheric model for determining realistic profiles of constituents for each pixel of a three-dimensional grid. The idea is that such a model provides the equivalent of an "interpolation" for resolving the atmospheric structure in the point of interest (where in general the vertical structure is unknown). The similarity with an interpolation procedure underlines the way the atmospheric model calculates the atmosphere conditions for custom coordinates. By using a physical model describing atmosphere spatial and time evolution, given starting and boundary conditions (from station measured data), the atmosphere structure can be determined in any point.

2.3 Introducing the computational approach

The estimate of the amount of radiation reaching the ground requires taking into account: viewing geometry, Sun position and light scattering and absorption phenomena within the atmosphere and with the ground. The light propagation through a medium with scattering and absorption is described by the radiative transfer equation (RTE) as explained in paragraph 2.5. The RTE is usually resolved by applying a radiative transfer software model (the radiative transfer model used in this work will be described in paragraph 4) passing it as input the optical parameters of the atmosphere. Thus the necessary condition for calculating the ground irradiation is the specification of atmosphere scattering and absorption properties (these properties will be defined in paragraph 2.4).

A plane parallel structure is usually assumed when modeling the atmosphere, i.e. the atmosphere is divided in horizontal layers or levels, with constituents concentration definite in each layer, so that the optical parameters can be calculated as a function of those concentrations for each step of the altitude. Those assumptions raise the problem of prescribing realistic data for characterizing the atmospheric column.

Although *in situ* measurement is the straightforward way (i.e. the atmospheric column is measured by sounding for determining profiles of pressure, temperature, concentration of atmospheric constituents), this method for characterizing the Earth atmosphere can't always be applied, because it needs a sounding campaign to be performed over long times and with high cadence around the point of interest using ground based lidar, since the atmosphere changes rapidly (timescales of $1\,h$ are typical) with a spatial inhomogeneity on a scale of tens of kilometers.

Satellite derived data offers a different approach to atmosphere characterization: with remote sensing images in specific wavelength bands (from visible to far infrared), large areas of the planet can be observed simultaneously, thus obtaining (using inversion techniques) a continuous spatial and temporal mapping of the atmospheric parameters by an inversion of the problem of light propagation. The inverse problem in radiative transfer is to determine the structure of the medium from multiwavelength measurements.

Although the former approach offers an estimate of atmospheric parameters that could be sufficient for atmosphere optical properties characterization, it is

not the procedure adopted in this work: in fact, the cloudiness is determined from the analysis of the satellite image in visible band. Using the same images for both cloudiness estimate and atmospheric parameters retrieval brings to a dependency of these parameters (data are not independent), so, despite the internal consistency of the data, a correct study of cloud structure data regarding the atmospheric structure must be provided *independently* of the image of the clouds.

In this work, a structure for the local atmosphere comes from a meteorological model. Using low resolution gridded data from global models and atmospheric profiles measured by ground station, the model provides a consistent low-resolution atmospheric structure to be used as input for the radiative transfer model.

The data used in this procedure are:

- the image of radiance seen from the satellite;
- an atmospheric profile of constituents for optical properties determination in each layer of the plane parallel atmosphere;
- ground irradiation measured from the ground by sensor in visible - near infrared ($335 - 2200\,nm$) an UV ($280 - 360\,nm$) bands.

This work is structured as follows:

- Calculation of time sequences of atmospheric profiles using an atmospheric model (MM5, described in paragraph 5.1). The output of the model is a gridded data: each pixel of the grid containing atmospheric parameters as a function of the altitude.
- Verification/testing of the atmosphere models for consistency, both internally, for precision estimate, and respect with the sounding measured in different stations.
- The atmosphere is considered as plane parallel, with parameters depending only on the altitude. This approach doesn't take into account the three-dimensional structure of the atmosphere, so, to be used as input in the radiative transfer model, a composite atmospheric profile is generated taking into account the three-dimensional structure from MM5 data for the point of interest. This point represents an innovative approach to atmosphere characterization, allowing one dimension atmosphere model (with each parameter as a function of altitude) to be generated taking into account the three-dimensional gridded data.
- The composite atmosphere is used as input for the radiative transfer model: UVSPEC, part of the libRadtran distribution [32] is used for ground irradiation computations.
- Ground measured irradiation in visible and UV bands, as well as the satellite-determined cloudiness estimation, are discussed. These measurements are used for comparison with the simulated ones.
- Because there are uncalibrated free parameters in this approach (i.e. aerosol amount, cloud liquid and ice drop size distribution) the simulation are provided for a range of parameters and the result are discussed. For providing

an order of magnitude for the parameters not provided by the atmospheric model (i.e. cloud drop radius), ground measured aerosol data are analyzed and discussed.

- The simulations of ground irradiation in visible and UV bands and of the corresponding satellite-observed cloudiness amount are provided using the libRadtran UVSPEC radiative transfer code with the composite atmospheric profile in input, calculated for each time step of the meteorological simulation and for the corresponding Sun position.

The novelty of this method consists in using the MM5 atmospheric model output as input for radiative transfer calculation by defining a new "composite" atmosphere. Such a composite atmosphere is obtained from three-dimensional data for the current geometry (Sun and ground point positions) of the system.

2.4 Optical parameters definitions

2.4.1 Radiance and irradiance

In studying the propagation of light in the atmospheric medium, the variable of interest is the *radiance* (intensity, surface brightness).

The radiance L_λ crossing a surface A (see figure 1) is defined as the mean power crossing the unit of surface normal to the direction defined by $\hat{s}$, for unit of wavelength λ, for unit of solid angle Ω around $\hat{s}$:

$$L_\lambda = \frac{dP}{d\lambda\, d\Omega\, dA\, \hat{n} \cdot \hat{s}} \tag{1}$$

Thus radiance units are $W\, m^{-2}\, sr^{-1} \mu m^{-1}$.

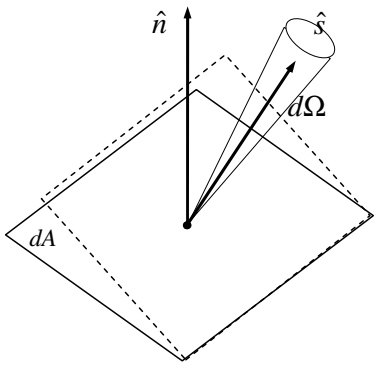

Figure 1: Radiance definition

The *irradiance* (or flux) E_λ is defined by fixing a plane (i.e. the ground) and integrating in the semi solid angle the radiance L_λ (see figure 2):

$$E_\lambda = \int_{2\pi} cos\theta\, L_\lambda d\Omega \tag{2}$$

where is θ the angle of incidence of L_λ with the normal $\hat{n}$ to the surface. Irradiance units are $W\, m^{-2}\, \mu m^{-1}$. Depending on the semi solid angle chosen for

integration, the considered irradiance is named *downwelling* (light incident on the upper surface from the overlying strata) or *upwelling* (i.e. ground or cloud reflected toward the sky). In the latter case, considering the ground as a Lambertian diffuser (i.e. reflected radiance is distributed isotropically: $L_\lambda = L_{0\lambda}$) the irradiance takes the form of:

$$E_\lambda = \int_0^{\frac{\pi}{2}} \int_0^{2\pi} cos\theta \, L_{0\lambda} sin\theta d\theta d\varphi = \pi L_{0\lambda} \tag{3}$$

In case of a mono-directional radiance (represented by a Dirac Delta distribution) $L_\lambda = \delta(\Omega - \Omega_0) L_{0\lambda}$ (i.e. extra atmospheric radiance from the Sun impinging at the top of the last atmospheric layer) the corresponding irradiance is:

$$E_\lambda = \int_{2\pi} cos\theta \delta(\Omega - \Omega_0) L_{0\lambda} d\Omega = L_{0\lambda} cos\theta_0 \tag{4}$$

where θ_0 is the angle of incidence of the radiation on the plane.

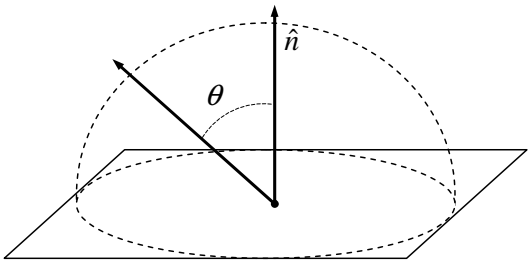

Figure 2: Irradiance definition

In the following formula, fixing a wavelength range $[\lambda_0, \lambda_1]$, we define the spectrally integrated radiance for a fixed position in the space as:

$$L = \int_{\lambda_0}^{\lambda_1} L_\lambda d\lambda \tag{5}$$

and the spectrally integrated irradiance as:

$$E = \int_{\lambda_0}^{\lambda_1} E_\lambda d\lambda \tag{6}$$

2.4.2 Approximations in this formulation

The source of radiance in the Earth atmosphere in the wavelength of interest of this work (UV, visible and near infrared) is the Sun. Thus, in the following equations the contribution due to thermal emission of ground and atmosphere itself is neglected.

The system is considered to be in steady state, that is the propagation of light in the medium is considered instantaneous, and the polarization of the photons is not considered, so we are dealing with radiation averaged over all polarizations, ignoring the dependence of the scattering on the polarization.

2.4.3 Direct and diffuse components

Scattering and absorption coefficients are defined by taking a volume of the medium and considering the ratio between scattered (or absorbed) power for volume unit and the impinging power for surface unit for a fixed wavelength:

$$\sigma_{s,a} = \frac{\text{impinging power for surface unit}}{\text{scattered (absorbed) power for volume unit}} \tag{7}$$

the dimensions of scattering (absorption) coefficient are the reciprocal of a length and vary with the wavelength.

From Lambert-Beer's law[4], the change of radiance for monochromatic radiation along a path ds for scattering or absorption events is:

$$dL_\lambda = -\left(\sigma_{s\,\lambda} + \sigma_{a\,\lambda}\right) L_\lambda ds = -\sigma_{e\,\lambda} L_\lambda ds \tag{8}$$

where $\sigma_{e\,\lambda} = \sigma_{s\,\lambda} + \sigma_{a\,\lambda}$ is the extinction coefficient at wavelength λ. For irradiance the equation is just the same.

The non-dimensional quantity

$$d\tau_\lambda = \sigma_{e\,\lambda}\,(s)\,ds \tag{9}$$

is the optical depth at wavelength λ, a natural unit for express the "opacity" along a path between two points in the atmosphere[5].

In case of spectrally integrated radiance[6], using the nomenclature introduced in paragraph 2.4.1, the optical depth can be defined as:

$$dL = -\sigma_e L\,ds = -L\,d\tau \tag{10}$$

Considering an observer on the ground, the total downwelling ground global (or total) irradiance G_λ coming from the Sun and spectrally integrated can be divided into two components:

$$G = I + D \tag{11}$$

where I is the direct component, that is the photons that have not been scattered, and D the diffuse component, the scattered photons that reach the ground plane with a different angular distribution.

Let's now consider the τ along the vertical direction in a plane parallel atmosphere: figure 3 shows the typical τ calculated on a vertical path from the altitude in abscissa to infinite in visible - near infrared bands. The altitude at which the atmosphere can be considered transparent ($\tau \to 0$) will be called hereafter the Top Of Atmosphere (TOA).

For an observer on the ground, the vertical optical depth from TOA to the ground is a measure of atmospheric opacity in the wavelength band[7] of interest.

[4] Lambert-Beer's law assumes that the absorption coefficient is independent of the radiance: this hypothesis is satisfied in a planetary atmosphere.

[5] From equation (7) it follows that τ can also be considered as the mean number of scattering events along a path s, being $\frac{1}{\sigma_e}$ the mean free path between two events of scattering and/or absorption.

[6] This is the case of radiances or irradiances measured by an instrument. Irradiance is integrated in the instrument wavelength range (band) and weighed by a response function.

[7] The definition of TOA depends, in fact, by the wavelength, due to the dependency of the extinction coefficient on the wavelength.

Following the literature, in this work the TOA has been fixed at $120\,km$, a value that allows the atmosphere to be considered transparent in the wavelength of UV, visible and near infrared[8].

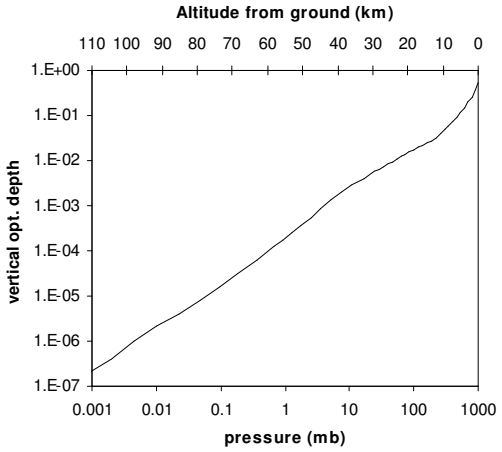

Figure 3: Typical optical depth from altitude (or pressure) in abscissa to infinite for a cloud free atmosphere in a $350-2200\,nm$ wavelength band. The TOA can be fixed at the altitude in which the optical depth can be considered negligible. The profile has been obtained using a spring-summer standard atmosphere with rural aerosol with $20\,km$ visibility from libRadtran library (the package will be introduced in sec. 4).

There is a fundamental difference in direct and diffuse components: considering a plane parallel atmosphere, from the optical depth definition (eq. (10)) and from the knowledge of the value of the integrated extraterrestrial irradiance at the top of atmosphere I_{TOA} (the power emitted for an horizontal surface area by the Sun integrated on the wavelength) the direct component can be derived analytically:

$$I = I_{TOA} \exp\left(-\frac{\tau}{cosSZA}\right) \tag{12}$$

where $\tau(x,y) = \int_0^{z_{TOA}} \sigma_e(x,y,z)\,dz$ is the total optical depth from ground to the TOA calculated in direction normal to the ground plane and SZA the solar zenith angle (see figure 4).

Considering the Sun direction normal to the ground plane ($SZA = 0°$), the term $T = e^{-\tau}$ is named the vertical transmittance of the atmosphere in the band of interest.

In contrast, the diffuse component D doesn't have a simple form. The scattered radiation, when the scattering event occurs, changes the direction of propagation (in this work we are considering the case of elastic scattering). The angular distribution of the scattering angle is described by the phase (or scattering) function $p(\gamma)$ (where γ is the scattering angle between incident and scattered direction). The value of $p(\gamma)$ depends on the real part of the refractive index of the scattering particle and on the wavelength . In case of molecular

[8]This definition of TOA comes from the use of the libRadtran software package used in this work. The atmosphere can be considered optically transparent also at lower altitude.

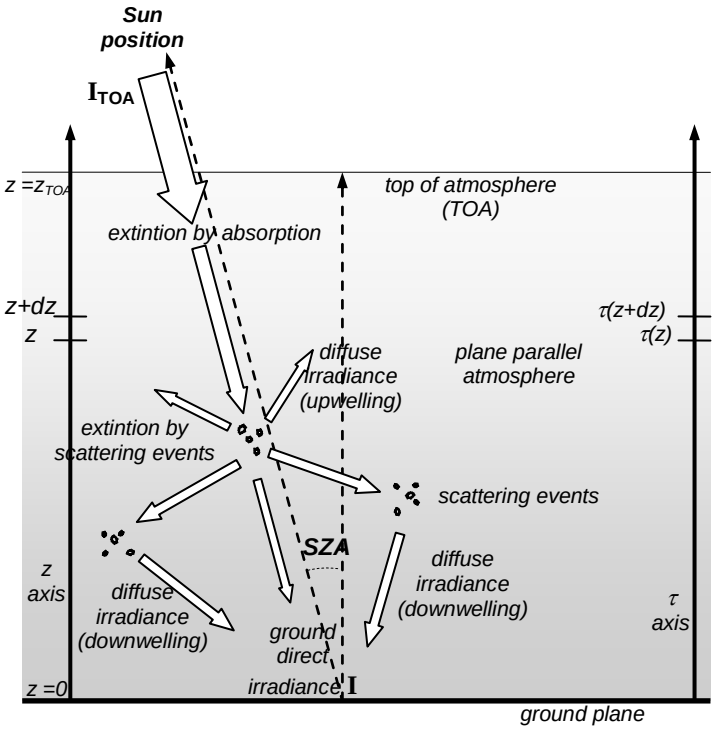

Figure 4: Plane parallel atmosphere: from the vertical optical depth and geometric parameters, the direct component of ground irradiance can be calculated with eq. (12). Diffuse contribution impinges the ground from every direction of the semi solid angle.

(Rayleigh [48]) scattering, p has the form:

$$p(\gamma) = \frac{3}{16\pi}\left(1 + \cos^2\gamma\right) \tag{13}$$

In case of aerosol scattering (i.e. by dust particles, water drops or ice crystals) the shape of $p(\gamma)$ is a function of the radial distribution of the particles radius and of the relative refractive index of air and the particle itself. The determination of diffuse radiation distribution thus requires a different approach: the solution of the radiative transfer equation (RTE) in this geometry.

Both diffuse and direct components of the solar radiation can reach the ground (in general modeled as a Lambertian diffuser with absorption properties). For characterizing the ground properties we'll introduce the definition of the ground albedo a, as the ratio between the reflected global irradiance (G_-) and the downwelling one (G_+):

$$a = \frac{G_-}{G_+} \tag{14}$$

Different definitions of albedo are used in literature for taking into account not Lambertian properties of the surface. In this work we'll consider the ground as Lambertian, thus using formula 14 for albedo definition.

In syntheses, if we want to calculate the direct component of the irradiance, the knowledge of the atmospheric structure allows to determine it; if we are dealing with the determination of the diffuse components, we have to resolve the RTE using numerical techniques, i.e. using a radiative transfer model.

2.5 The Radiative Transfer Equation (RTE)

As we have seen in paragraph 2.4, the interaction between radiation and atmospheric components (without considering thermal emission[9]) can be classed as either scattering or absorption, in a word, by extinction.

The RTE describes the budget of radiance (with wavelength λ) propagating in direction $\hat{\mathbf{s}}$ crossing a surface normal to the direction $\hat{\mathbf{n}}$ [23]. The phenomena contributing to the received radiance L_λ are: the loss due to extinction phenomena and the increase of received radiation by a source term, in our hypothesis given only by the scattering of the diffuse radiation in direction $\hat{\mathbf{s}}$. The RTE describing the transfer of monochromatic radiation at wavelength λ through a plane parallel medium[10] (scattering and absorption properties depending on the z coordinate only) is then given by:

$$L_\lambda(\mu, z) = -\frac{\mu}{\sigma_e}\frac{dL_\lambda}{dz} + \frac{\sigma_s}{\sigma_e}\int_{4\pi} p_\lambda\left(\hat{\mathbf{s}} - \hat{\mathbf{s}'}\right) L_\lambda d\Omega' \tag{15}$$

with $\mu = cos\theta$, where θ is the angle between $\hat{\mathbf{s}}$ and $\hat{\mathbf{n}}$.

In the RTE the first term on the right takes into account the radiance extinct passing through the optical depth $d\tau = \sigma_e dz$ with an angle θ with respect to the zenithal direction $\hat{\mathbf{n}}$, the second term considers the radiance that, from any directions $\hat{\mathbf{s}'}$ (that is, integrated on the solid angle), is scattered in the direction $\hat{\mathbf{s}}$ with a probability distribution given by the scattering function $p\left(\hat{\mathbf{s}} - \hat{\mathbf{s}'}\right)$. Thermal contributions are not considered because the radiative transfer occurs in a spectral interval in which the thermal contribution is negligible.

The atmospheric properties in each layer are described by the corresponding scattering and absorption coefficients and scattering function. The solution of this equation for a plane parallel atmosphere requires the use of a numerical radiative transfer model (RTM). Fixing the atmospheric parameters, the RTM can calculate both radiances in a definite direction and irradiances at ground, thus it will be used for simulating the radiance scattered by atmosphere and ground observed by the satellite and the ground irradiance measured by the ground instruments. The RTM used in this work is UVSPEC (described in sec. 4).

2.6 Plane parallel atmosphere

The atmosphere is a complex multiphase, multi-component physical system consisting of gas and condensed phases. The concentration of atmospheric components depends on altitude, temperature and pressure conditions and on aerosol

[9] The emission due to the temperature (Plank law) in UV, visible and near infrared bands is negligible, so the only source of radiation is considered to be the Sun, thus thermal emission can be ignored.

[10] Earth curvature is neglected. This also allows the delta approximation for the direction of incidence of the irradiance at the TOA.

and particulate suspension near the ground surface. Aerosol concentration depends on both the natural events (e.g. dust, pollen, marine salt, clouds) and human activities (e.g. smog, soot, industrial aerosols). Usually the aerosol concentration decreases with the altitude. Both gaseous and aerosol components cause the electromagnetic radiation to be scattered and absorbed. The atmosphere can be considered locally flat and divided in horizontal layers. This is a good approximation[11] since the altitude scale is small relative to the Earth radius, so that curvature can be neglected. This assumption is at the basis of both the MM5 atmospheric model (described in paragraph 5.1) and the radiative transfer model (sec. 4). A plane parallel atmosphere can be characterized by different values of the specific constituents in each layer or level. The optical properties (i.e. scattering and absorption) are determined by the profile of constituents. In this formulation, the atmosphere can be represented as a spatial and vertical grid (this is the representation used for MM5 output).

The literature often uses the concept of a standard atmosphere [35]. Such an atmosphere is a reference atmosphere, usually representative of a cloud free situation, with scattering and absorption coefficients referring to climatic and seasonal standard situations (i.e. a typical mid-latitude summer atmosphere with a spring-summer rural aerosol profile). Due to the local and temporal variability of atmospheric parameters, the standard atmosphere is different by the real atmosphere. A realistic atmospheric profile referred to the vertical of a ground point matches the measured profile (for example from a sounding campaign).

The model should produce a realistic atmosphere (with its profile of constituents in each layer), and the radiative transfer model should reproduce the response of a ground sensor (i.e. it simulates the propagation of radiation from the Sun to the ground), and also simulate the satellite response (the observed cloud cover). The simulated and measured satellite data can then be compared to determine a relation between cloud cover (integrated on the line of sight, the satellite imagery) and atmospheric vertical profile. This is the goal of the modeling.

In this work the atmospheric model provides realistic atmospheric profiles and the radiative transfer model provides the correct estimate both for ground radiation (taking into account scattering and absorption properties) and for satellite observed radiation.

There is a further step to introduce: radiative transfer models usually use a *homogeneous* plane parallel representation of the atmosphere, each layer has optical properties depending on altitude only. Because the light crosses different columns of atmosphere, using a uniform plane in each level does not capture the horizontal inhomogeneity of the atmosphere. Furthermore, in mountainous zones, a small displacement on the ground produces a rapid change in altitude, thus the atmospheric profile varies extremely rapidly[12]. Thus for these reasons, in paragraph 2.7 we now describe how a composite model is computed and used.

[11] Considering a plane parallel (i.e. flat) atmosphere is correct as long as the model is kept within the angular limits imposed by the deviations relative to a finite, curved atmosphere and it represents a reasonable approximation of the reality.

[12] A description of the topography effect on the atmospheric profile will be provided in section 5, introducing the meteorological model description. In particular, see par. 5.1.1, 5.1.2 and fig. 31.

2.7 Plane parallel atmosphere vs. the new composite atmosphere model

Although the *homogeneous* plane parallel atmosphere is a good compromise between the need of an analytical method for solving the problem of light propagation in a scattering and absorbing medium and a realistic model for the atmosphere, it doesn't take into account its three-dimensional structure.

Such a condition is evident in the real world when, for example, half of the sky is cloud covered and the other half is clear: the position of the Sun plays a fundamental role in the observed radiation. Seen from an observer at ground level, the radiation along the line of sight toward the Sun will be mostly extinguished and diffused by the cloud cover if the Sun direction passes through the covered part of the sky, or much less diffuse if it passes from the clear sky.

Since the atmospheric model provides a grid with profiles of atmospheric constituents, the simpler way to include in the homogeneous plane parallel atmosphere is to consider only a single point on the grid, corresponding to the geographic position of the point for which the simulation is performed. The light can, however, cross columns of the atmosphere (with different constituent profiles) which are not considered, producing incorrect modeling of all those conditions (i.e. sunset) in which the Sun is near the horizon[13].

For this work, an alternative approximation of a composite atmosphere has been developed. Figure 5 displays the model grid, each point being characterized by a different profile of constituents, pressure and temperature. An observer at ground level in a point with geographic coordinates x, y sees the Sun in the sky in a position described by the SZA (Solar Zenith Angle: the angle respect to the normal to the ground plane of incidence of the light) and by the SAA (Solar Azimuth Angle: the angle respect to the north towards east) on the horizontal plane. In the upper part of figure 5 the arrow points in the direction given by the solar azimuth angle, in the lower part the angle of the arrow with the vertical defines the solar zenith angle.

The composite atmosphere includes the intersection of the Sun-observer line-of-sight with the grid boundaries and, at the altitude corresponding to the intersection points, the atmospheric profile is *cut* and replaced with the profile of the next-crossed pixel. This procedure is iterated until the line exits from the atmosphere. The technique is the same as "short characteristics" in the radiative transfer literature. It is the formal solution of the radiative transfer equation for the direct ray if scattering is ignored. As shown in fig. 5, the MM5 simulation provides the atmosphere structure from the ground to approximately 16 km. This is the realistic atmosphere (i.e. physically consistent) determining the main contribution to ground radiation. The upper part of the atmosphere is required by the radiative transfer model, being higher layers relevant for optical radiative transfer calculations (the reference library of profiles for different latitude and seasons used by the radiative transfer code UVSPEC considers the TOA to be around 120 km) but it produces negligible contribution for the final

[13] In fact, when the Sun position is near the horizon, there is also the effect due to Earth curvature. Earth curvature can be usually neglected due to other unmodeled events occurring during light propagation at low solar position (presence of obstacles on the ground plane, shading of the ground, etc.). The effect due to Earth curvature is neglected both by the plane parallel model and by the composite model described in this paragraph. In practice, when the Sun is low enough (elevation angle less than 10°), the curvature is not the principal source of error for the model.

ground result[14]. For linking the MM5 and the standard atmospheres the two profiles are joined together: for layers from ground to the higher altitude of the MM5 data the parameters altitude steps, pressure, temperature and water vapor mixing ratio are taken from MM5 and the profiles of O2, CO2, O3, NO2 gases (not provided by MM5) are scaled proportionally to air density profile ratio between the MM5 and the standard profiles and re-interpolated at MM5 altitude steps; a standard atmospheric profile from the UVSPEC library is used for the corresponding season and latitude for layers from the higher altitude of the MM5 data to the TOA. The procedure JOIN_PROFILES is used for creating the composite atmosphere (see paragraph A.1).

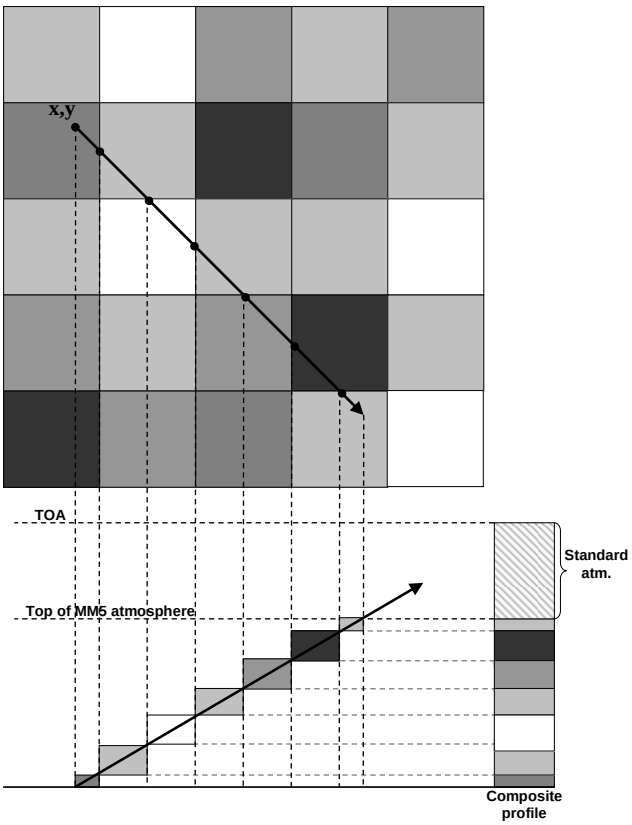

Figure 5: Composite atmosphere creation from a parallel layer atmosphere: from the ground to the higher altitude of the MM5 data the composite atmosphere is created taking the atmospheric profiles section on the Sun-observer line of sight. The standard atmosphere is used for "filling" the layers from the top of MM5 atmosphere to the TOA. Air gases are scaled in proportion to the MM5 air density.

[14] An exception is represented by ozone absorption for UV bands: optically significant concentrations of ozone are present in atmosphere above the MM5 upper limit, but the ozone concentration is set in the radiative transfer model independently of the MM5 profile.

2.8 Reflectance and transmittance model

To evaluate the total reflectance observed in direction of the satellite line of sight we consider the radiation propagating from the Sun in direction given by the angle SZA (Solar Zenith Angle) in a homogeneous plane parallel atmosphere (figure 6), each layer having a fixed value for the vertical optical depth. Defining τ_i as the vertical optical depth (see paragraph 2.4.3) of the layer i, the vertical transmittance T can be defined in each layer i by

$$T_i = exp(-\tau_i) \tag{16}$$

Denoting the transmittance in direction given by angle SZA for radiation propagating toward ground as T_i^+ and the transmittance at the angle VZA (Visual Zenith Angle) for radiation propagating towards the satellite as T_i^-, we have the following relations in the $i-th$ layer:

$$T_i^- = e^{-\frac{\tau_i}{cosVZA}} = T_i^{\frac{1}{cosVZA}} \tag{17}$$

$$T_i^+ = e^{-\frac{\tau_i}{cosSZA}} = T_i^{\frac{1}{cosSZA}} \tag{18}$$

Considering the atmosphere as non-absorbing, the reflectance can be defined as:

$$R_i^- = 1 - T_i^+ = 1 - T_i^{\frac{1}{cosSZA}} \tag{19}$$

$$R_i^+ = 1 - T_i^- = 1 - T_i^{\frac{1}{cosVZA}} \tag{20}$$

with the ground albedo (see formula 14) represented by the term $R_0^- = a$.

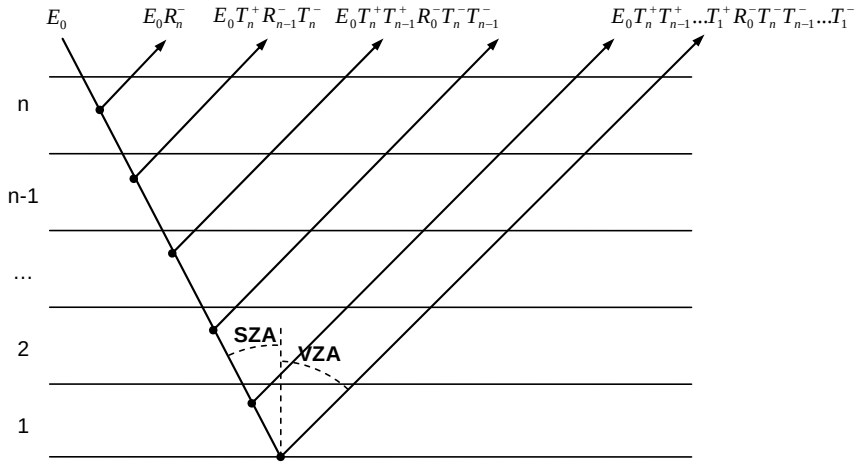

Figure 6: Reflectance model

It follows[15] that the total reflectance R_{tot} observed by the satellite is:

$$\begin{aligned} R_{tot} = R_n^- + T_n^+ R_{n-1}^- T_n^- + T_n^+ T_{n-1}^+ R_{n-1}^- T_{n-1}^- T_n^- + \ldots = \\ = \sum_{i=1}^{n+1} \left(\prod_{j=i}^{n} T_j^+ \, R_{i-1}^- \, \prod_{j=i}^{n} T_j^- \right) \end{aligned} \tag{21}$$

[15] The product $\prod_{j=i}^{n} \ldots$ has to be considered 1 for $i > n$

so:

$$R_{tot} = \sum_{i=2}^{n+1} \left[\left(\prod_{j=i}^{n} T_j \right)^{\left(\frac{1}{cosSZA} + \frac{1}{cosVZA}\right)} \left(1 - T_{i-1}^{\frac{1}{cosSZA}} \right) \right] + \\ + a \left(\prod_{j=1}^{n} T_j \right)^{\left(\frac{1}{cosSZA} + \frac{1}{cosVZA}\right)} \tag{22}$$

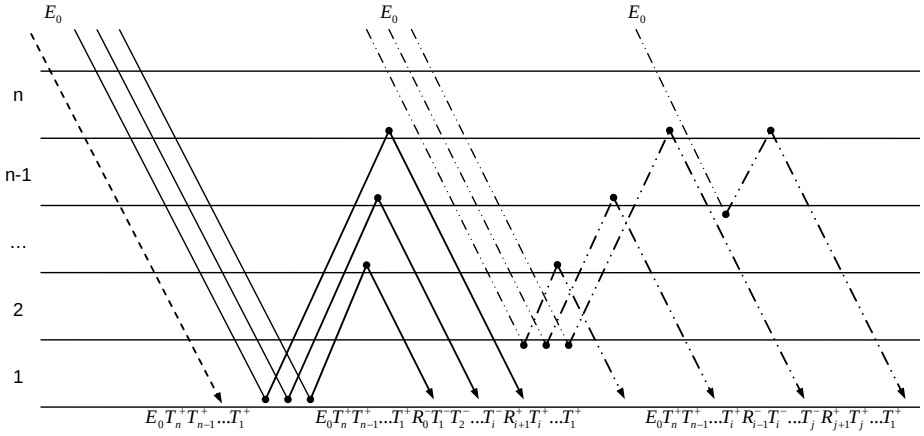

Figure 7: Transmittance model. Different contributions can be distinguished: direct radiation on the left (segmented line on the left), ground and atmosphere reflected radiation (continuous line in the center of the figure) and radiation trapped between atmospheric layers (on the right).

To determine the transmittance observed on the ground plane (see figure 7) we consider the contribute $T_n^+ \dots T_1^-$ given by the transmittance of all layers (direct contribution, see paragraph 2.4.3) plus the contributions given by reflections between layers and between ground and layers, so the total contribution to ground transmittance T_{tot} is:

$$T_{tot} = T_n^+ \dots T_1^+ + \sum_{k=2}^{n} T_n^+ \dots T_1^+ R_0^- T_1^- \dots T_{k-1}^- R_k^+ T_{k-1}^+ \dots T_1^+ + \\ + \sum_{k=2}^{n} T_n^+ \dots T_2^+ R_1^- T_2^- \dots T_{k-1}^- R_k^+ T_{k-1}^+ \dots T_1^+ + \dots \tag{23}$$

that becomes (where j and k are the layers in which the scattering occurs):

$$T_{tot} = \prod_{i=1}^{n} T_i^+ \left[1 + \sum_{k=2}^{n} \sum_{j=0}^{k-1} \left(R_j^- \prod_{i=j+1}^{k-1} T_i^- R_k^+ \prod_{i=j+1}^{k-1} T_i^+ \right) \right]. \tag{24}$$

Rewriting the formula (24) using the vertical transmittance T_i and using the relation $R_0^- = a$, it follows:

$$T_{tot} = \prod_{i=1}^{n} T_i^{\frac{1}{cosSZA}} \left\{ 1 + \sum_{k=2}^{n} \left[a \left(1 - T_k^{\frac{1}{cosVZA}} \right) \right. \right. \\ \prod_{i=1}^{k-1} T_i^{\left(\frac{1}{cosVZA} + \frac{1}{cosSZA}\right)} + \left(1 - T_k^{\frac{1}{cosVZA}} \right) \\ \left. \left. \sum_{j=1}^{k-1} \left(\left(1 - T_j^{\frac{1}{cosSZA}} \right) \prod_{i=j+1}^{k-1} T_i^{\left(\frac{1}{cosVZA} + \frac{1}{cosSZA}\right)} \right) \right] \right\} \tag{25}$$

with the first, constant, term into the first parenthesis taking into account the direct radiation from the Sun to the ground and the sum on k considering the contribution due to the diffuse radiation scattered toward ground by the $k-th$ layer. The latter contribution can be further divided, the term with the ground albedo estimating the radiation reflected first by the ground and then by each $k-th$ atmospheric layer and the second term (sum on $j = 1 \ldots k-1$) estimating the radiation reflected first by the $j-th$ layer and then reflected again by the $k-th$ layer towards ground without interacting with the ground plane. The different contributions are represented in figure 7).

Comparing this model with the radiative transfer code UVSPEC must be noted that the direct contribution to the ground irradiance ($I_{TOA} \prod_{i=1}^{n} T_i^+$) is expected to be the same for both UVSPEC and this model (the composite atmosphere *is* in fact a plane parallel atmosphere obtained by combining different atmospheric profiles in the direction of the line of sight of the Sun). The major differences are expected in the diffuse irradiance calculation, due to the scattering being computed in one direction only and not integrated over the solid angle. In practice, by separating the components into T and R, we are assuming that the transmission is only direct and the scattering is purely backward. Moreover, in such a simplified model, the diffuse contribution takes into account the multiple reflection between layers, but multiple scattering events and Lambertian diffusion by ground are neglected and, also considering single scattering events only, the scattering function is not weighted by the angle of viewing.

The approach described here resembles the principle used in Monte Carlo radiative transfer simulations. In such an approach, the different contributions to the observed radiation are estimated by simulating the trajectories of "photon packets". The simulation is performed by extracting the single photon trajectory by calculating, for each segment of the trajectory, the absorption or scattering distance between two points and the photon direction after the scattering event using random number extraction. The probability distribution used for each random number is calculated as a function of the optical characteristics of the medium. After a statistically relevant number of photons has been received in a fixed solid angle (simulating the sensor), the ratio between the number of received and launched photons converges to the ratio between the irradiance impinging at the top of the atmosphere and the ground or satellite measured radiance, thus the Monte Carlo method can be considered as the simulation of a representative set of all the contribution to the received radiation[16]. As in Monte Carlo modeling, the simple model for reflectance and transmittance calculation described in fig. 6 and 7 considers the different contributions to the radiation observed from the satellite or at ground. The algorithm is the same for the direct ray in the two treatments, the difference is the flexibility of having multiple columns while maintaining the planar geometry. This is an essential change since, even for the diffuse calculation, all existing models (with the exception of the Spherical Harmonic Discrete Ordinate Method (SHDOM) [21], http://nit.colorado.edu/shdom.html) consider a single-column approach, i.e. a *homogeneous* plane parallel atmosphere.

[16]The description given here for a Monte Carlo model applied to atmospheric radiative transfer is necessarily condensed and simplistic. For an example of a working Monte Carlo model developed for radiative transfer calculation and a more detailed description of the method, see e.g. [34].

The transmittance shown in figure 8 is calculated using both the model described in this paragraph and by launching UVSPEC. The discrepancies between the curves are due to the diffuse radiation model. In figure 9 the mismatch of the diffuse contribution is evident. The direct contribution is defined, on the contrary, exactly in the same way for both models, so the corresponding curves perfectly overlap. The software procedures used for calculating reflectance and transmittance are listed in A.6.

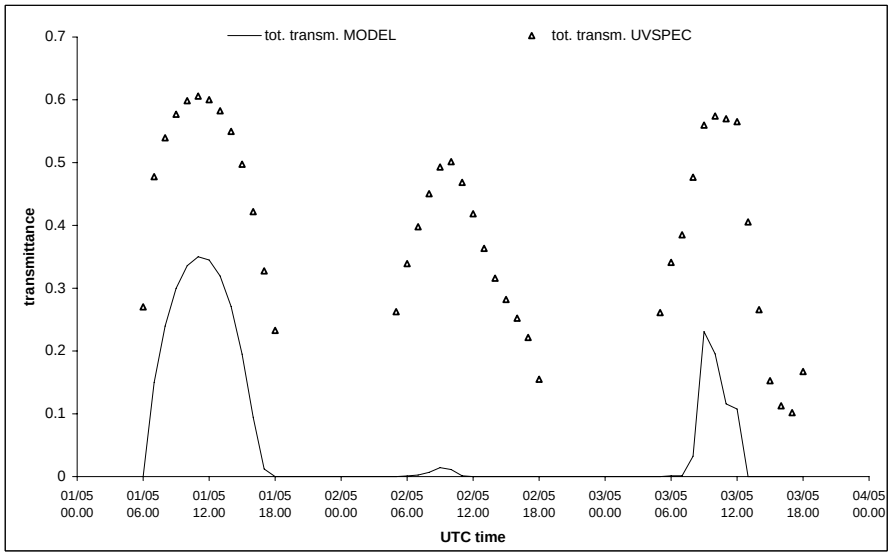

Figure 8: Transmittance comparison between UVSPEC derived transmittance and the model described here for the UV range: discrepancies are due to diffuse radiation model, mainly for values corresponding to cloudy situations (characterized by unmodeled multiple scattering events).

2.9 Increase of ground irradiance by broken clouds

The composite atmosphere takes into account the three-dimensional structure of the atmosphere, but, in fact, when running into the radiative transfer model, its structure is one-dimensional (parameters depending on altitude only).

A ground measurement of irradiance and of its direct and diffuse components with clouds modeled as layers brings to an enhancement of the diffuse components versus the total irradiance respect to the clear sky case, due to the greater optical depth (increase of scattering events $\rightarrow$ increase of diffusion and absorption). In contrast, the direct contribution decreases relative to clear sky for the same reasons.

A broken cloud layer produces a different ground irradiance. In the case presented in figure 10, the direct contribution is unchanged compared to clear sky, but the diffuse component increases because of cloud scattering. Depending on the phase function, a diffuse contribution can be seen at the ground plane within a smaller incidence angle, thus contributing to total irradiance more than in a clear sky situation. This is enhanced when the scattering is mainly

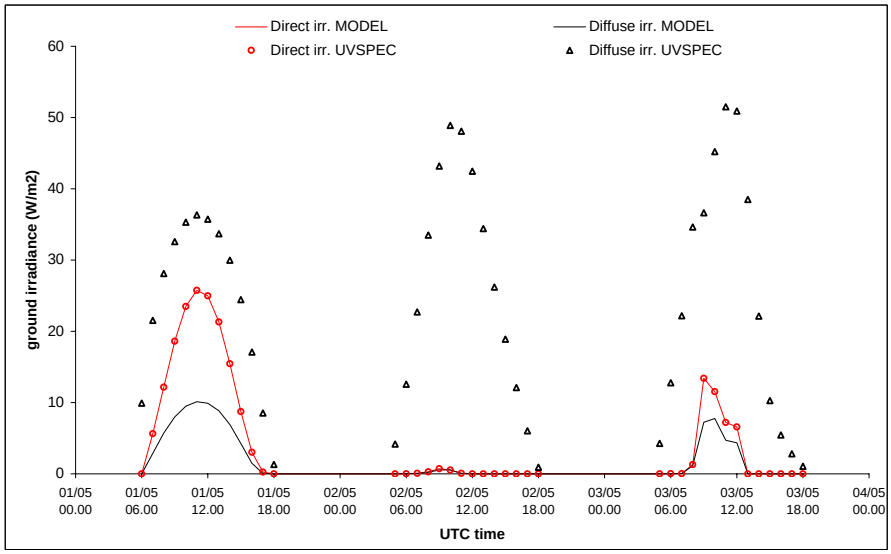

Figure 9: Direct and diffuse ground irradiance comparison: discrepancies due to diffuse radiation modeling are evident in the curve obtained from the simple transmittance model. Values for direct irradiance are calculated by Lambert-Beer law in the same way in both model and corresponding curves overlap.

due to large particles (Mie scattering): the typical scattering phase function (see 2.4.3) for aerosols (i.e. cloud water drops) is more peaked in the forward direction than Rayleigh scattering. In contrast, with broken clouds, as in figure 11, the reflectance observed from satellites can be reduced with respect to a uniform cloud cover,since part of the radiation is "trapped" between the ground and the cloud layer. The simple example shown in fig. 10 and 11 provides a model for this phenomena that is currently under study and represents a future development of this thesis. Increased ground irradiances due to broken clouds have been measured and are shown in figure 12, together with the corresponding image observed by the Meteosat Second Generation satellite (satellite data will be described in paragraph 6.2).

2.10 Ground contribution in UV exposure

The increase of ground irradiance is enhanced when the diffuse component is large with respect to the total, as in the UV band, due to the greater Rayleigh optical depth. In the examples in figure 10, the ground contribution has been neglected, since ground reflectance (albedo) is in general small compared to cloud reflectance. In the case of a non-negligible ground albedo, reflection and radiative trapping between the ground and clouds have to also be considered as contributions to total irradiance.

Since UV exposure is dangerous for humans, the ground contribution can't be ignored if the observer is standing near reflective surfaces (i.e. water) or high albedo terrains (sand, snow or ice covered soil): a significant body exposure can, in practice, arise from all these effects, so the simple shielding of direct

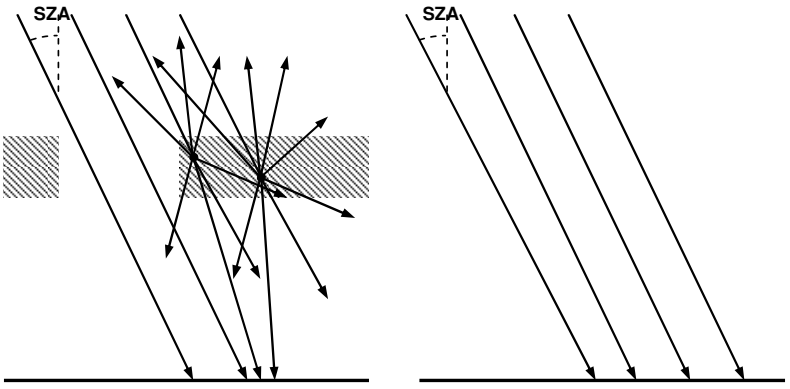

(a) Broken clouds (b) clear sky

Figure 10: Broken cloud situation and ground irradiance: if direct contribution can pass trough the "hole", both diffuse and direct ground irradiance are increased relative to the clear sky case.

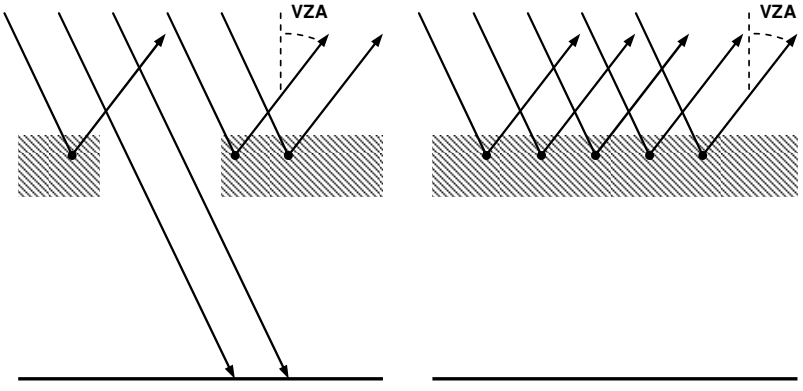

(a) Broken clouds (b) total cloud cover

Figure 11: Broken cloud situation and satellite observed reflectance: broken cloud situations can decrease the radiation diffused towards the satellite, thus the observed reflectance results decreased.

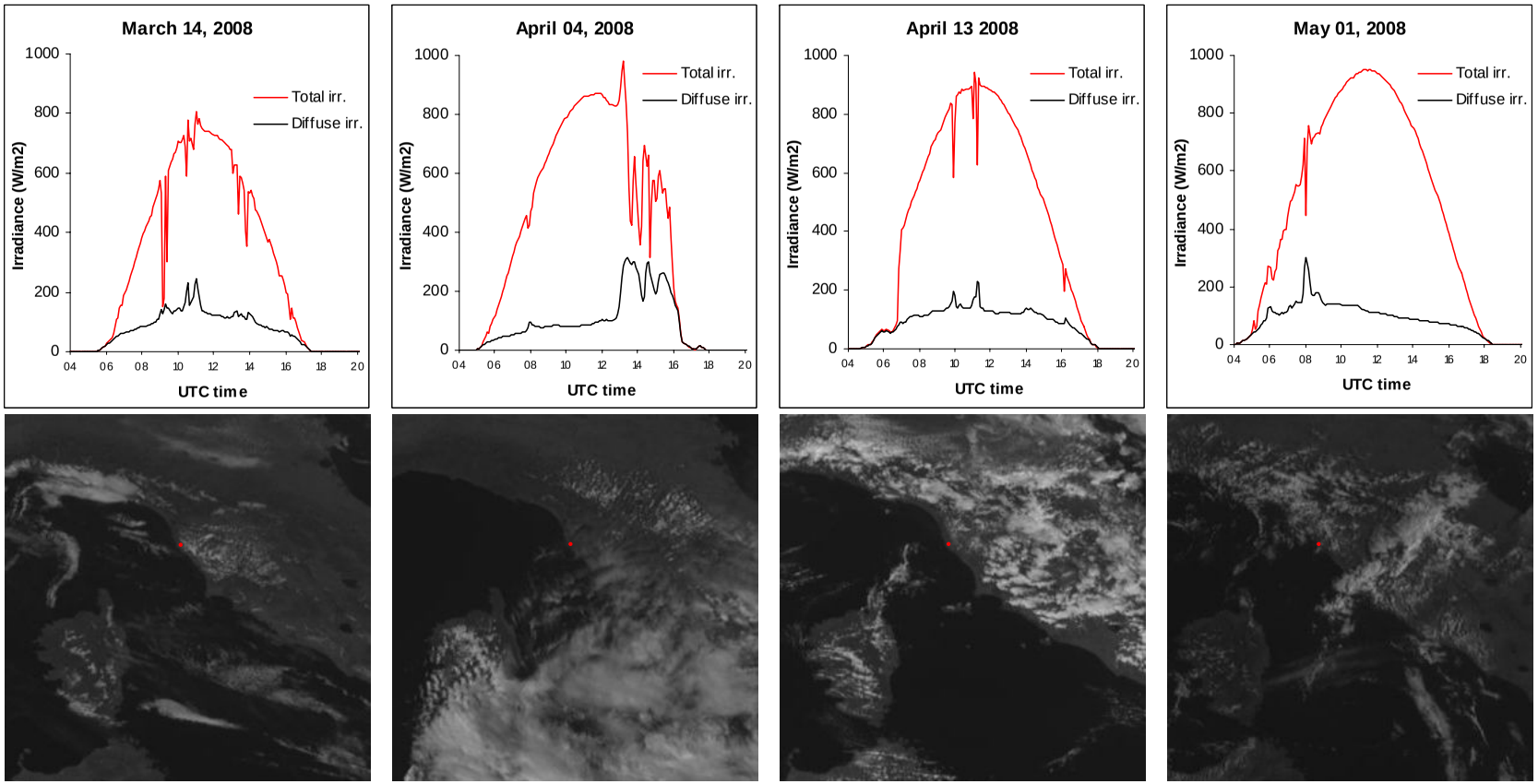

Figure 12: Examples of ground measured irradiance in broken cloud situations: the amplification effects are visible in measured values for total irradiance. Also the nearest Meteosat Second Generation image in visible band is displayed, for showing cloud position with respect to the ground sensor (represented as a red dot on the images). Satellite bands are described in detail in paragraph 6.2.

irradiance (i.e. standing under a umbrella) doesn't ensure protection from UV exposure.

2.11 Summary of the principal points of this section

In this section a new atmospheric model has been introduced: the composite atmosphere, taking into account the three dimensional structure of the atmosphere. The composite atmosphere is built from a grid of atmospheric profiles by cutting the profiles along the Sun direction and rearranging them in a new plane parallel atmosphere, used as input for the radiative transfer calculation.

A simple radiative transfer calculation, that will be further developed, has been introduced. The model determines the different contributions to the satellite observed radiance and ground irradiance (fig. 10 and 11).

The effects of non-uniform cloud cover are naturally included, the predicted effects have been measured with ground sensors and are shown in fig. 12. These effects will be considered during the development of future atmosphere models.

3 Ground measured data

3.1 The use of ground measured data in this work

Ground measured data are needed for the validation of the composite profile approach. The validation is performed by comparing the measured ground irradiance with the simulated values by the use of the radiative transfer model UVSPEC. Formally the use of the term validation isn't completely appropriate for this comparison: this is due to the practical lack of all the values for atmosphere characterization, that is the aerosol model to be selected in the radiative transfer code and the characteristics of the clouds. Although some characteristics can be derived by the knowledge of the local conditions of the locality of interest (for example, the literature offers typical "average" profiles of aerosol for different winter/summer and latitude range conditions), there are free parameters that remain unknown, that is they are not provided neither by the atmospheric model nor by direct measurements. The cloud drop radius (and ice drop shape) is a typical unmeasured parameters, subject to a rapid change in timescales of minutes, thus also a raw estimation of this type of parameters is in practice extremely difficult. In this work the radiative transfer simulations are performed using a range of the main unknown parameters, but the order of magnitude needs to be found by the statistical analysis of the aerosol (cloud drops are in fact aerosol particulate). In general, the problem of performing a realistic simulation of the ground irradiance is how to choose, from the MM5 predictions for the presence of clouds, some parametrization for the drop properties. For the analysis of aerosol properties, the AERONET (AErosol RObotic NETwork, http://aeronet.gsfc.nasa.gov) data have been chosen. AERONET data offers a wide database of aerosol size distributions, allowing the simulation of the corresponding optical characteristics.

Although AERONET data don't characterize the aerosol distribution as a function of the altitude (the aerosol measurements are obtained by lidar measurements, thus they correspond to an integration on the entire atmospheric column), aerosol characteristics are easily recognizable by the analysis of the size distribution, allowing the identification of aerosol origin, for example by wind load or water vapor condensation.

3.2 Ground sensors and acquisition campaign

Ground irradiance in UV and visible - near infrared bands has been measured using sensors located at the southern end of Livorno, at coordinates 43.506°N, 10.322°E, on the top of a building (approximately $10\,m$ ASL). The sensors integrate the impinging radiation over the upper hemisphere with respect to the local surface normal, thus performing a measurement of the irradiance.

The sensor is a Davis Instruments UV Sensor model 7841 (figure 13). Its spectral response matches very closely the Erythemal Action Spectrum, defined by McKinlay and Diffey [33], that is the standard representation of human skin sensitivity to UV radiation (shown in figure 14 together with the sensor response curve). The sensor measures the total UV irradiance (direct plus diffuse). The UV measurements are relative: the sensor provides a linear response with respect to the ground UV irradiance.

Irradiance in visible and infrared bands has been measured using two pyra-

Figure 13: Davis Instruments UV Sensor model 7841 (image from www.davisnet.com).

nometers (distributed by Delta Ohm), named LP PYRA 03 and LP PYRA 12, respectively Second and First Class Pyranometer according to ISO 9060. The pyranometers are based on a thermopile sensor: radiation is absorbed by the thermopile black surface (with Lambertian response), creating a temperature difference between the center of the thermopile and the body of the instrument. The temperature difference generates a voltage. In order to provide thermal insulation, to reduce the sensitivity to thermal radiation and to protect against dust and humidity, the instrument is covered by two glass domes. The spectral band is determined by the transmission of the glass domes.

The LP PYRA 12 instrument measures only the diffuse component of the total ground irradiance by the use of a shading ring that blocks direct irradiation. To impede the direct component, the ring must cover the apparent path of the Sun in the sky, thus the sensor must be properly oriented: the sensor body must face the Sun at local noon (azimuth angle 180°) [17] and must be rotated about to keep the ring axis parallel to that of the Earth (figure 15). Then the ring must be shifted along the sliding bars according with the current solar declination angle δ (angle between the Sun rays and the plane of the Earth's equator. Because the declination angle changes with the day of the year (DOY) due to the Earth's orbit (see chart b in figure 15), adjustments must be performed (approximately every two days) to keep the thermopile shaded and avoid direct irradiance contribution to the measured value. Figure 16 shows the change of the daily apparent trajectory of the Sun during the year. Changes to be performed in shading ring position are listed in a table provided with the instrument for all the year.

Measured values from all sensors are sampled by a datalogger. Averaged (by integration) values are stored every 5 minutes throughout the day.

The following contributions have been measured by the sensors:

- total irradiance (direct plus diffuse components) by LP PYRA 03 and UV Sensor 7841 in UV and visible - near infrared range;

[17] Orientation toward the Sun is performed by comparing the shading in both sides of a groove.

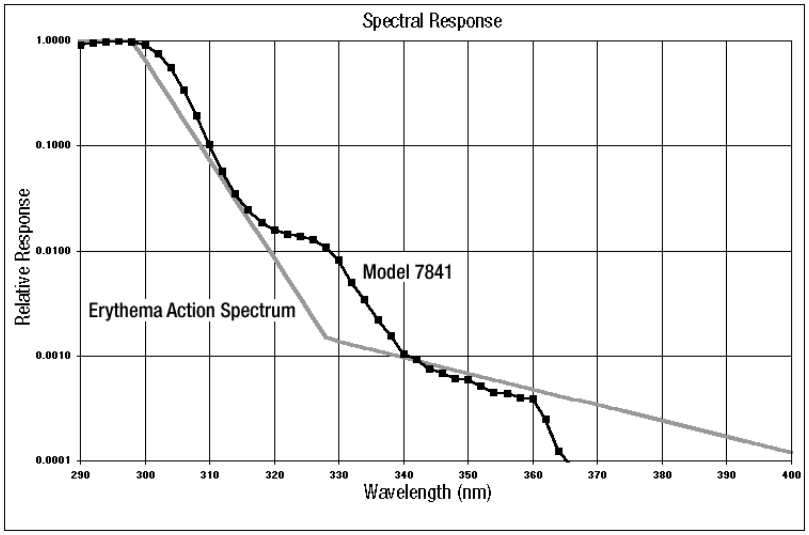

Figure 14: Davis Instruments UV Sensor model 7841 spectral response (from sensor data sheet www.davisnet.com).

- diffuse irradiance by LP PYRA 12 in the visible - near infrared range.

Direct irradiance in visible - near infrared band can be measured by difference between LP PYRA 03 and LP PYRA 12.

The characteristics of the instruments are summarized in the table 1.

Images of the instruments and ground measurement site are shown in figure 17 and 18.

3.3 AERONET aerosol data

The AERONET (AErosol RObotic NETwork) program is a federation of ground-based remote sensing aerosol networks [44, 15, 36, 25] established by NASA (www.nasa.gov) and LOA-PHOTONS (http://loaphotons.univ-lille1.fr/photons). The program provides a long-term public domain database of aerosol optical properties obtained by inversion techniques from ground measurements.

For investigating the characteristics of the particle size distribution of aerosols an automatic IDL procedure has been written for fitting all daily data provided by AERONET. Given the volume particle size distribution $dV/d\,(ln(r))$, the following distribution (sum of three logarithmic Gaussians [36]) has been fitted on AERONET data for Ispra (45.803°N, 8.627°E):

$$\frac{dV}{d\,(\ln(r))} = \sum_{i=1}^{3} A_i \exp\left(-\frac{(ln\,(r) - u_i)^2}{2\,c_i^2}\right) \tag{26}$$

The log-normal fit of eq. (26) is based on the expected statistical distribution for aerosols formed under normal nucleation conditions. Representing volume particle size distributions in logarithmic scale facilitates reporting the size distribution over a wide range. Moreover, logarithmic size distributions implicitly assume equal logarithmic intervals, corresponding to different aerosol sources,

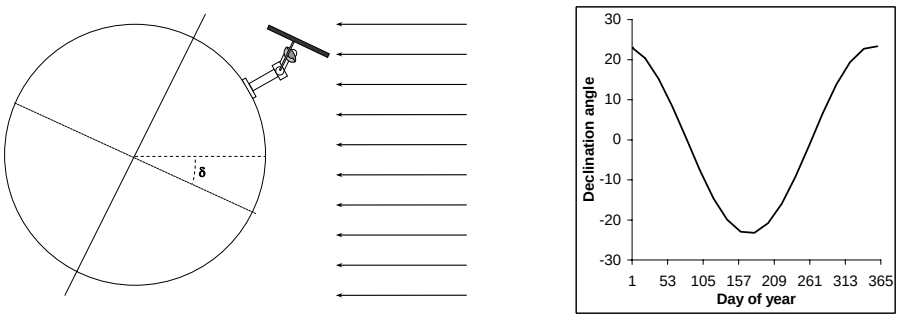

(a) (b)

Figure 15: Sensor position with respect to the Earth axis (a): the shading ring must be periodically adjusted for taking into account the change of the declination angle δ during the year (b). The shading disk of LP PYRA 12 instrument needs to be adjusted every two days for following the change in declination angle. See also figure 16 for an explanation in terms of solar zenith angle.

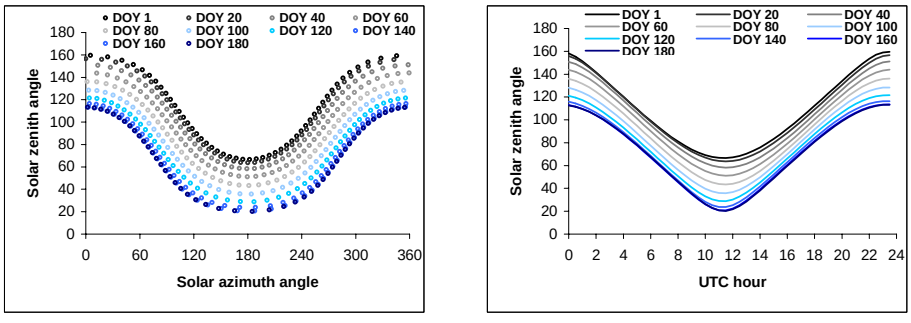

(a) (b)

Figure 16: Solar zenith angle vs. solar azimuth angle (a) and solar zenith angle vs. UTC time (b) at sensors coordinates (43.506°N, 10.322°E) for different days of the year (DOY). Curves are shown only for the first part of the year: after the minimum corresponding to summer solstice, the solar zenith angle increases until the winter solstice). The shading disk of LP PYRA 12 instrument needs to be frequently adjusted for following the Sun position on different curves.

	LP PYRA 03	**LP PYRA 12**	**Davis Instruments 7841**
Integration time for averaging	300 s	300 s	300 s
Sensor type	thermopile sensor	thermopile sensor	Semiconductor photodiode
Spectral range	$335\,nm - 2200\,nm$	$335\,nm - 2200\,nm$	$280\,nm - 360\,nm$
Cosine response	$\pm 22\,W\,m^{-2}$	$\pm 18\,W\,m^{-2}$	$\pm 4\,\%$ of reading (0° to 65° incident angle) and $\pm 9\,\%$ of reading (65° to 85° incident angle)
Measuring uncertainty	$\pm 2.5\,\%$	$\pm 1.5\,\%$	$\pm 8\,\%$
Measured components of ground irradiance	Total irradiance (direct + diffuse)	Diffuse irradiance	Total irradiance (direct + diffuse)
Sensor geographic position	43.506°N, 10.322°E, altitude $10\,m$ ASL	43.506°N, 10.322°E, altitude $10\,m$ ASL	43.506°N, 10.322°E, altitude $10\,m$ ASL

Table 1: Summary of the principal characteristics of ground sensors used in this thesis. LP PYRA 03 and LP PYRA 12 are yearly calibrated. The table uses the uncertainty from the calibration report, obtained by comparison with a calibrated source.

(a) LP PYRA 12 pyranometer

(b) LP PYRA 03 pyranometer

Figure 17: The LP PYRA 12 and LP PYRA 03 instruments for diffuse and total ground irradiance measurement. The shading ring of LP PYRA 12 prevents the direct contribution from contributing to the received irradiance.

whose radii having different order of magnitude. As an example a subset of these distributions is shown in figure 19. From the fit, the parameters A_i, c_i and u_i ($i = 1 \ldots 3$) have been determined and are given for all the datasets (years from 1997 to 2007) in figures 20 to 23. The IDL procedure performs the fit[18] using equation (26). If the fit doesn't converge or the code detects absurd values (e.g. negative values) for the parameters of one of the logarithmic Gaussians, the fit is repeated using only 2 Gaussians (eq. (26) for $i = 1, 2$). The charts and the table in figure 24 summarize the mean values obtained for each parameter of the three logarithmic distributions and the corresponding standard deviation.

Since this type of measurement is obtained by lidar measurements, it doesn't characterize the aerosol distribution as a function of the altitude, but it represents the integration on the entire atmospheric column. Nevertheless, aerosol characteristics are easily recognizable from the peaks of the distribution in formula (26). The log-normal distribution with mean radius r_1 around $0.1\mu m$ (see table in figure 24) is presumably given by the background aerosol above the 2-3 km, due to small particles that are usually present in the atmospheric column regardless of soil and atmospheric conditions[19]. The aerosol with the largest mean radius r_2 can be attributed to soil-generated particulate (natural or anthropogenic aerosol loading due to winds and boundary layer turbulence) in the layers near the ground (between the ground and the first $2-3\,km$) and (partly)

[18] In the code, the IDL-supplied function `CURVEFIT` has been used. The function uses a gradient-expansion algorithm to compute a non-linear least squares fit to a user-supplied function (in our case equation (26)) with a given number of parameters (A_i, c_i and u_i, $i = 1 \ldots 3$).

[19] A description of this type of aerosol inside the radiative transfer model used in this thesis will be given in paragraph 4.3.

Figure 18: The measurement site at 43.506°N, 10.322°E (represented by a red square on the image) in an orthophoto from Google Earth service (http://earth.google.it/).

to largest water and ice condensation phenomena at greater altitude, the typical particle radius being in the range $1 - 10\,\mu m$. The intermediate mean radius r_3, not always present in every sample, can be well explained by condensation of water vapor, as suggested by the largest width of the distribution with respect to the mean radius, and can be located between the ground and approximately 10 km of altitude.

We note that, for ground irradiance radiative transfer simulations, for aerosol and, in particular, clouds characterization (since clouds are a type of aerosol), we don't use the radius obtained by fit of AERONET data. In fact the model requires an altitude dependent radius for clouds description, and a choice for the non-cloud aerosol profile depending on the characteristic of the simulated site (further details in paragraph 4.3, in particular in table 2). For radiative transfer calculations in a cloudy atmosphere the radius of cloud drops needs to be specified, and such a parameter is not provided either by the meteorological simulations nor by direct local measurements, remaining undetermined. For this reason, in sec. 7, the simulations are performed for a range of fixed values of cloud drop radius. Therefore AERONET data provide an order of magnitude estimate for the liquid water and ice drop radius of the clouds as an input for the radiative transfer model.

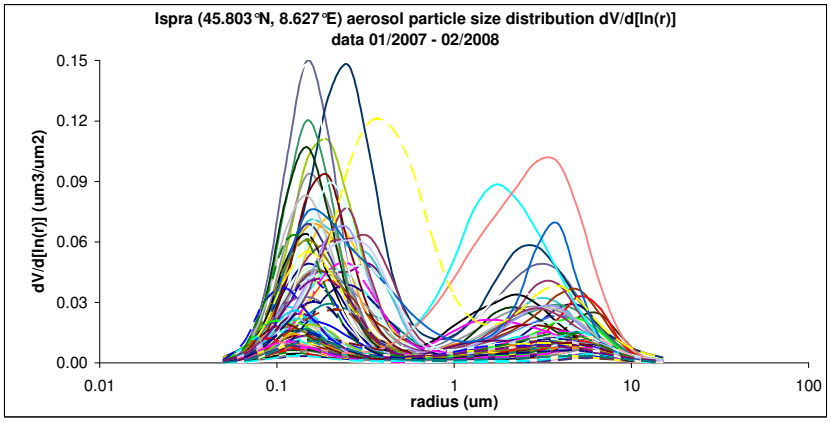

Figure 19: Aerosol particle size distribution $dV/d\,(\ln(r))$ in Ispra (45.803°N, 8.627°E). A subset of the data between January 2007 and February 2008 is shown for intelligibility of the chart. The first peak on the left of the log-normal distribution characterizes the background aerosol (above the 2-3 km), made up of small particles usually present in the atmospheric column regardless of soil and atmospheric conditions. On the contrary, the right peak represents the soil-generated aerosol (due to wind load) in the boundary layer and to largest water and ice condensation phenomena at higher altitude. An intermediate larger distribution, not always observed, is explained by water vapor condensation. Cloud drop radius is then expected to be in the range between $1-10\,\mu m$ or bigger (because the data are cloud-screened: the inversion model used for AERONET aerosol characteristics doesn't apply in case of cloud cover).

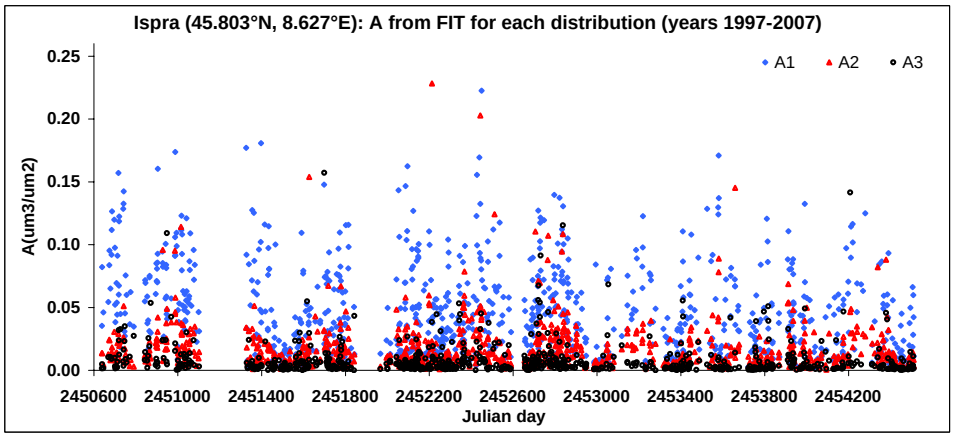

Figure 20: A from fit for each distribution

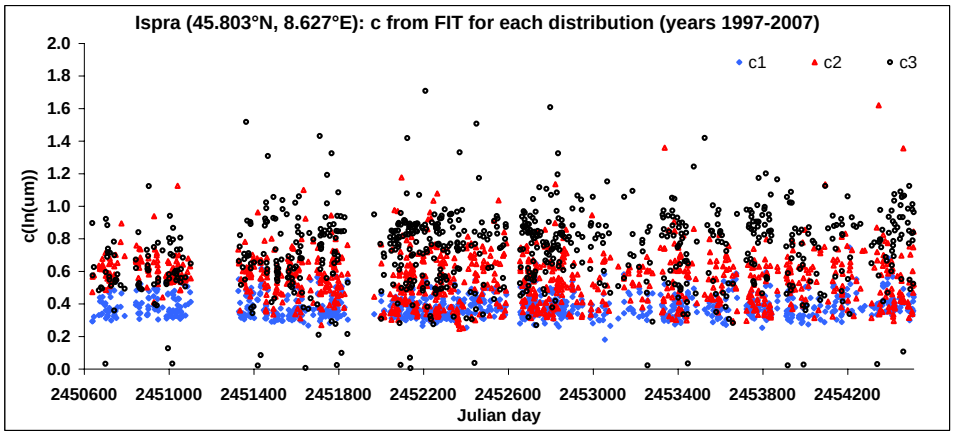

Figure 21: c from fit for each distribution

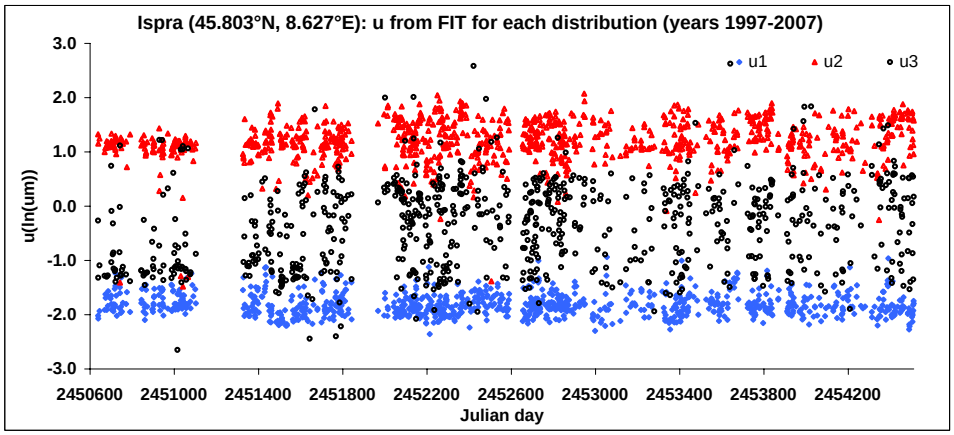

Figure 22: u from fit for each distribution

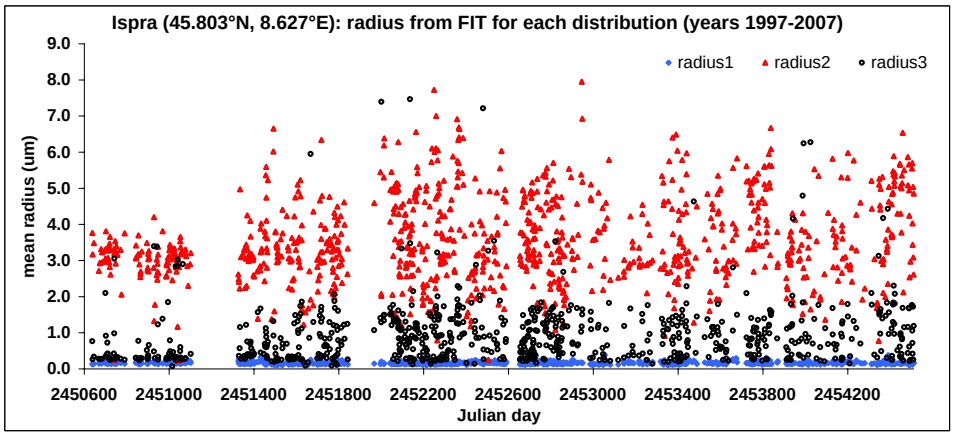

Figure 23: r from fit for each distribution. Strongly deviant values for radius 3 can be ascribed to soil generated particles due to wind load (see also discussion in [49], pp. 53).

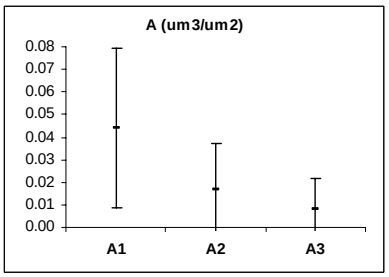

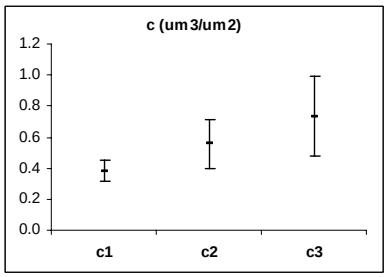

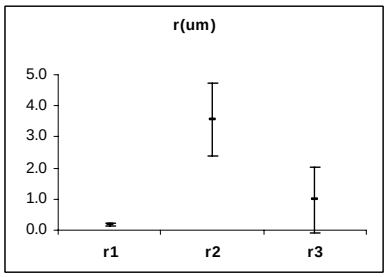

	mean	st. dev.
A_1(um3/um2)	0.044	0.036
A_2(um3/um2)	0.017	0.021
A_3(um3/um2)	0.008	0.014
c_1(um3/um2)	0.383	0.067
c_2(um3/um2)	0.557	0.157
c_3(um3/um2)	0.734	0.257
r_1(um)	0.166	0.038
r_2(um)	3.549	1.180
r_3(um)	0.972	1.055

Figure 24: Mean and standard deviation for A, c and r parameters of eq. (26).

4 The UVSPEC radiative transfer model

4.1 Use of the radiative transfer model

Radiative transfer models are used for simulating the propagation of the light in the atmosphere. In general a radiative transfer code considers a plane parallel atmosphere, whose layer being characterized by optical parameters depending on the altitude coordinate. The geometry in which the radiative transfer equation is resolved is three-dimensional, but the characterization of the physical system is one-dimensional (atmospheric layers have flat boundaries, , consequently the ground is considered as flat). Although this way of approaching the simulation of light propagation in a real atmosphere is in general accurate enough, there are situations in which the irradiation estimate depends not only on the vertical structure, but also on the spatial structure of the atmosphere around the observer. The case of irregularly distributed cloud cover offers an adequate representation of a system in which the measured ground irradiance depends on the Sun position as well as on the cloud position with respect to the observer.

Usually, also if a three-dimensional atmosphere is provided in input (we can consider, without loss of generality, a grid in which each pixel represents a profile of atmospheric constituents), the atmosphere characterization is not only plane-parallel, but also "single-pixel", in the sense that the profile is taken from the pixel of the grid corresponding to the observer position, regardless of the structure of the profiles of the surrounding pixels. This means that the entire atmospheric structure is described by the profile corresponding to the observer vertical profile. Such an atmosphere produces a prediction of the observed irradiance that is independent on the direction of propagation of the incoming light. Any change in the atmosphere opacity in the surrounding pixel doesn't affect the simulated ground irradiance. On the contrary, in the *real* problem, a change in cloud constellation around the observer makes the observer irradiance strongly dependent on the Sun position (as pointed out, for example, in the description of broken cloud effects in par. 2.9). As a consequence, light propagation depends not only on the local profile (the profile on the vertical of the observer) but also on the profiles of the surrounding pixels (even far away from the observer position).

A description of the phenomena occurring in non-plane-parallel atmospheric situation has already been provided, and a simple model (although inaccurate for precise radiative transfer calculations) has been introduced as a possible approach to a more realistic model. Nevertheless, the composite atmosphere approach represents a way of considering the differences between the pixels of the profile grid (i.e. the spatial variation of the profiles of the three-dimensional atmospheric model) by selecting a privileged direction (the Sub-observer line of sight) for determining a new profile. Then the composite profile can be employed in the radiative transfer model. In this thesis, the radiative transfer code for comparing the simulation of the ground and satellite measurements is the UVSPEC program, part of the libRadtran [32] atmospheric radiative transfer software package, a freely available library of radiative transfer routines and programs.

UVSPEC solves the Radiative Transfer Equation (RTE) by calculating the radiation field in the Earth's atmosphere for a given set of input parameters.

An UVSPEC run needs an input file, consisting of single line entries, each making up a complete input to the UVSPEC program. First on the line comes the parameter name, followed by one or more parameter values. UVSPEC can calculate irradiance, radiance, transmittance and reflectance (spectral or integrated quantities). The program offers different algorithms for the solution of the radiative transfer equation. In this work the multi-stream discrete ordinates radiative transfer equation solver DISORT (DIScrete Ordinates Radiative Transfer [45]) has been used. DISORT is a general and versatile plane-parallel radiative transfer procedure used in many atmospheric radiative transfer codes and applicable to a large wavelength range from the ultraviolet to radar regions of the electromagnetic spectrum for a multi layered plane parallel medium.

4.2 Spectral and spectrally integrated calculations

UVSPEC offers different ways of spectral calculations:

- Spectrally resolved calculation in the UV and visible spectral range;
- Line-by-line calculation using user-defined molecular absorption data;
- Band parametrization.

The spectrally resolved calculation and the line-by-line calculation are more or less exact methods, although very slow. A spectrally resolved calculation is the most direct way, used especially in the ultraviolet and visible spectral range, where gas absorption generally occurs in broad bands with only slow spectral variation. So, a wavelength resolution of $1\,nm$ is usually sufficient to obtain the spectral output in this range. Absorption cross sections for various species are included in UVSPEC, among them the most important are O_3, O_2, H_2O, CO_2, NO_2. In the infrared, however, molecular absorption spectra are characterized by narrow absorption lines. There are two ways to treat these:

- line-by-line calculations or
- band parametrization.

Line-by-line calculations are spectral calculations resolved at high wavelength resolution, but they need spectrally resolved absorption cross section profiles determined from database such as HITRAN ([40]), which is usually the standard for such calculations. Such a database database contains the parameters describing the shape of specific spectral lines and the continuum contribution. In this way the atmospheric absorption can be determined for the wavelengths of interest as a function of the concentration, pressure and temperature of the atmospheric gases. Band parametrization such as the Kato correlated-k distribution [29] and pseudo-spectral calculation such as the molecular absorption parametrization from LOWTRAN/SBDART [38] are approximations that provide a compromise between accuracy and computation time. In this thesis the most accurate band parametrization, the correlated-k method, is used. The Kato correlated-k method is a powerful way to calculate spectrally integrated quantities: the solar spectrum is split up into 32 bands, then the spectrally integrated quantity (irradiance or radiance) is simply the sum of the outputs for each band (the program support a specific command for obtaining Kato spectrally

integrated output). Although uncertainty is high for all bands above 2.5 micron, the integrated shortwave radiation (the sum of all 32 bands) is calculated with high accuracy because:

- the bands above 2.5 micron give only a little contribution to the integrated irradiance;
- errors on single bands are random.

4.3 Aerosols

Aerosol extinction is a principal contributor to the optical depth, especially in the visible. Clouds, composed of water as liquid drops and ice crystals, are an ensemble of aerosols. But aerosols are also present even in a cloud-free atmosphere, due to the action made by winds and to natural and anthropogenic phenomena occurring at ground (dust, combustion, pollen, urban and industrial activities, etc.). Depending on the location, the aerosol type changes and optical properties of the atmosphere are affected.

In the UVSPEC model, the aerosol specifications are based on the work of Shettle (1989) [43]. This default aerosol can be modified by the user to match the real conditions which the simulation refers to. In the Shettle model, aerosol has a reference profile depending on the season and the climatic zone, defined by an average profile for different situations as for the standard atmosphere introduced in paragraph 2.6. Table 2 lists the aerosol types considered by the model. In this thesis, considering the characteristic of the locality in which ground data have been collected (far from the center of Livorno, since aerosol composition is affected mainly by surrounding rural zones), the aerosol type used is the rural aerosol[20].

Aerosol type	**Altitude range from the ground**
Rural type aerosols	0-2 km
Maritime type aerosols	0-2 km
Urban type aerosols	0-2 km
Tropospheric type aerosols	above 2 km

Table 2: Aerosol type in the UVSPEC model

Excluding clouds, aerosols in Earth atmosphere are concentrated mainly in the first $2\,km$ from the ground. At higher altitude, the aerosol optical depth drops and only a tropospheric aerosol can be found, made up of smaller particles less than $0.5\,\mu m$ (visible in the AERONET aerosol data in paragraph 3.3, figure 23).

[20] Although the region where we made the irradiance measurements is near the sea and a few km away from a harbor with industrial activities, the rural model better matches the aerosols of the locality. In fact, maritime refers to the aerosols typical of oceanic environment and urban type aerosol is typical of heavily polluted or urbanized zones, so both of them would not realistically describe the characteristics of the atmosphere around the ground sensors.

Since the optical properties of the atmosphere are affected by aerosols especially in near ground layers, the light extinction due to aerosols can be expressed in terms of visibility, i.e. a parameter correlated with the optical depth measured horizontally instead of vertically. UVSPEC code uses visibility (expressed in km) as a scaling factor for the aerosol extinction coefficient profile, so that an increase of horizontal visibility brings to a corresponding scaling of the integrated vertical optical depth. The relation between visibility and aerosol integrated optical depth and single scattering albedo is shown in figure 25. The dependency of the aerosol profile by the altitude is shown in figure 26 for different aerosol models in different wavelength bands. The different effects due to aerosol type on ground irradiance are shown in chart 27 and 28 for direct and diffuse UV irradiance[21] for different values of visibility. The effects due to seasonal changes in the constituents atmospheric profile are shown in chart 29 and 30.

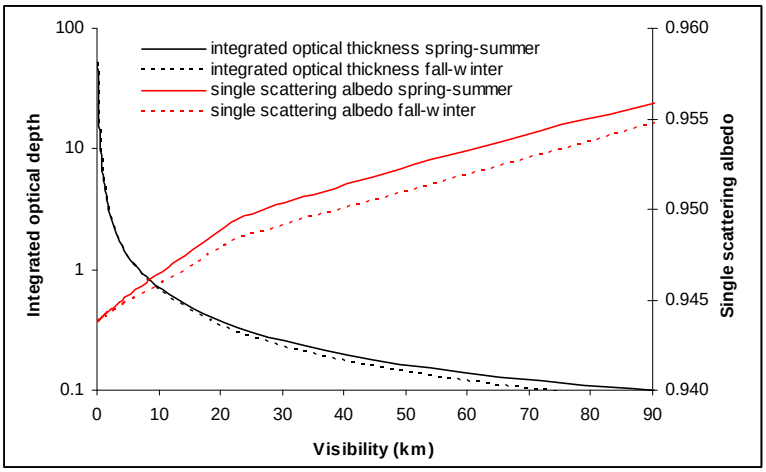

Figure 25: Integrated optical depth for a wavelength of $550\,nm$ due to aerosols only and aerosol single scattering albedo as a function of the visibility parameter (km) in UVSPEC for aerosol type rural in different seasons.

[21] Simulations have been performed for ozone values expressed in Dobson units (DB). One Dobson unit refers to a layer of ozone that would be 10 μm thick under standard temperature and pressure ($273.15\,K$, $100\,kPa$).

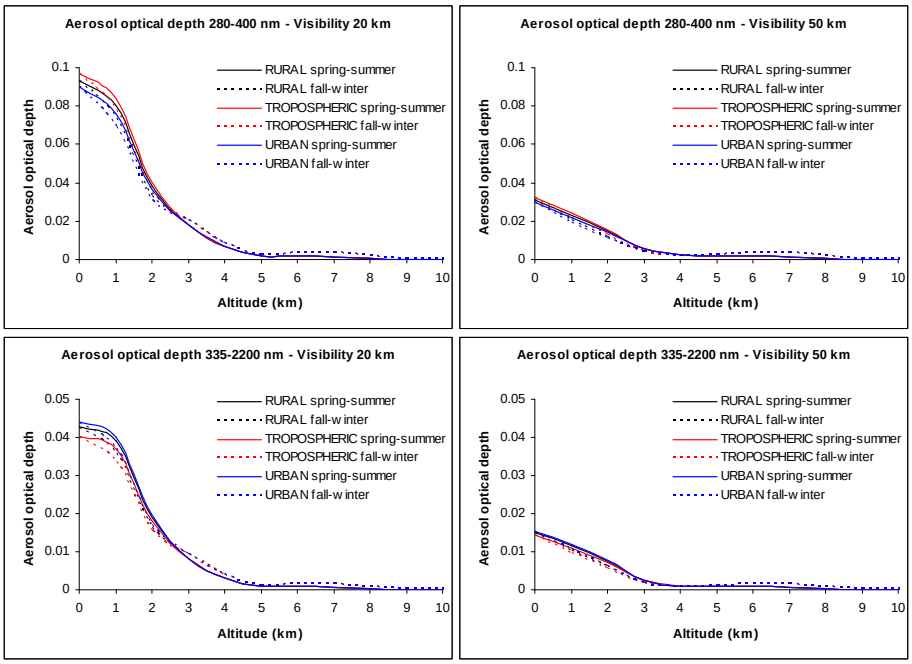

Figure 26: Aerosol optical depth from altitude in abscissa to the top of atmosphere for different aerosol type used by UVSPEC for different values of visibility, season and wavelength band.

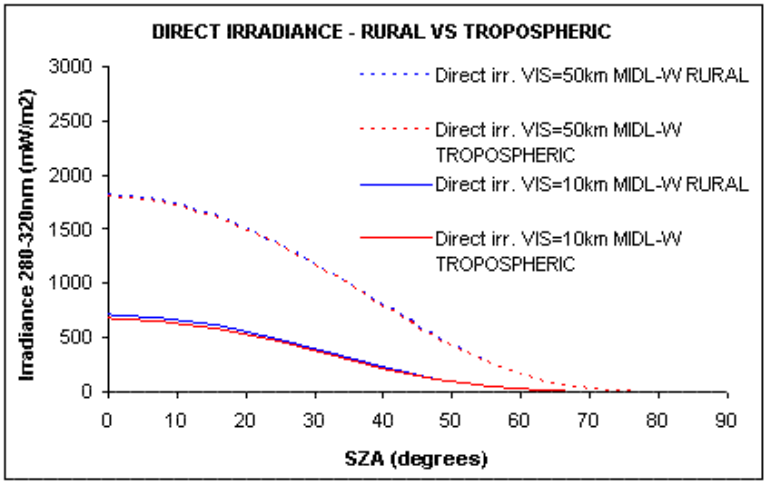

Figure 27: Comparison between direct irradiance values in the band $280-320nm$ using two different models for aerosol: rural and tropospheric. UVSPEC Input data: atmosphere type MIDLATITUDE-WINTER, visibility value of 50 km and 10 km, ozone 350 DU, ground albedo 0.017 (typical of the vegetation).

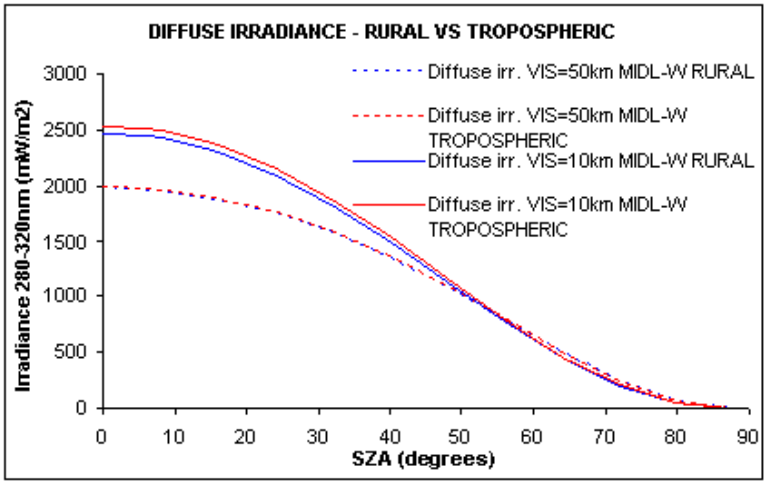

Figure 28: Comparison between diffuse irradiance values in the band $280 - 320nm$ using two different models for aerosol: rural and tropospheric. UVSPEC input data as in chart 27.

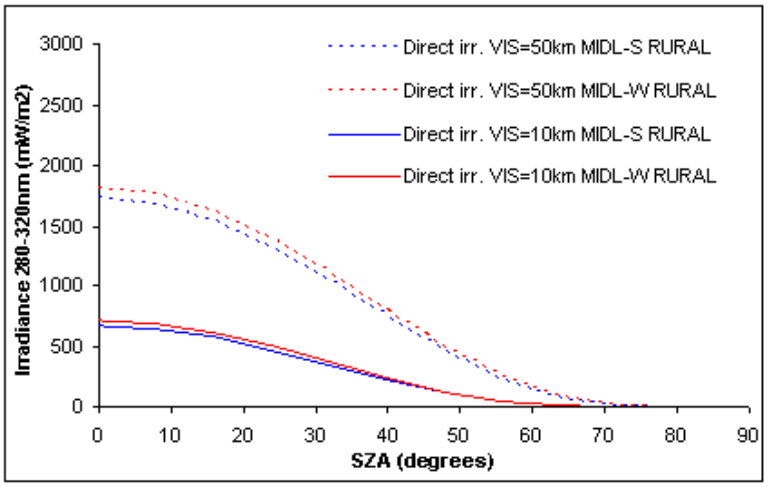

Figure 29: Comparison between direct irradiance values in the band $280-320nm$ using two different models for aerosol: rural and tropospheric. UVSPEC Input data: atmosphere type MIDLATITUDE-WINTER, visibility value of 50 km and 10 km, ozone 350 DU, ground albedo 0.017 (typical of the vegetation).

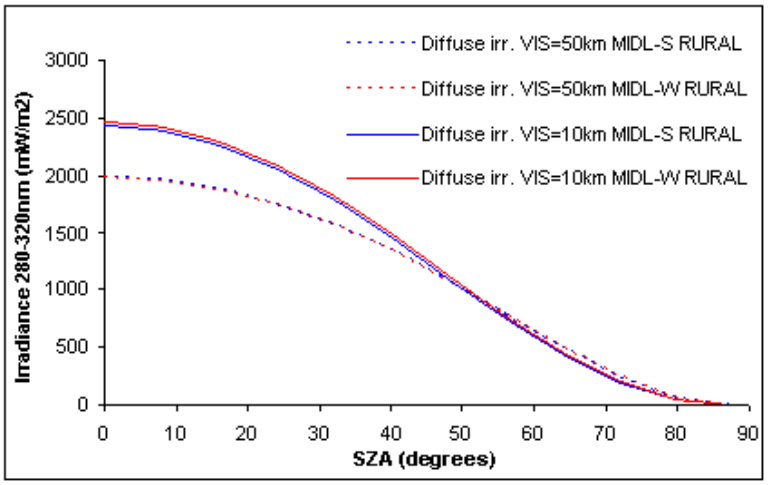

Figure 30: Comparison between diffuse irradiance values in the band $280 - 320nm$ using two different models for aerosol: rural and tropospheric. UVSPEC Input data as in chart 29.

4.4 Setting up the atmosphere

UVSPEC offers default atmospheric profiles (standard atmospheres) for different climatic zones (i.e. subarctic, midlatitude, tropical, U.S. standard) and seasons (winter or summer). These standard atmospheres are representative of a cloud free situation and are referred to climatic and seasonal standard conditions, as explained in paragraph 2.6. Profiles of standard atmosphere require:

- altitude above sea level in km;
- pressure in hPa;
- temperature in K;
- air density in cm^{-3};
- ozone density in cm^{-3};
- oxygen density in cm^{-3};
- water vapor density in cm^{-3};
- CO2 density in cm^{-3};
- NO2 density in cm^{-3}.

These profiles can be modified by the user. This is the step that substitutes the composite atmosphere described in paragraph 2.7 for the standard atmosphere, using MM5 (sec. 5) in the lower layers with the upper part of the standard atmosphere (not considered by the meteorological simulation) linked to the lower layers. The procedure carried on for the new composite atmosphere profiles creation is discussed in detail in A.2.1. In appendix A is described also the IDL code used to generate the atmosphere files for UVSPEC.

4.5 Ice and liquid water clouds

By default, the atmosphere defined for UVSPEC is representative of a cloud free situation. The user can, however, include water or ice clouds by generating a cloud water/ice file consisting of:

- altitude in km;
- liquid or ice water content in g/m^3;
- effective droplet radius in μm.

The water content is returned by the run of MM5 atmospheric model, and the radius (not provided by the numerical simulation) has been extrapolated using AERONET data (paragraph 3.3). The procedures for ice and liquid water profiles creation is discussed in detail in A.2.2, together with the IDL code for automatic file generation from the atmospheric model output.

5 The atmospheric model

5.1 The MM5 model

5.1.1 MM5 model definition

The PSU/NCAR mesoscale model is a limited-domain, terrain-following model designed to simulate or predict mesoscale and regional-scale atmospheric circulation, that is to perform a meteorological prediction. The following definitions define a mesoscale model:

- mesoscale-alpha: the spatial range covers a 200-2000 km area with a temporal step of 6 h – 2 days (it's used to model jet streams, small hurricanes, weak anticyclones);
- mesoscale-beta: with dimensions of 20-200 km and a time step of 30 min – 6 h (used to provide atmospheric vertical profiles, local and mountains wind, mesoscale convective complexes, large thunderstorms); - mesoscale-gamma: with dimensions between 2 and 20 km and 3-30 min time step (for thunderstorms, large cumulus, large tornadoes).

MM5 is used in this thesis to provide atmospheric vertical structure, thus the scale used is the mesoscale-beta. In particular, by performing a post analysis using low resolution gridded data and station measured atmospheric profiles, MM5 determines: pressure, temperature, water vapor mixing ratio and cloud, snow and ice water content profiles for the location of interest (in this thesis the location of the irradiance sensors). The model was developed by Pennsylvania State University and the National Center for Atmospheric Research (www.ncar.ucar.edu). It is supported by several auxiliary programs, which are referred to collectively as the MM5 modeling system. MM5 is freely provided and maintained by the Mesoscale Prediction Group in the Mesoscale and Microscale Meteorology Division, NCAR (www.mmm.ucar.edu/mm5). The model conventions, coordinate system and MM5 program flow are described in the next paragraphs. Appendix C details the entire procedure of code customization applied to the MM5 runs needed in this thesis.

5.1.2 MM5 vertical grid

MM5 input and output data are grid-referenced. Since the atmosphere is in hydrostatic equilibrium, a monotonic variation of pressure with the altitude means that the geometric altitude z or the pressure p are equally valid coordinates. The use of the pressure as a vertical coordinate is useful when the atmosphere is close to be in hydrostatic equilibrium. MM5 model uses the sigma coordinates system. The sigma coordinate system [51] is pressure based and normalized, so it conforms to natural terrain. It defines the base at the model's ground level. The vertical coordinate is terrain following meaning that the lower grid levels follow variable isobars. With σ there is no need to detail boundaries at terrain gradients, while the upper surface is assumed to be flat. A dimensionless quantity is used to define the model levels. Thus, considering a point in coordinates x, y, the vertical position in the atmosphere is expressed as:

$$\sigma(x,y) = \frac{p(x,y) - p_t}{p_s - p_t} \tag{27}$$

where p is the pressure of the point, p_s the pressure at the reference surface, p_t the pressure at the top of the domain, as in figure 31. Thus, the modeling system calculates its data on isobaric surfaces, but these need to be interpolated to the model's vertical coordinate before being input to the model.

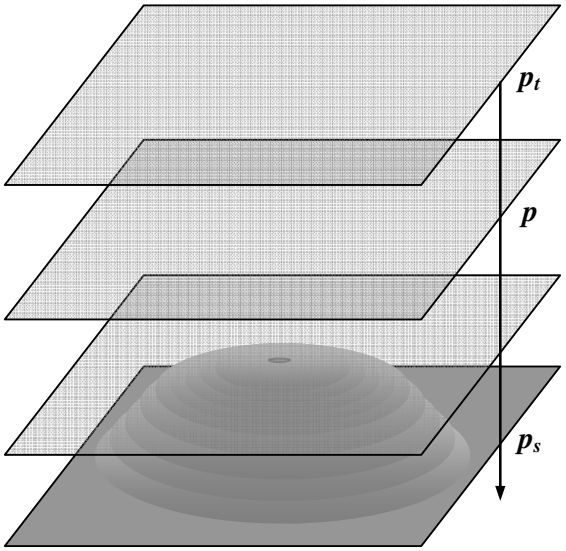

Figure 31: Schematic representation of the isobars in presence of terrain gradient. Sigma coordinate are normalized, so that lower sigma levels follow the terrain and the upper level is flat.

5.1.3 MM5 horizontal grid

MM5 model uses a Cartesian coordinate system. Using a Cartesian coordinate system instead of the full spherical coordinates means that the surface is locally considered "flat" (for this reason it is said to be a mesoscale model) using the tangent-plane approximation: the Earth's surface in the vicinity of a point is considered to be a plane tangent to the Earth spheroid in that point and the apparent gravity is directed perpendicular to the plane, even at finite x, y displacements. The lines of latitude and longitude form a regular rectangular grid on the tangent plane.

5.1.4 MM5 momentum equations

An MM5 run is performed by solving the dynamical model equations. We have to introduce the special symbol $\frac{D}{Dt}$ as the material derivative: any quantity s will be a function of three position coordinates x, y, z and of time: $s = s(t, x, y, z)$. If s is changed by ds, the independent variables change by:

$$\delta s = \frac{\partial s}{\partial t}\delta t + \frac{\partial s}{\partial x}\delta x + \frac{\partial s}{\partial y}\delta y + \frac{\partial s}{\partial z}\delta z \tag{28}$$

For calculating the change experienced by a fluid particle, we need to choose $\partial x, \partial y, \partial z$ to be consistent with the displacement of the particle in the time interval. If we denote the velocity $\mathbf{v}$ of the fluid with components given by u, v, w, then:

$$(\partial x, \partial y, \partial z) = (u, v, w)\delta t \tag{29}$$

We define now the material derivative as:

$$\frac{D}{Dt} = \lim_{\delta t \to 0} \frac{\delta s}{\delta t} \tag{30}$$

so:

$$\frac{Ds}{Dt} = \left(\frac{\partial s}{\partial t} + u\frac{\partial s}{\partial x} + v\frac{\partial s}{\partial y} + w\frac{\partial s}{\partial z}\right) \tag{31}$$

or

$$\frac{D}{Dt} = \frac{\partial}{\partial t} + \mathbf{v} \cdot \nabla \tag{32}$$

To develop an expression of the law of motion, the momentum equation has to be written (at the moment in an inertial frame):

$$\frac{D\mathbf{v}}{Dt} = -\frac{1}{\rho}\nabla p + \mathbf{g_t} \tag{33}$$

where p is the pressure, ρ the density of the air and $\mathbf{g}_t$ the gravity acceleration. This is one of Navier-Stokes equation for fluids (the viscosity is at the moment neglected). Changing the inertial frame used for eq. (33) in a frame rotating with the Earth with angular velocity $\mathbf{\Omega}$ at latitude ϕ, the moment must also contain a term due to centrifugal and Coriolis accelerations. Calling $\mathbf{g}$ the apparent gravity as the sum of $\mathbf{g}_t$ and the centrifugal force, it follows:

$$\frac{D\mathbf{v}}{Dt} + 2\mathbf{\Omega} \times \mathbf{v} = -\frac{1}{\rho}\nabla p + \mathbf{g} \tag{34}$$

and the equation for each component of the moment in x, y, z direction is:

$$\frac{Du}{Dt} + 2\Omega w cos\phi - 2\Omega v sin\phi = -\frac{1}{\rho}\frac{\partial p}{\partial x} \tag{35}$$

$$\frac{Dv}{Dt} + 2\Omega u sin\phi = -\frac{1}{\rho}\frac{\partial p}{\partial y} \tag{36}$$

$$\frac{Dw}{Dt} - 2\Omega u cos\phi = -\frac{1}{\rho}\frac{\partial p}{\partial z} - g \tag{37}$$

$sin\phi$ taking into account the Earth's angular velocity in the local vertical.

Applying eq.(34) to synoptic-scale systems (i.e. ranging in size from several hundred kilometers to several thousand kilometers) implies the following assumptions:

- vertical velocities are typically $\approx 10\,cm\,s^{-1}$ (timescale $\approx 1\,day$, typical distances $\approx 10\,km$)[22];
- horizontal velocities are typically $\approx 10\,m\,s^{-1}$ (timescale $\approx 1\,day$, typical distances $\approx 1000\,km$;)
- the term $2\Omega w cos\phi$ is smaller of the term $2\Omega v sin\phi$ of a ratio $\approx \frac{w}{v} \approx 10^{-3}$ (considering a typical latitude of 45°) and can be ignored at high accuracy;
- $\frac{Dw}{Dt} \approx \frac{10\,cm\,s^{-1}}{1\,day} \ll g$ and $2\Omega u cos\phi \ll g$.

To first order, the momentum equations become:

$$\frac{Du}{Dt} - fv = -\frac{1}{\rho}\frac{\partial p}{\partial x} \tag{38}$$

$$\frac{Dv}{Dt} + fu = -\frac{1}{\rho}\frac{\partial p}{\partial y} \tag{39}$$

$$\frac{\partial p}{\partial z} = -\rho g \tag{40}$$

where $f = 2\Omega sin\phi$ is the Coriolis parameter.

The eq. (40) is the hydrostatic equation[23]. It is important to emphasize that the assumption is not that vertical acceleration is zero, but that it's small enough for considering the atmosphere in hydrostatic balance. With eq. (40) is impossible to calculate the vertical acceleration, for this reason, the model first resolves the equations for momentum, then it calculates the density distribution using thermodynamic and pressure equations (see paragraph 5.1.6).

The assumption now is that the basic horizontal wind may be represented by the geostrophic wind, meaning a wind velocity for which the Coriolis acceleration balances the horizontal pressure force. The balance between Coriolis and horizontal pressure-gradient forces can be written as:

$$fv = \frac{1}{\rho}\frac{\partial p}{\partial x} \tag{41}$$

and

$$fu = \frac{1}{\rho}\frac{\partial p}{\partial y} \tag{42}$$

Horizontal winds can be written as $\mathbf{u} = \mathbf{u_g} + \mathbf{v}$. The semigeostrophic approximation replaces horizontal winds $\mathbf{v}$ by their geostrophic values ($\mathbf{u_g}$) in the horizontal acceleration terms of the momentum equations, considering the horizontal advection (the process of transport of an atmospheric property solely by the velocity field) in the thermodynamic equation being purely geostrophic advection. The semigeostrophic approximation is used in the analysis of synoptic-scale systems, in which winds can be approximated by their geostrophic values. The geostrophic approximation becomes poorer near the ground for the effect of

[22] These assumptions are not valid in storms, strongly convecting systems or terrain-forced flow

[23] Eq. (40) is the hydrostatic equation in the co-rotating frame, not the hydrostatic equation in general.

frictional forces (on a scale of few meters, thus not affecting the atmospheric optical properties considered in this thesis). The difference between the real value of wind velocity and the geostrophic wind is known as ageostrophic wind. The wind speed near the ground can be modeled by adding a negative acceleration term in the momentum equation depending on the terrain surface roughness.

5.1.5 Nesting

Surface, boundary conditions and atmospheric data refer to the horizontal latitude and longitude grid. The user defines one or different domains for the MM5 run by fixing a central point for the grid and a length for the side of each pixel of the grid. The horizontal grid allows interactions between different user-defined domains, taking into account the possibility of multiple nesting. Usually an external domain, with a coarser resolution, contains a nested domain with a finer resolution. Each sub-domain has a "mother domain" in which it is completely embedded. In MM5 the nesting can be done using a one-way or two-way configuration:

- In the one-way nesting the model is first run to create an output (mother domain). Initial conditions are established by taking the variable values at ground by a climatic global model distributed on the web for the interval of interest (more details in paragraph 5.1.7 for description of the source of the data). Then the output is interpolated and a boundary file is created. A typical boundary file may be hourly (dependent upon the output frequency of the coarse domain), and can be time-interpolated to supply the nest domain with a finer temporal resolution. The nest may also be initialized with enhanced-resolution data and terrain model (consistent with the coarser mesh in the boundary zone). We have to introduce here the condition for convergence for solving partial differential equations numerically: the Courant–Friedrichs–Lewy condition (CFL condition [11]). For the algorithm to provide stable results, the time step used must be less than the time for a pressure (sound) wave to travel to an adjacent grid point. In formulas:
$$\frac{\mathbf{v}\Delta t}{\Delta x} < C \tag{43}$$
The relation between spatial grid step and temporal step must respect the CFL condition. Following MM5 documentation we choose the spatial and time steps with respect to (43).

- Two-way nesting uses a feedback from the inner to the mother domain: the nest's input from the coarse mesh comes via its boundaries, while the feedback to the coarser mesh occurs over the nest interior. In this way, the outer domain provides boundary condition for each of the inner domains. The advantage in using this option is that the model has lateral boundary conditions that use consistent physics with the coarse grid model and these conditions are available at a relatively high temporal frequency. For setting a two-way nested domain in MM5, the resolution of the inner domain must be 3 times finer than the resolution of the mother domain. Nesting is useful for having a high resolution around the point of interest and a mother domain covering a large area (for realistic simulation), thus increasing computation time.

5.1.6 MM5 equations

An MM5 run is performed by solving the dynamical model equations for the basic variables (excluding moisture[24]). First of all, we have to re-define the gas equation as:

$$p = \rho R T \tag{44}$$

where p is the pressure, ρ the density of the air, T the virtual temperature, $R = \frac{R_{gas}}{\bar{m}}$, $R_{gas} = 8.3143 JK^{-1}mol^{-1}$ the gas constant, $\bar{m}$ the mean molar mass for dry air (averaging over dry constituent gas components). The term T as virtual temperature takes into account the amount of water vapor mixing ratio q (mass of water vapor per unit mass of dry air) in the general case of wet air. It is indeed convenient considering R as constant (since the components of dry air are approximately constant) and applying the definition of virtual temperature for taking into account the variability of the water vapor in wet air:

$$T = \frac{1 + \frac{q}{\epsilon}}{1 + q} T_{true} \backsimeq T_{true}\,(1 + 0.622q) \tag{45}$$

where T_{true} is the real temperature and ϵ is the ratio of the molecular weight of water vapor and dry air.

The thermodynamic equation is derived from the gas equation (eq. (44)). By defining $\alpha = \frac{1}{\rho}$, it follows:

$$R\,dT = dp\,\alpha + p\,d\alpha \tag{46}$$

By substituting $R = c_p - c_v$:

$$c_p dT - \alpha\,dp = c_v dT + p\,d\alpha = dQ \tag{47}$$

with Q diabatic (involved in the transfer) heat, c_p specific heat at constant pressure, c_v specific heat at constant volume and applying the material derivative definition (eq. (32)) to the first and third term of eq. (47), it follows:

$$c_p \frac{DT}{Dt} = \frac{1}{\rho}\frac{Dp}{Dt} + \dot{Q} \tag{48}$$

Applying the material derivative definition to eq. (44) and defining $p = p_0 + p'$, with p_0 reference pressure, brings to:

$$\frac{\partial T}{\partial t} = -\mathbf{v}\cdot\nabla T + \frac{1}{\rho c_p}\left(\frac{\partial p'}{dt} + \mathbf{v}\cdot\nabla p' - p_0 g w\right) + \frac{\dot{Q}}{c_p} \tag{49}$$

For the pressure equation we have (by applying the material derivative to (44)):

$$\frac{1}{p}\frac{Dp}{Dt} = \frac{1}{\rho}\frac{D\rho}{Dt} + \frac{1}{T}\frac{DT}{Dt} \tag{50}$$

Substituting the continuity condition $\frac{1}{\rho}\frac{D\rho}{Dt} = -\nabla\cdot\mathbf{v}$ and the equation (48) in (50), it follows:

[24] Moisture is considered by using the virtual temperature (see following lines)

$$\frac{1}{p}\frac{Dp}{Dt} = -\nabla \cdot \mathbf{v} + \frac{\dot{\mathsf{Q}}}{\mathsf{c_p}T} + \frac{1}{c_p \rho T}\frac{D\rho}{Dt} \tag{51}$$

Fixing $\gamma = c_p/c_v$(where γ is the adiabatic index and c_v the specific heat at constant volume), brings to:

$$\frac{Dp}{Dt} = -\gamma\rho\nabla \cdot \mathbf{v} + \frac{\gamma\rho\dot{\mathsf{Q}}}{\mathsf{c_p}\mathsf{T}} \tag{52}$$

and the pressure equation can be written as:

$$\frac{\partial p'}{\partial t} - p_0 g w + \gamma p \nabla \cdot \mathbf{v} = -\mathbf{v} \cdot \nabla p' + \frac{\gamma p}{T}\frac{\dot{Q}}{c_p} \tag{53}$$

The pressure increase due to heating which forces the air to expand is neglected in the model in both thermodynamic and pressure equation.

An MM5 model treats the equations in terrain following sigma coordinates (see paragraph 5.1.2) finite differenced on the dominion grid and resolve them applying, for each point, a leapfrog algorithm. In the leapfrog scheme, the variables values at time n are used to step the variables from time $n-1$ to $n+1$. However, for certain terms, the model time step is too long for stability: these terms have to be calculated with a shorter time step, therefore the algorithm resolves "fast" terms (pressure gradients, divergence terms, u, v, w, p') by updating more frequently these variables when the time step is split. A schematic representation of the leapfrog scheme is provided in appendix B.

Note that the particle size isn't treated in the MM5 calculations. This is the reason of the statistical study of the AERONET aerosol size distribution in par. 3.3. For the run of the radiative transfer code a value for the cloud drop radius must be associated with each condensed atmospheric for determining the corresponding optical properties. Such a parameter is undetermined by the output of the meteorological simulation.

5.1.7 Using MM5

Since MM5 produces a regional model, it requires initial as well as boundary conditions (i.e. topography). Gridded data are needed to cover the entire time period for providing boundary conditions for a model run. As introduced in paragraph 5.1.1, MM5 performs a post-analysis to obtain a "downscaling" of the data (from low-resolution gridded data and station measured atmospheric profiles) for characterizing the atmosphere around the irradiance sensors. The changes needed for customizing the code are described in appendix C.

Terrestrial and isobaric meteorological data are horizontally interpolated from a latitude-longitude mesh to a custom high-resolution domain. Meteorological data for setting the boundary and initial conditions are downloaded from NOMADS servers [41] and interpolated on the horizontal grid and, since the interpolation does not provide mesoscale details, they may be augmented with station data (ground measured data and vertical profiles by atmospheric sounding). This technique (objective analysis) uses a standard algorithm (Cressman scheme: see appendix C) for calculating a new grid corrected with the station data. Together with this interpolation, a vertical interpolation from pressure levels to the sigma coordinate system of MM5 is also performed. As explained

in paragraph 5.1.2, sigma surfaces near the ground closely follow the terrain, and the higher-level sigma surfaces tend to approximate isobaric surfaces.

5.1.8 The MM5 final output

The final output of MM5 is a four-dimensional data file containing, for each time step (for the purposes of this thesis the time step has been set to $1h$), the values of the atmospheric profiles of pressure, temperature, mixing ratio and cloud constituents plus grid-referred data. This file uses a sigma-coordinates system that needs to be converted to pressure levels from the ground to the upper level. Finally, the tool **MM5toGrADS** converts the MM5 file in pressure-level vertical coordinates in a GrADS-compatible format, to be open and read with the software package GrADS (described in paragraph 5.3). GrADS software is used by the `LAUNCH_GRADS` procedure (see A.2) to access the MM5 data.

5.2 Validation analysis of the MM5 simulations

5.2.1 Why a validation analysis is needed

The initial aim of this thesis was to develop a tool for providing ground irradiance map in a cloudy atmosphere, and the use of the MM5 model for providing the structure of a realistic (three-dimensional) atmosphere was planned as a prediction tool. Although the possibility of using a meteorological prediction (i.e. a forecast) is not precluded in the final structure of the work (on the contrary, it is indeed an attractive possibility for a future development of the research), the thesis, in its actual form, develops, together with the problems dealing with the traditional plane parallel modeling of the atmosphere, the "composite atmosphere" approach that takes into account different profiles of an atmospheric grid (although the composite atmosphere is still plane parallel), in opposition to the traditional "vertical-column only" model that characterizes the atmospheric plane parallel layers using a punctual profile of the datacube.

The differences between the two approaches are given, in practice, by the presence of condensed layers in some profiles of the input grid (i.e. zones with cloud layers) on the line of sight of the Sun, thus the composite profile depends by the atmospheric three-dimensional grid as well as by the Sun-observer relative position at fixed time. Other atmospheric characteristics, i.e. the pressure, the temperature or the relative humidity profiles (when uncondensed) have little or no impact on wavelength integrated quantities and direct - diffuse radiation ratio (although they have a strong impact on the spectral lines). Nevertheless, in the following paragraphs, the ground measured dewpoint and temperature profiles (from atmospheric soundings) are compared with the corresponding profiles determined by MM5 using objective analysis (i.e. soundings from different stations are used as "control point" for the MM5 run) and the differences are discussed. In fact, this comparison verifies that the models predicts correctly the global structure (that is, both cloud fraction and altitude of the cloud layers). A comparison between the direct and diffuse components of the ground irradiance (calculated by the UVSPEC radiative transfer model) is also presented for examining the atmosphere model consistency with respect to the soundings measured in different stations.

A further remark relates to the use of nesting (see par. 5.1.5) in the MM5 simulations: although only one way nested simulations have been used in this

work, the possibility of running a nested domain is an interesting possibility for the future development of the model. Nesting would provide a forecast with high spatial resolution around the locality of interest taking advantage of physically consistent and high temporal frequency boundary conditions from the mother domain.

5.2.2 Atmospheric structure influence in irradiance calculation

As described in paragraph 2.3, the output produced by the atmospheric model provides the structure for the atmosphere, thus the consistency of the MM5 data needs to be verified. Considering a point on the surface, the satellite measurement depends on the entire atmospheric profile. This is a fundamental point for a correct understanding of the radiative transfer in the atmosphere. For this reason the composite atmosphere model has been set up: in this way, a realistic model of the atmosphere can be used for simulating the measured radiation.

For verifying the data consistency a dataset of three winter days has been chosen: days 17-19 January 2008. The mid-winter time ensures the absence of fast convective phenomena (typical of midlatitude summer conditions), thus it legitimates the use of a time step of $1h$ for the MM5 simulation output data (a compromise between the need of a reasonable computation time length and a time resolution comparable with the MSG satellite data). Furthermore, days 17-19 January 2008 are intended to be representative of the atmospheric conditions in both cloudy and cloudless conditions. Winter is a typical difficult case. During the selected days, all stations were available, the dataset overlapped a period of measurements, and there were no unusually difficult phenomena to treat during this period nor large frontal systems (see the weather map in fig. 32). Further details about the choice of the dataset are given in par. 5.2.4.

We consider at this point the relation between the observed data (satellite and ground measured) and the atmospheric structure: the atmospheric model from MM5 is used as input for the radiative transfer model for simulating the observed ground irradiance or the satellite observed radiance. The satellite response is *simulated* using the model composite atmosphere described in paragraph 2.7 and, if the simulation is verified by comparison with ground data, the relation between the atmospheric structure and the measured data is established.

The simulation of the downwelling irradiance is considered here for comparison with the ground measured data. For a realistic simulation, both direct and diffuse components of ground irradiance (introduced in paragraph 2.4.3) need to be determined. The simulation has been performed with the radiative transfer model by postulating a homogeneous plane parallel atmosphere, whose layers corresponding to the composite atmosphere. For direct irradiance determination, only the vertical optical depth is necessary. The complete structure has been considered for calculating the irradiance angular distribution in the point of interest, that is the diffuse contribution. For this reason the total (direct plus diffuse) contribution needs the predicted altitude of the cloud layers.

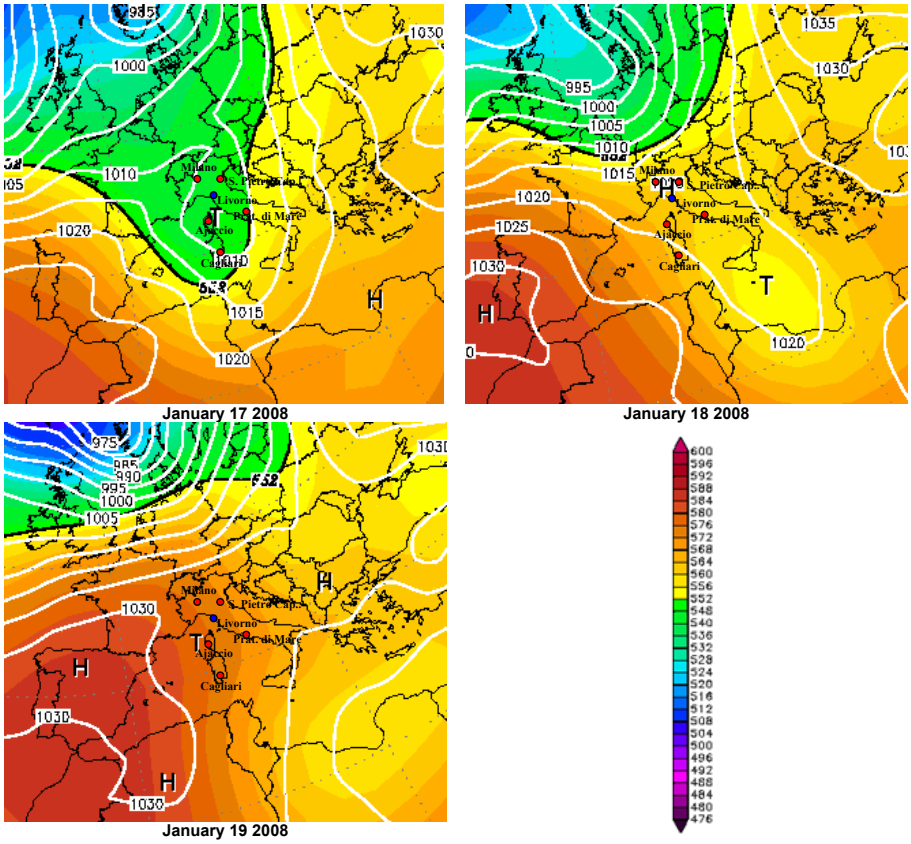

Figure 32: Map of the atmospheric pressure at ground (isobaric lines) and at 500 hPa geopotential height, i.e. approximately at 5520 m above sea level, (in colors, values in the legend in hPa) at 00:00 UTC for the winter dataset, days 17-19 January 2008. The positions of the stations used for the validation analysis (Cagliari, Milano, Ajaccio, Pratica di Mare, S. Pietro Capofiume) and of the measurement site in Livorno are indicated by red and blue circles. The dataset of days 17-19 January 2008 has been chosen for the absence of large frontal systems and fast convective phenomena. Data from www.wetterzentrale.de.

5.2.3 Atmospheric structure influence on the satellite image

The visible channel of the Meteosat Second Generation satellite (described in paragraph 6.2) allows the monitoring of the cloud cover on the point of interest with a time resolution of 15 minutes. The observed spatial structure of cloud cover depends on the vertical structure of the atmosphere at each point.

The MM5 simulation grid is three-dimensional and different pixels are used to determine the composite atmosphere profile. The sensitivity of the radiative transfer calculation model to the structure of the employed atmosphere must be investigated.

Different structures of the atmosphere produce different remote sensing images. As an example, let's consider the optical depth τ (eq. (9)) measured along the line of sight from the Sun to an observer at ground. Fixing the vertical optical depth τ_v in cloud cover conditions, the change of $\tau = \tau(SZA)$ as a function of the solar zenith angle SZA depends on the structure of the atmosphere. In a homogeneous atmosphere $\tau = \tau_v / cos(SZA)$ and, for $SZA \to 90^\circ$ $\tau \to \infty$. This trend is not simply described by trigonometric functions if the structure along the line of sight of the Sun is, for example, fractal. In the latter case the optical depth τ could reduce, because, at any scaling factor, there is always a non-zero probability for a beam to pass through "empty space" in the cloud structure along the line of sight (except for $SZA = 90^\circ$).

The optical depth τ estimated by satellite images can correspond , depending on atmosphere structure at the point of interest, to different values of the optical depth in the line of sight of the Sun measured by an observer at ground, bringing to completely different values of the estimated ground irradiance.

5.2.4 Dewpoint and temperature diagrams: sensitivity test

The dewpoint temperature T_d is the temperature to which air must be cooled at constant pressure to reach saturation. Thus dewpoint temperature is a measure of atmospheric relative humidity.

When the temperature T of air reaches T_d, we have the condensation of water drops and the creation of the cloud. The estimate of T and T_d reveals the existence of a condensed layer, thus the presence of clouds (ice clouds if the temperature is lower than the condensation point).

As said in paragraph 5.1.7, since the interpolation does not provide mesoscale details, the initial conditions may be combined with station data, by using the objective analysis (for further details about the setting used in the simulation see appendix C). The stations have been chosen around the measurement site in Livorno (lat. 43.51° N, lon. 10.32° E), as shown in the image of fig. 33.

As a verification of the atmospheric model, for the diagrams in figures 34-43, the same simulation has been performed using soundings from different stations and verifying the temperature and the dewpoint temperature profiles in two stations. Data have been downloaded from University of Wyoming: http://weather.uwyo.edu/upperair/sounding.html.

The points used for verification are the station in:

- Cagliari (latitude 39,22° N, longitude 9.05° E),
- Milano (latitude 45.43° N, longitude 9.27° E).

The station measured input data used for objective analysis in the atmospheric models are from stations:

- Ajaccio (latitude 41.92° N, longitude 8.80° E),
- Pratica di Mare, Roma (latitude 41.65° N, longitude 12.45° E),
- S. Pietro Capofiume, Bologna (latitude 44.65° N, longitude 11.61° E).

The test was performed by comparing the simulated profiles with the measured ones in days 17-19 January 2008, using different groups of ground station soundings for objective analysis.

The MM5 model was able to qualitatively reproduce the temperature profiles (as in diagrams for Cagliari at 18/01/2008 00:00 UTC time) but there are some discrepancies. In some comparisons (as in the profiles of the 19/01/2008 00:00 UTC for Milano, the disagreement of the data is due to sampling resolution of the sounding. In other cases (as in the diagrams of Cagliari for the sounding performed in the day 20/01/2008 at 00:00 UTC) the general trend is correctly reproduced, but the measured and simulated structure are quantitatively different. We note that none of these structures produce condensation (temperature is far away from dewpoint temperature) and, at lower levels, the trend is well reproduced.

For determining how well the atmosphere is reproduced by MM5 and for verifying that the models predict correctly the global structure (that is, both cloud fraction and altitude of the cloud layers) the comparison between the output of the radiative transfer model has been performed. A list of the main parameters used for the MM5 simulations are summarized in tab. 3).

Tables 4 and 5 give the result for simulated ground irradiance using a composite atmosphere from the 12:00 UTC of each day and using each set of simulations fixing the cloud drop radius (respectively) at 10 and $20\,nm$. The tables contain the value of direct, diffuse and total ground irradiance and, in the three columns on the right, the ratio (%) with the result using the MM5 run processed without objective analysis (that is using only the global model initial condition and no soundings, the so-called *control run*).

The maximum difference is found for day 18/01/2008 ($\sim 30\%$, without considering conditions of saturation in which the direct contribution is totally extinct), because the temperature and dewpoint temperature curves are close and, increasing the information about the state of atmosphere (by adding soundings with objective analysis), temperature and dewpoint curves can be found overlapping (condensation occurs when $T \leq T_d$) bringing to different vertical cloud profiles (i.e. different vertical optical depth) for runs obtained using different soundings. Other differences are in the range of few percent, confirming that the control run alone is in almost all the cases sufficient for a correct description of the atmospheric structure.

Some remarks must be given about the choice of the dataset for this validation analysis. The dataset shows the presence of clouds at different altitude (i.e. compare figure 34, charts of days 17 and 18 at 12:00), allowing different distributions of the cloud profiles along the atmospheric column. Moreover, such a comparison uses pressure vs. temperature curves different with respect to a standard atmosphere, allowing both pointing out the differences between MM5 profiles and measured data, and evaluating the results with respect to a real (not only realistic, that is *standard*) cloudy atmosphere.

MM5 run parameters	Parameter values
Grid spatial resolution	$5\,km$ grid centered on coordinates 43.50°N, 10.32°E (Livorno, position of the ground sensors)
NOMADS grid resolution	10 minutes of arc (approximately 18.5 km)
Temporal resolution of output data	$1\,h$
Grid projection type	Mercator projection
Dominion type	One way nested

Table 3: Summary of the MM5 run parameters. The same parameters have been used for the simulations in sec. 7. Further details about the simulations are described in appendix C.

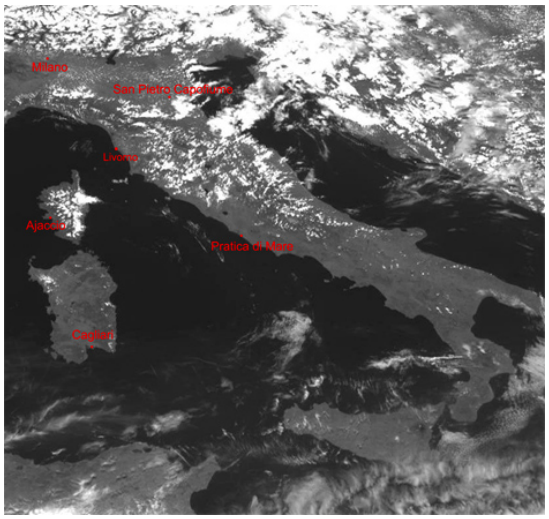

Figure 33: Position of the stations used for the MM5 objective analysis on the Meteosat Second Generation image for May 1 2008 12:00: Cagliari (lat. 39,22° N, lon. 9.05° E), Milano (lat. 45.43° N, lon. 9.27° E), Ajaccio (lat. 41.92° N, lon. 8.80° E), Pratica di Mare, Roma (lat. 41.65° N, lon. 12.45° E), S. Pietro Capofiume, Bologna (lat. 44.65° N, lon. 11.61° E). Note that the stations have been chosen around the measurement site in Livorno (lat. 43.51° N, lon. 10.32° E).

5.2.5 Summary of the validation analysis

The complete atmosphere structure needs to be considered for calculating the irradiance angular distribution in the point of interest, that is the diffuse contribution to ground irradiance, thus, for calculating the total ground irradiance (direct plus diffuse contributions), the position of the clouds needs to be known. Being MM5 data the input for our model of composite atmosphere, the con-

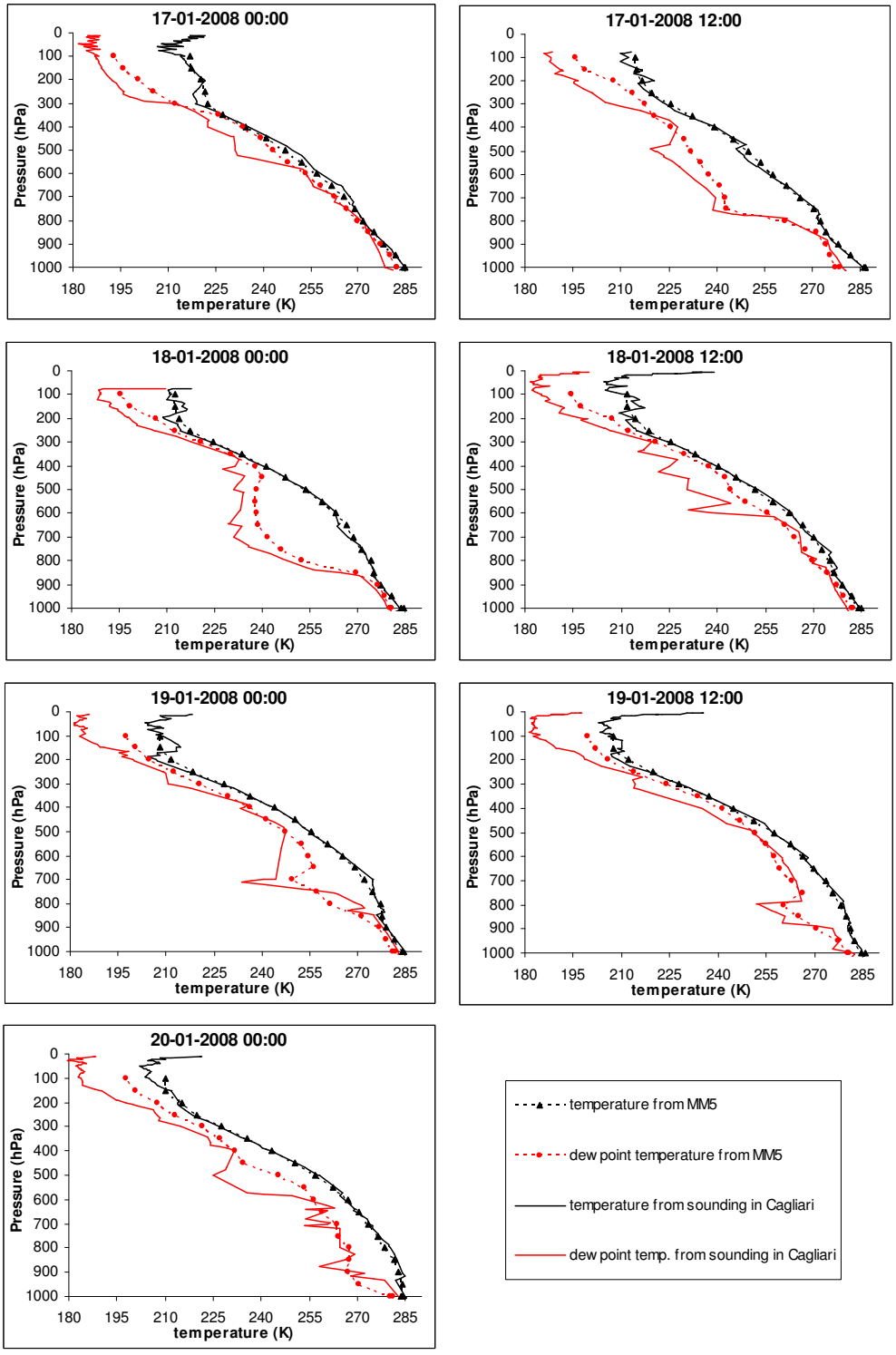

Figure 34: Profiles of temperature and dewpoint temperature in Cagliari (latitude 39.22° N, longitude 9.05° E) from MM5 simulation using sounding from station in Ajaccio (latitude 41.92° N, longitude 8.80° E) and Pratica di Mare (latitude 41.65° N, longitude 12.45° E).

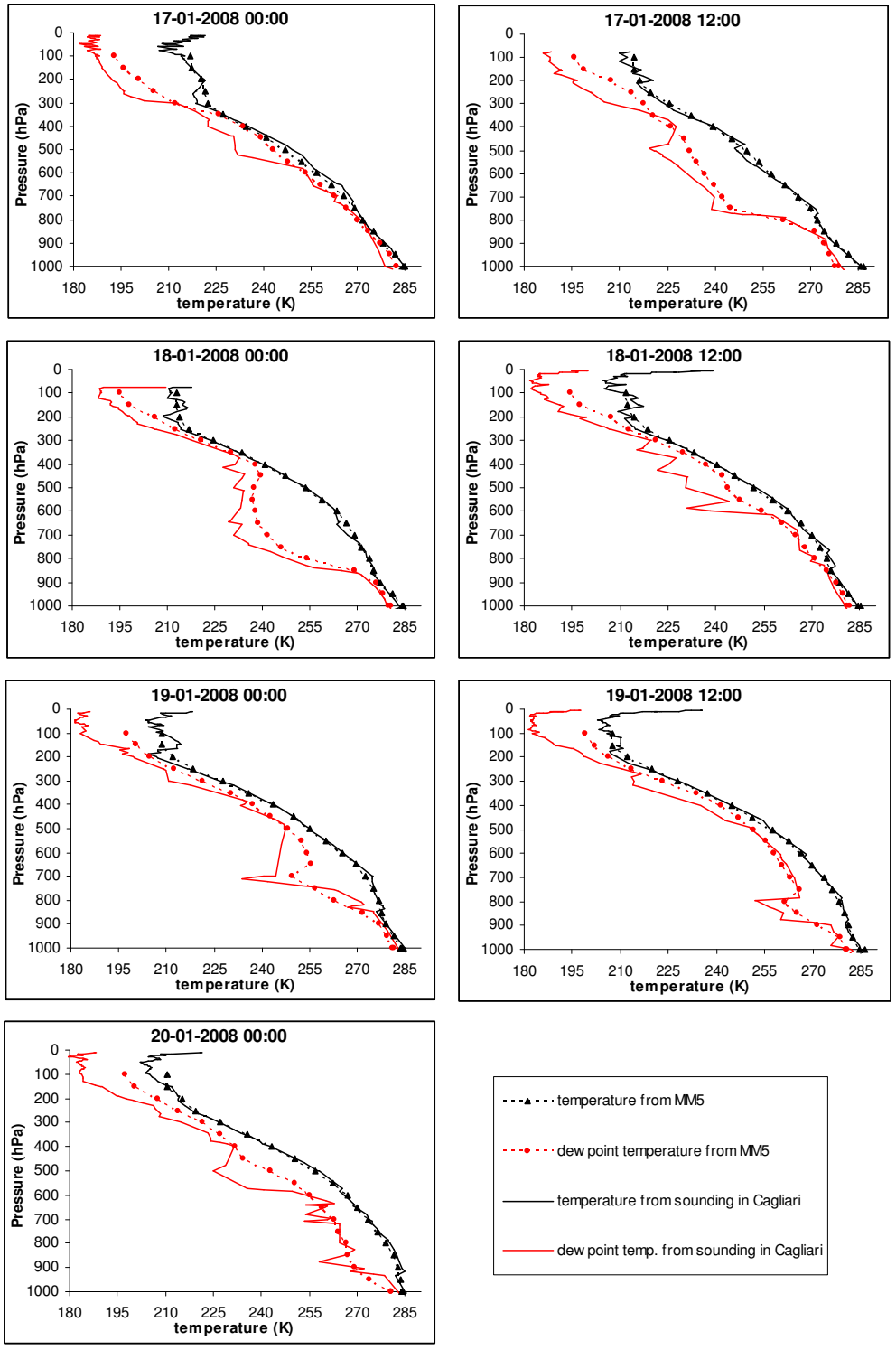

Figure 35: Profiles of temperature and dewpoint temperature in Cagliari (latitude 39.22° N, longitude 9.05° E) from MM5 simulation using sounding from station in Ajaccio (latitude 41.92° N, longitude 8.80° E) and S. Pietro Capofiume (latitude 44.65° N, longitude 11.61° E).

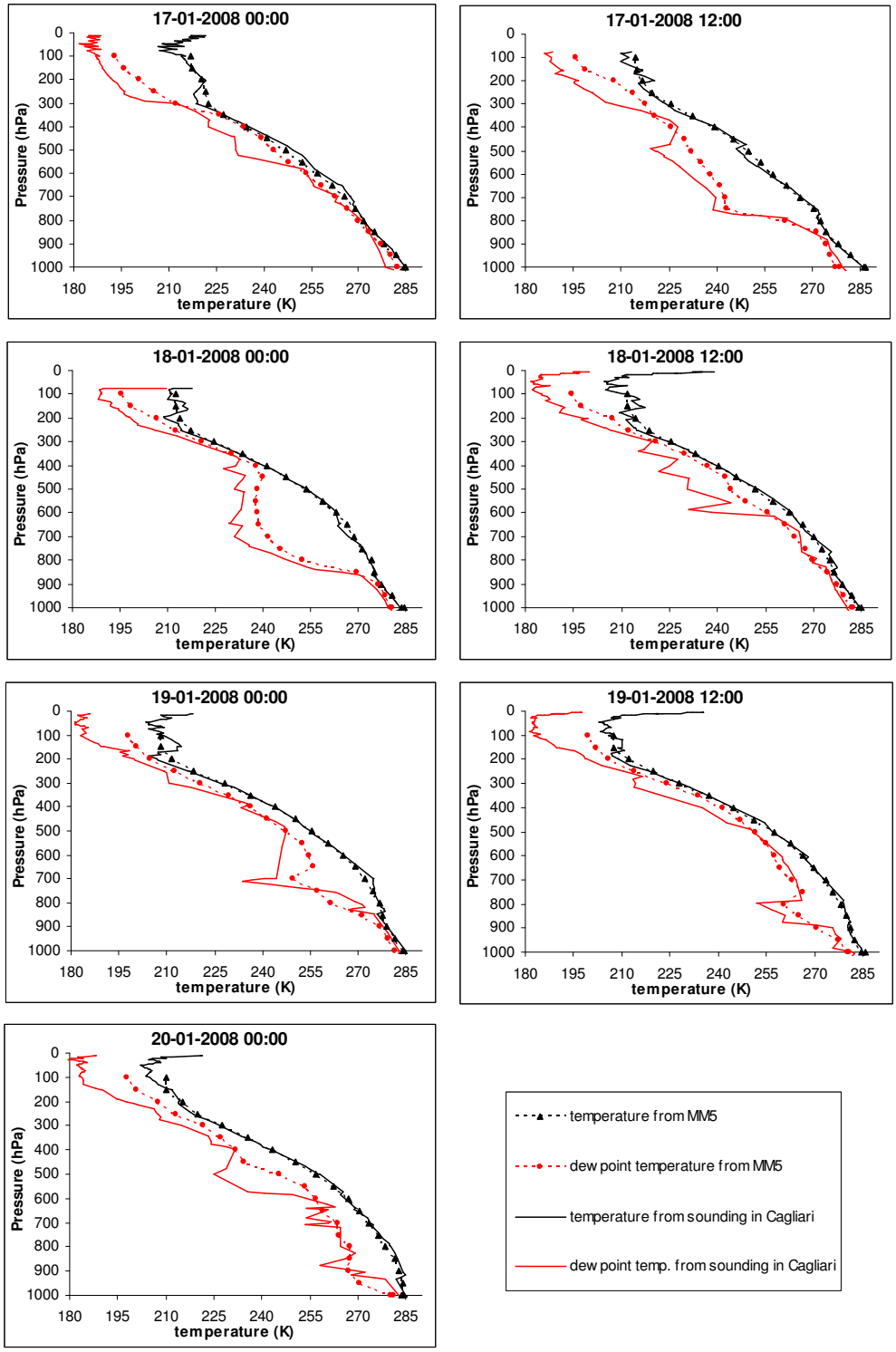

Figure 36: Profiles of temperature and dewpoint temperature in Cagliari (latitude 39.22° N, longitude 9.05° E) from MM5 simulation using sounding from station in S. Pietro Capofiume (latitude 44.65° N, longitude 11.61° E).

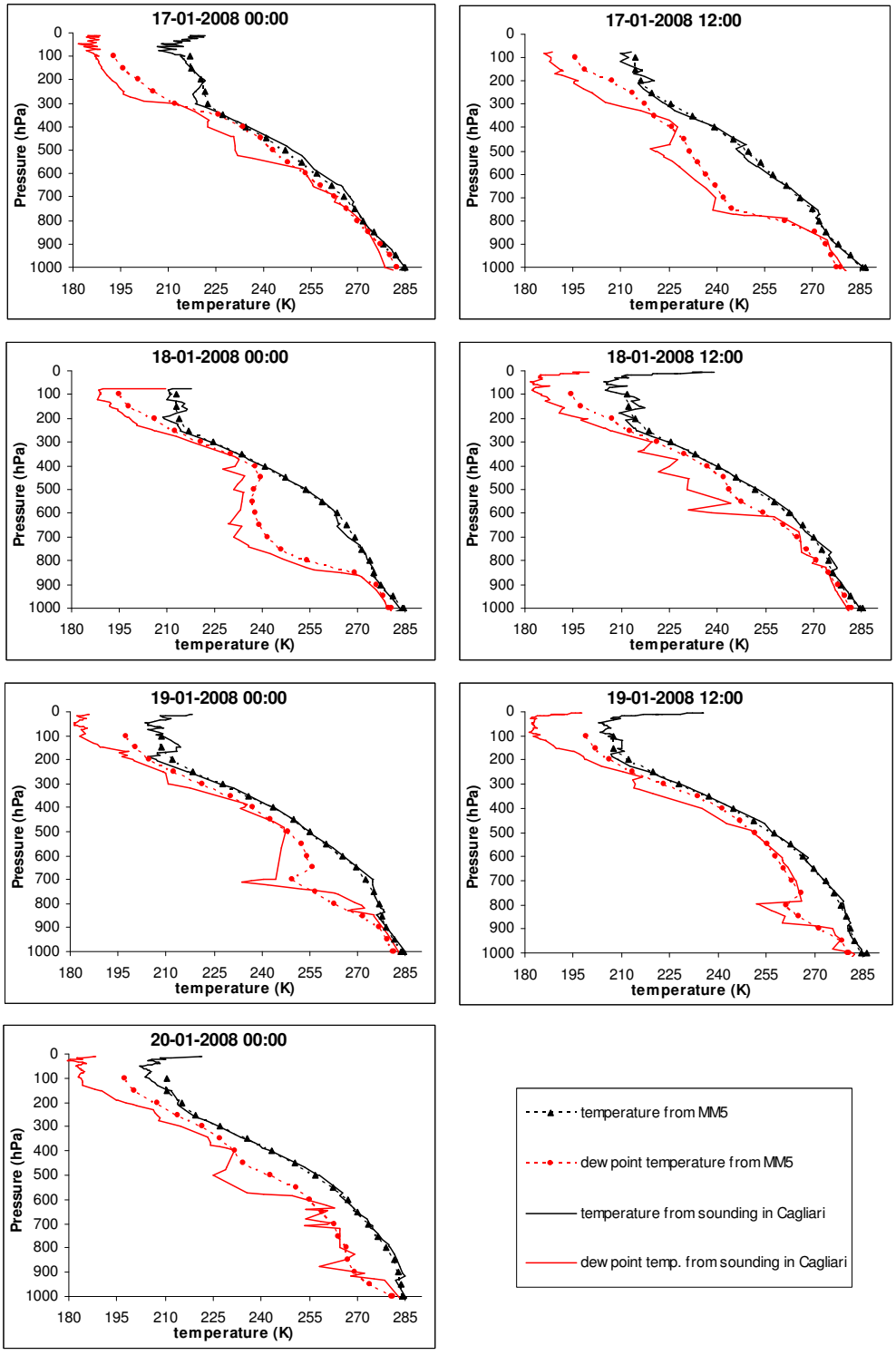

Figure 37: Profiles of temperature and dewpoint temperature in Cagliari (latitude 39.22° N, longitude 9.05° E) from MM5 simulation using sounding from station in S. Pietro Capofiume (latitude 44.65° N, longitude 11.61° E) and Pratica di Mare (latitude 41.65° N, longitude 12.45° E).

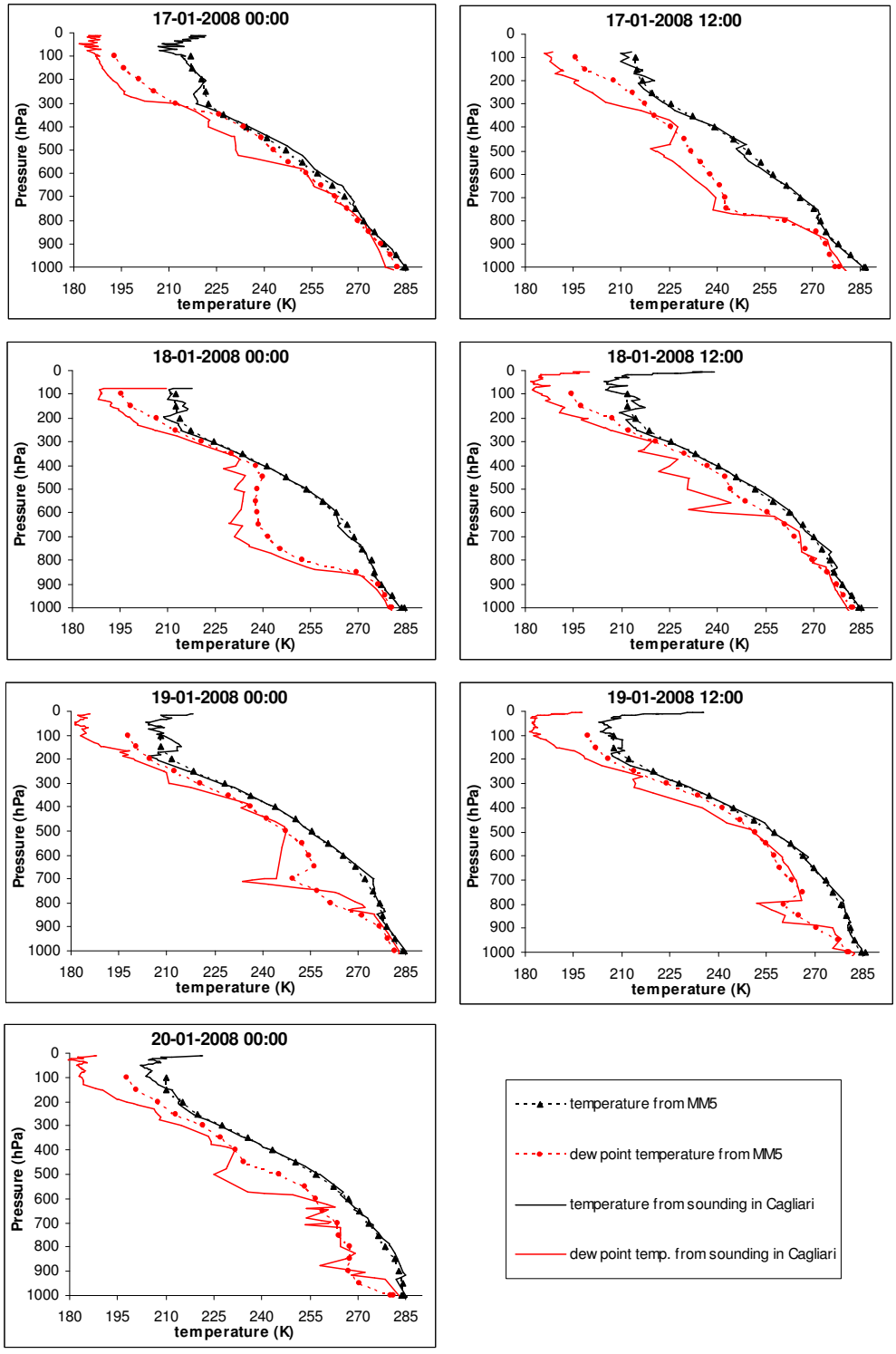

Figure 38: Profiles of temperature and dewpoint temperature in Cagliari (latitude 39.22° N, longitude 9.05° E) from MM5 simulation using control run (no sounding data).

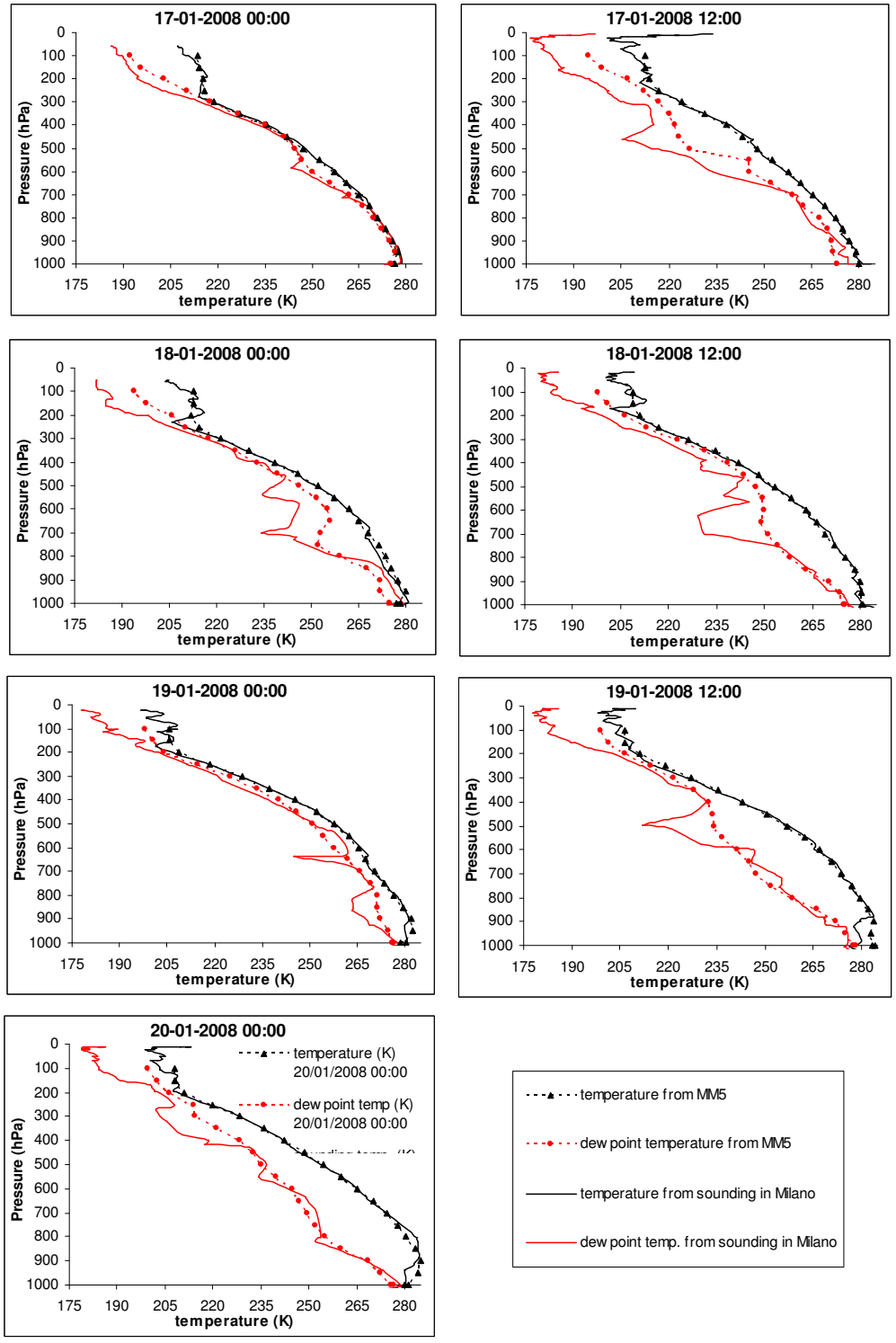

Figure 39: Profiles of temperature and dewpoint temperature in Milano (latitude 45.43° N, longitude 9.27° E) from MM5 simulation using sounding from station in Ajaccio (latitude 41.92° N, longitude 8.80° E) and Pratica di Mare (latitude 41.65° N, longitude 12.45° E).

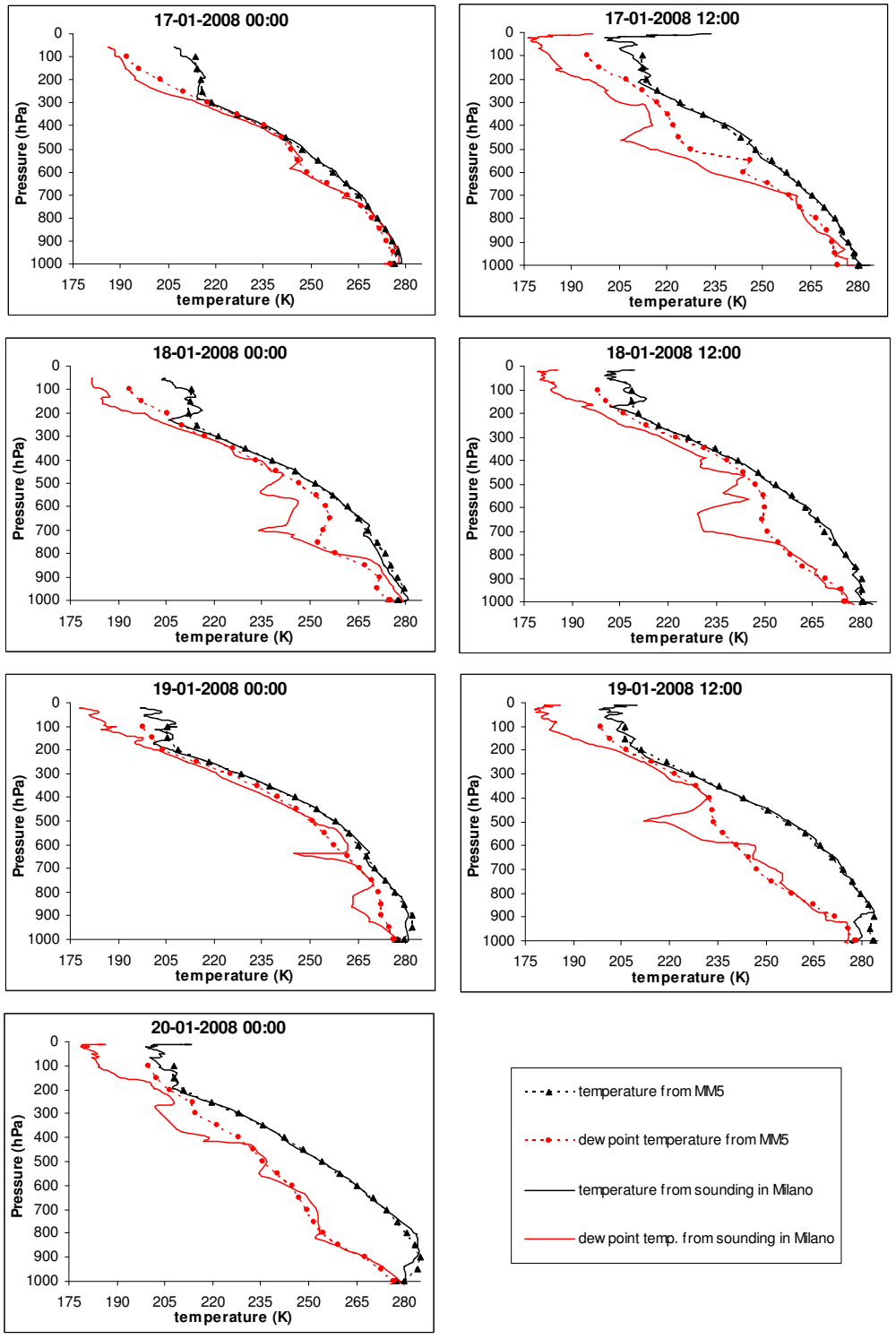

Figure 40: Profiles of temperature and dewpoint temperature in Milano (latitude 45.43° N, longitude 9.27° E) from MM5 simulation using sounding from station in Ajaccio (latitude 41.92° N, longitude 8.80° E) and S. Pietro Capofiume (latitude 44.65° N, longitude 11.61° E).

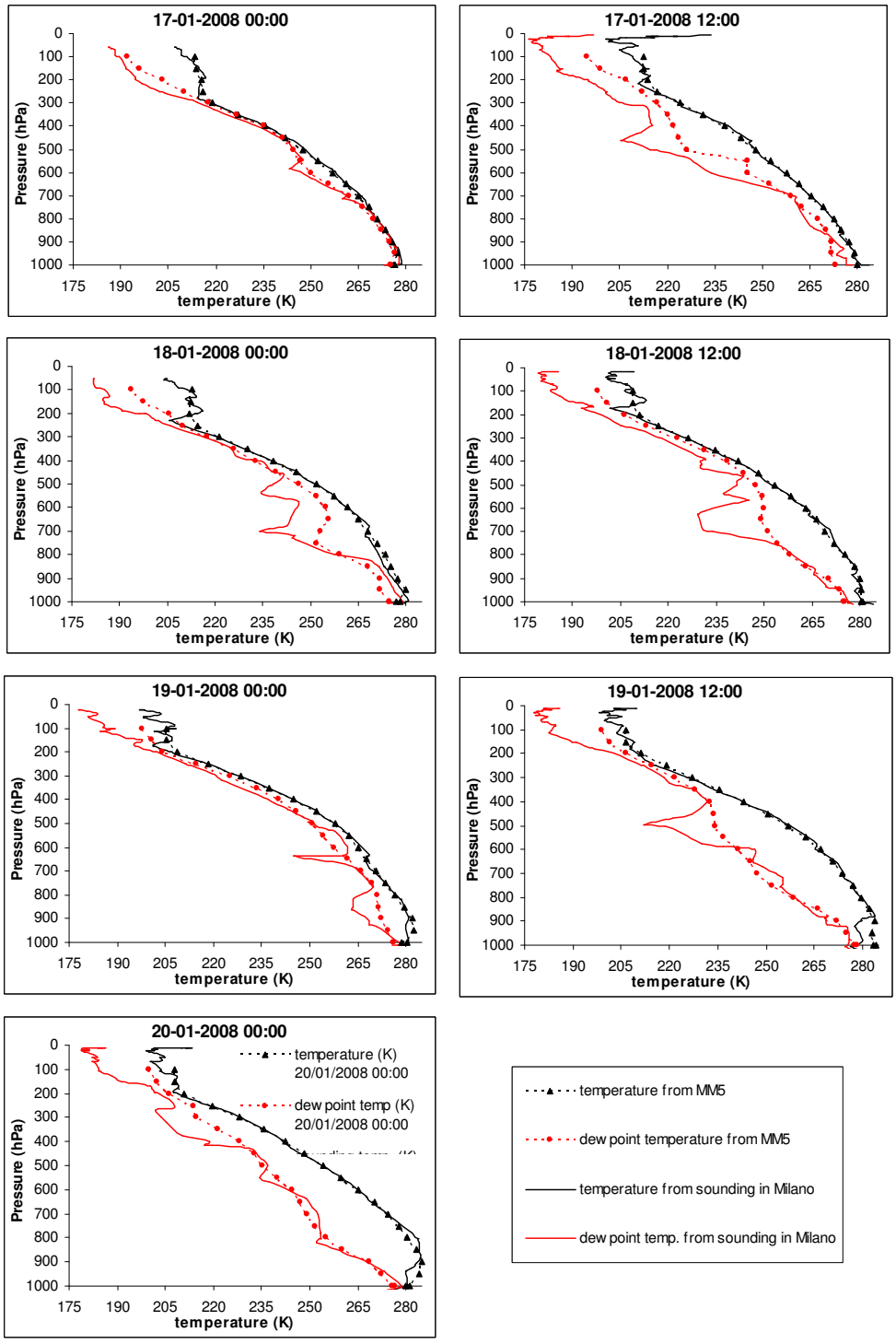

Figure 41: Profiles of temperature and dewpoint temperature in Milano (latitude 45.43° N, longitude 9.27° E) from MM5 simulation using sounding from station in S. Pietro Capofiume (latitude 44.65° N, longitude 11.61° E).

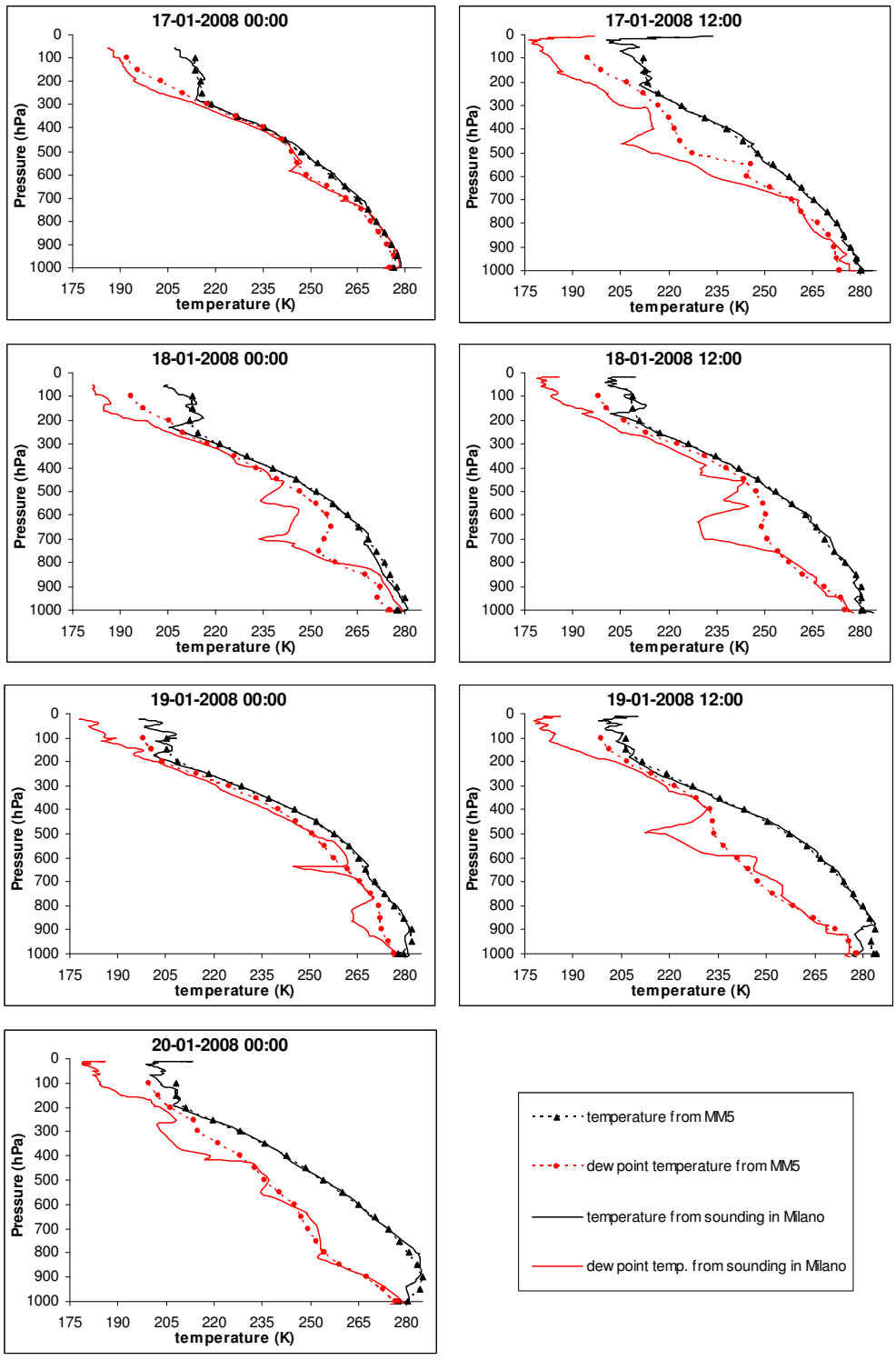

Figure 42: Profiles of temperature and dewpoint temperature in Milano (latitude 45.43° N, longitude 9.27° E) from MM5 simulation using sounding from station in S. Pietro Capofiume (latitude 44.65° N, longitude 11.61° E) and Pratica di Mare (latitude 41.65° N, longitude 12.45° E).

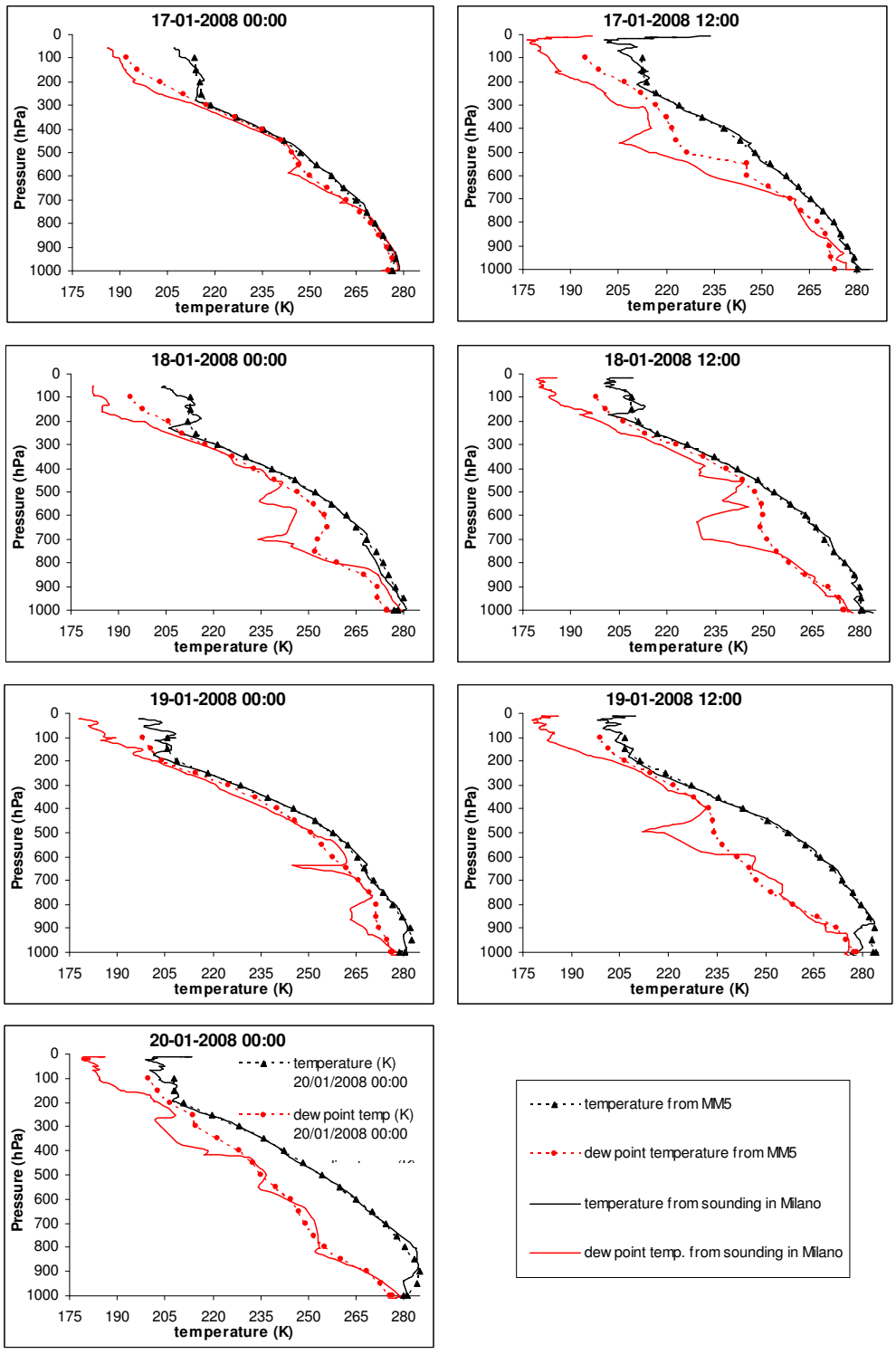

Figure 43: Profiles of temperature and dewpoint temperature in Milano (latitude 45.43° N, longitude 9.27° E) from MM5 simulation using control run (no sounding data).

	Ground irradiance			% run with no sounding		
17/01/2008 12.00	**Dir. irr. (W/m2)**	**Diff. irr. (W/m2)**	**Tot. irrad (W/m2)**	**Direct (%)**	**Diffuse (%)**	**Total (%)**
Cagliari using sounding Ajaccio - S. Pietro Cap.	1.68E-01	1.38E+00	1.55E+00	100	100	100
Cagliari using sounding Prat. di Mare - Ajaccio	1.68E-01	1.38E+00	1.55E+00	100	100	100
Cagliari using sounding S. Pietro Cap.	1.68E-01	1.38E+00	1.55E+00	100	100	100
Cagliari using sounding S. Pietro Cap. - Prat. di Mare	1.68E-01	1.38E+00	1.55E+00	100	100	100
Cagliari no sounding	1.68E-01	1.38E+00	1.55E+00	100	100	100

18/01/2008 12.00	**Dir. irr. (W/m2)**	**Diff. irr. (W/m2)**	**Tot. irrad (W/m2)**	**Direct (%)**	**Diffuse (%)**	**Total (%)**
Cagliari using sounding Ajaccio - S. Pietro Cap.	1.19E-14	8.24E-01	8.24E-01	-	99	99
Cagliari using sounding Prat. di Mare - Ajaccio	1.34E-07	1.09E+00	1.09E+00	-	131	131
Cagliari using sounding S. Pietro Cap.	1.18E-07	1.09E+00	1.09E+00	-	131	131
Cagliari using sounding S. Pietro Cap. - Prat. di Mare	1.28E-07	1.09E+00	1.09E+00	-	131	131
Cagliari no sounding	2.49E-14	8.32E-01	8.32E-01	100	100	100

19/01/2008 12.00	**Dir. irr. (W/m2)**	**Diff. irr. (W/m2)**	**Tot. irrad (W/m2)**	**Direct (%)**	**Diffuse (%)**	**Total (%)**
Cagliari using sounding Ajaccio - S. Pietro Cap.	1.17E-03	9.19E-01	9.20E-01	99	100	100
Cagliari using sounding Prat. di Mare - Ajaccio	8.08E-04	8.91E-01	8.91E-01	69	97	97
Cagliari using sounding S. Pietro Cap.	8.31E-04	8.93E-01	8.93E-01	71	97	97
Cagliari using sounding S. Pietro Cap. - Prat. di Mare	8.10E-04	8.91E-01	8.91E-01	69	97	97
Cagliari no sounding	1.18E-03	9.19E-01	9.21E-01	100	100	100

17/01/2008 12.00	**Dir. irr. (W/m2)**	**Diff. irr. (W/m2)**	**Tot. irrad (W/m2)**	**Direct (%)**	**Diffuse (%)**	**Total (%)**
Milano using sounding Ajaccio - S. Pietro Cap.	4.40E-02	8.90E-01	9.34E-01	99	100	100
Milano using sounding Prat. di Mare - Ajaccio	4.46E-02	8.91E-01	9.35E-01	101	100	100
Milano using sounding S. Pietro Cap.	4.47E-02	8.91E-01	9.36E-01	101	100	100
Milano using sounding S. Pietro Cap. - Prat. di Mare	4.47E-02	8.91E-01	9.35E-01	101	100	100
Milano no sounding	4.43E-02	8.90E-01	9.34E-01	100	100	100

18/01/2008 12.00	**Dir. irr. (W/m2)**	**Diff. irr. (W/m2)**	**Tot. irrad (W/m2)**	**Direct (%)**	**Diffuse (%)**	**Total (%)**
Milano using sounding Ajaccio - S. Pietro Cap.	2.08E-04	5.93E-01	5.93E-01	103	100	100
Milano using sounding Prat. di Mare - Ajaccio	3.75E-04	6.18E-01	6.19E-01	186	105	105
Milano using sounding S. Pietro Cap.	3.79E-04	6.19E-01	6.19E-01	188	105	105
Milano using sounding S. Pietro Cap. - Prat. di Mare	3.76E-04	6.18E-01	6.19E-01	187	105	105
Milano no sounding	2.02E-04	5.91E-01	5.91E-01	100	100	100

19/01/2008 12.00	**Dir. irr. (W/m2)**	**Diff. irr. (W/m2)**	**Tot. irrad (W/m2)**	**Direct (%)**	**Diffuse (%)**	**Total (%)**
Milano using sounding Ajaccio - S. Pietro Cap.	1.56E-02	8.38E-01	8.53E-01	100	100	100
Milano using sounding Prat. di Mare - Ajaccio	1.56E-02	8.37E-01	8.53E-01	100	100	100
Milano using sounding S. Pietro Cap.	1.56E-02	8.37E-01	8.53E-01	100	100	100
Milano using sounding S. Pietro Cap. - Prat. di Mare	1.56E-02	8.37E-01	8.53E-01	100	100	100
Milano no sounding	1.56E-02	8.38E-01	8.53E-01	100	100	100

Table 4: Direct, diffuse, total ground irradiance and their ratio (in %) with respect to the case with no sounding simulated with UVSPEC using the atmospheric profiles of figures 34-43 and 10 μm cloud drop radius.

	Ground irradiance			% run with no sounding		
17/01/2008 12.00	**Dir. irr. (W/m2)**	**Diff. irr. (W/m2)**	**Tot. irrad (W/m2)**	**Direct (%)**	**Diffuse (%)**	**Total (%)**
Cagliari using sounding Ajaccio - S. Pietro Cap.	1.68E-01	1.38E+00	1.55E+00	100	100	100
Cagliari using sounding Prat. di Mare - Ajaccio	1.68E-01	1.38E+00	1.55E+00	100	100	100
Cagliari using sounding S. Pietro Cap.	1.68E-01	1.38E+00	1.55E+00	100	100	100
Cagliari using sounding S. Pietro Cap. - Prat. di Mare	1.68E-01	1.38E+00	1.55E+00	100	100	100
Cagliari no sounding	1.68E-01	1.38E+00	1.55E+00	100	100	100

18/01/2008 12.00	**Dir. irr. (W/m2)**	**Diff. irr. (W/m2)**	**Tot. irrad (W/m2)**	**Direct (%)**	**Diffuse (%)**	**Total (%)**
Cagliari using sounding Ajaccio - S. Pietro Cap.	6.28E-08	1.10E+00	1.10E+00	-	99	99
Cagliari using sounding Prat. di Mare - Ajaccio	1.77E-04	1.30E+00	1.30E+00	-	117	117
Cagliari using sounding S. Pietro Cap.	1.66E-04	1.30E+00	1.30E+00	-	117	117
Cagliari using sounding S. Pietro Cap. - Prat. di Mare	1.73E-04	1.30E+00	1.30E+00	-	117	117
Cagliari no sounding	9.00E-08	1.11E+00	1.11E+00	100	100	100

19/01/2008 12.00	**Dir. irr. (W/m2)**	**Diff. irr. (W/m2)**	**Tot. irrad (W/m2)**	**Direct (%)**	**Diffuse (%)**	**Total (%)**
Cagliari using sounding Ajaccio - S. Pietro Cap.	1.50E-02	1.17E+00	1.18E+00	100	100	100
Cagliari using sounding Prat. di Mare - Ajaccio	1.25E-02	1.14E+00	1.16E+00	83	98	98
Cagliari using sounding S. Pietro Cap.	1.27E-02	1.15E+00	1.16E+00	84	98	98
Cagliari using sounding S. Pietro Cap. - Prat. di Mare	1.25E-02	1.14E+00	1.16E+00	83	98	98
Cagliari no sounding	1.51E-02	1.17E+00	1.18E+00	100	100	100

17/01/2008 12.00	**Dir. irr. (W/m2)**	**Diff. irr. (W/m2)**	**Tot. irrad (W/m2)**	**Direct (%)**	**Diffuse (%)**	**Total (%)**
Milano using sounding Ajaccio - S. Pietro Cap.	4.92E-02	8.97E-01	9.46E-01	100	100	100
Milano using sounding Prat. di Mare - Ajaccio	4.95E-02	8.98E-01	9.47E-01	100	100	100
Milano using sounding S. Pietro Cap.	4.96E-02	8.98E-01	9.48E-01	100	100	100
Milano using sounding S. Pietro Cap. - Prat. di Mare	4.96E-02	8.98E-01	9.47E-01	101	100	100
Milano no sounding	4.93E-02	8.97E-01	9.47E-01	100	100	100

18/01/2008 12.00	**Dir. irr. (W/m2)**	**Diff. irr. (W/m2)**	**Tot. irrad (W/m2)**	**Direct (%)**	**Diffuse (%)**	**Total (%)**
Milano using sounding Ajaccio - S. Pietro Cap.	3.64E-03	7.45E-01	7.49E-01	102	100	100
Milano using sounding Prat. di Mare - Ajaccio	4.85E-03	7.62E-01	7.67E-01	136	102	103
Milano using sounding S. Pietro Cap.	4.88E-03	7.63E-01	7.68E-01	136	102	103
Milano using sounding S. Pietro Cap. - Prat. di Mare	4.86E-03	7.63E-01	7.67E-01	136	102	103
Milano no sounding	3.58E-03	7.45E-01	7.48E-01	100	100	100

19/01/2008 12.00	**Dir. irr. (W/m2)**	**Diff. irr. (W/m2)**	**Tot. irrad (W/m2)**	**Direct (%)**	**Diffuse (%)**	**Total (%)**
Milano using sounding Ajaccio - S. Pietro Cap.	3.08E-02	8.86E-01	9.17E-01	100	100	100
Milano using sounding Prat. di Mare - Ajaccio	3.08E-02	8.86E-01	9.17E-01	100	100	100
Milano using sounding S. Pietro Cap.	3.07E-02	8.86E-01	9.16E-01	100	100	100
Milano using sounding S. Pietro Cap. - Prat. di Mare	3.08E-02	8.86E-01	9.17E-01	100	100	100
Milano no sounding	3.08E-02	8.86E-01	9.17E-01	100	100	100

Table 5: Direct, diffuse, total ground irradiance and their ratio (in %) with respect to the case with no sounding simulated with UVSPEC using the atmospheric profiles of figures 34-43 and 20 μm cloud drop radius.

sistency of this data need to be verified by comparison with ground station soundings (i.e. direct measurements of atmosphere profile).

The comparison of MM5 and measured data shows that MM5 model is able in reproducing qualitatively the temperature profiles, although there are discrepancies due to the disagreement. This is due to:

- different sampling resolution of the sounding and the MM5 simulation;
- differences in temperature and dewpoint temperature profiles, that is differences in predicting condensed layers especially if temperature and dewpoint temperature curves overlap;

For low levels, however, the profiles trend calculated by MM5 is well reproduced, also by the control run.

We notice also that a realistic atmosphere (obtained from direct measurements or MM5 data) is basically different from the standard atmosphere. Also, condensation phenomena are not considered by the standard atmosphere, as well as the seasonal (and even daily) temperature and dewpoint profile values distribution.

5.3 The GrADS program

The Grid Analysis and Display System (GrADS) is a public and freely downloadable software (www.iges.org/grads) distributed under the GNU General Public License. GrADS has been developed at the Institute of Global Environment and Society (IGES) and is currently maintained by the Centre for Ocean-Land-Atmosphere Studies (COLA). It is used for accessing and visualizing various gridded data formats. GrADS uses a four dimensions data environment: longitude, latitude, vertical level and time.

In this thesis GrADS is used to access MM5 output data and extract a profile of atmospheric constituents for a selected pixel of the grid (see paragraph 5.1.8). The IDL procedure `LAUNCH_GRADS` (described in paragraph A.2) allows GrADS commands to be executed for extracting, using as input the geographical coordinates of fixed point, the data referred to the corresponding pixel of the grid.

The conversion process for obtaining an MM5 output readable from GrADS (see paragraph 5.1.8) performs a grid adjustment. In the internal MM5 grid (see figure 44), data are referred to a grid pixel in the following way: the scalars (T, q, p', w and atmospheric constituents) are defined at the center of the grid pixel, while the northward (v) and eastward (u) velocity components are collocated at the corners of the pixels. GrADS joins the two grid together.

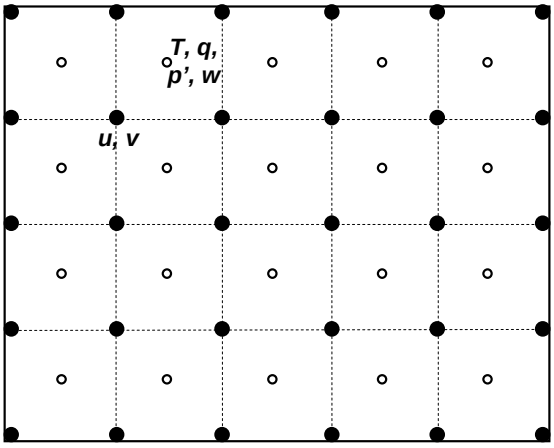

Figure 44: MM5 output data referred to the MM5 grid. The scalars (T, q, p', w and atmospheric constituents) are defined at the center of the grid square (white points), while the horizontal components u, v of velocity components are defined at the corners (black points). GrADS re-arranges all the data in a single grid.

6 Cloud cover estimate from satellite images

6.1 The use of satellite data in this thesis

Satellite data provide high spatial and time resolution images. A satellite measurement of the radiance reflected by the point of interest represents an alternative point of view for the composite atmosphere approach verification. A comparison of satellite observed data with the radiances simulated by the UVSPEC radiative transfer model would offers the possibility of analyzing the differences between the "on the vertical" plane parallel model and the new composite profile approach. The problem of performing a direct comparison with the satellite measured radiance is represented by the need of knowing the characteristics of the ground. Nevertheless, the main parameter of interest is the cloud cover (although the satellite observes a value integrated on the entire atmospheric column) and scientific literature offers a method developed for extracting a cloudiness index from the Meteosat Second generation satellite data. The so-called Heliosat method [14, 39], described in par. 6.4, represents a procedure for extracting (by comparison with historical series of images) a cloud index referred to cloud cover only. Although this method makes strong assumptions (e.g. about the aerosol amount and its angular properties or the temporal variability of the ground albedo), it represents a valid comparison tool.

Although the model is taken from literature, its implementation in IDL language as well as the procedure for the analysis of the time series of Meteosat Second generation images (to be used as flat field for the cloud index map extraction) has been carried out for the purposes of this thesis (par. 6.4-6.5).

6.2 Meteosat Second Generation image data

Meteosat Second Generation (MSG) is a set of four geostationary meteorological satellites that commenced operations in January 2004 and will operate until 2018. The MSG system radiometer, the Spinning Enhanced Visible and InfraRed Imager (SEVIRI), delivers daylight radiance images with a resolution sub-satellite point of 1 and 3 km, plus thermal information. The full disc view allows frequent sampling, every 15 minutes, enabling monitoring of rapidly evolving events.

The SEVIRI instrument acquires the image of the Earth disk from MSG spinning geostationary satellite. The scanning of the Earth disk is obtained by using the satellite spin ($\sim 100\,rpm$) in the East-West direction and, by stepping a flat scan mirror, in the South-North direction, as represented in figure 45.

The instrument generates images of the Earth in 12 spectral channels (or bands). SEVIRI channels are named either "cold" channels (IR3.9, IR6.2, IR7.3, IR8.7, IR9.7, IR10.8, IR12.0, IR13.4: thermal infrared channels) or "solar" ("warm") channels[25] (HRV, VIS0.6, VIS0.8, NIR1.6: reflected solar).

During each satellite rotation, deep space measurements are taken corresponding to zero input radiance for offset determination for each channel. For thermal channels calibration an onboard blackbody is also involved in the calibration process. Data are elaborated by Eumetsat and disseminated to users as Level 1.5 data.

The Level 1.5 data are processed from the Level 1.0 data by correcting all radiometric and geometric effects: the images are geolocated using a standardized projection. The resulting Level 1.5 image consists of Earth-located data in linear relation with the observed radiance. Images of the satellite received radiance are disseminated together with ancillary meteorological data derived from the analysis of all MSG band. Data physical units are obtained by scaling digital numbers into radiance values by applying an appropriate radiometric scale.

The ground resolution of MSG images as Level 1.5 data is shown in table 6: the sampling distance corresponds to 1 km at sub-satellite point (SSP) for High Resolution Visible channel (on a subset of Earth area) and 3 km at SSP for the other bands. Other information about MSG data dissemination chain, file format and image georeferencing steps are given in appendix D.

6.3 Cloud mask data

6.3.1 Cloud detection algorithm description

Together with the radiance data, the Eumetsat Data Dissemination service provides meteorological data products (MPEF) from the SEVIRI bands. In particular, the Cloud Mask meteorological product (CLM) provides a byte mask for classifying clouds, ground and sea pixels of the image. In this thesis CLM data are used to distinguish between cloudy and clear sky pixels of the image.

The MSG cloud detection algorithm is based on the threshold technique for scene classification, i.e. measurements in various bands[26] of a particular scene

[25] "Cold" because, for image acquisition in thermal infrared bands, the instrument must be cooled to avoid contribution due to the thermal emission of the instrument itself. "Solar" because in these bands the source of radiation is the Sun.

[26] Bands IR9.7 and HRV are not used in cloud detection algorithm: HRV channel is excluded

Band name	**Nominal central wavelength (μm)**	**Spectral range (μm)**	**Sample distance (sub-satellite point)**	**Bands**	**Band usage description**
VIS 0.6	0.635	0.56 - 0.71	3 km	Visible and near infrared	Clouds observation
VIS 0.8	0.81	0.74 - 0.88	3 km	Visible and near infrared	clouds observation
IR 1.6	1.64	1.50 - 1.78	3 km	Visible and near infrared	water, ice clouds and snow distinction
IR 3.9	3.92	3.48 - 4.36	3 km	Transmittance window	clouds and fog distinction
WV 6.2	6.25	5.35 - 7.15	3 km	Water vapor	Water vapor measurement
WV 7.3	7.35	6.85 - 7.85	3 km	Water vapor	Water vapor measurement
IR 8.7	8.70	8.30 - 9.10	3 km	Transmittance window	Liquid water and ice clouds distinction
IR 9.7	9.66	9.38 - 9.94	3 km	Ozone	Ozone measurement
IR 10.8	10.8	9.80 - 11.80	3 km	Transmittance window	Cloud and ground temperature measurement
IR 12.0	12.0	11.00 - 13.00	3 km	Transmittance window	Cloud and ground temperature measurement
IR 13.4	13.40	12.40 - 14.40	3 km	Carbon-dioxide	CO2 measurement
HRV	0.75	0.45-1.05	1 km	Visible and near infrared	Clouds observation in high resolution broadband

Table 6: MSG band characteristics and descriptions. From Eumetsat documentation "MSG Level 1.5 Image Data Format Description" [20] (www.eumetsat.int).

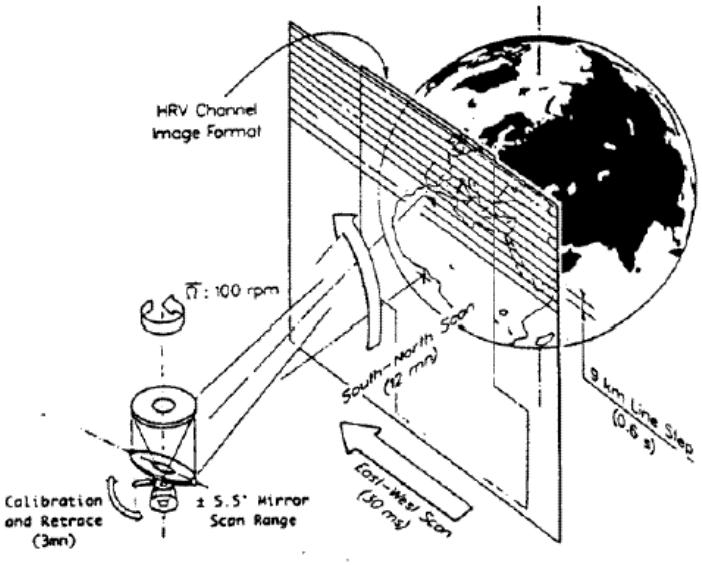

Figure 45: Earth imaging principle used by the SEVIRI instrument (from Eumetsat documentation "MSG Level 1.5 Image Data Format Description" [20], www.eumetsat.int).

are compared with clear sky reference values (from climatological reflectance data or, if present, from cloud free pixels of previous images, details in paragraph 6.3.2). For MSG the following groups of threshold tests have been defined (from Eumetsat documentation [19]):

Group 1: reflectance tests using the solar channels,

Group 2: reflectance difference tests (using all combinations of the solar channels),

Group 3: temperature tests using the IR window channels,

Group 4: temperature difference tests (using all combinations of channels $10.8\mu m$ and $12.0\mu m$ with all other IR/WV channels),

Group 5: standard deviation tests for the window channels on a moving 3 x 3 pixel target,

Group 6: snow and ice test,

Group 7: tests foreseen in future, e.g. dust storm test, volcanic ash cloud test.

6.3.2 Thresholds determination

Threshold tests are based on the following principle:

due to different ground resolution; channel IR9.7 is sensitive to ozone absorption and to the temperature of the surface, thus it provides no further information compared to different IR window channel as e.g. IR10.8.

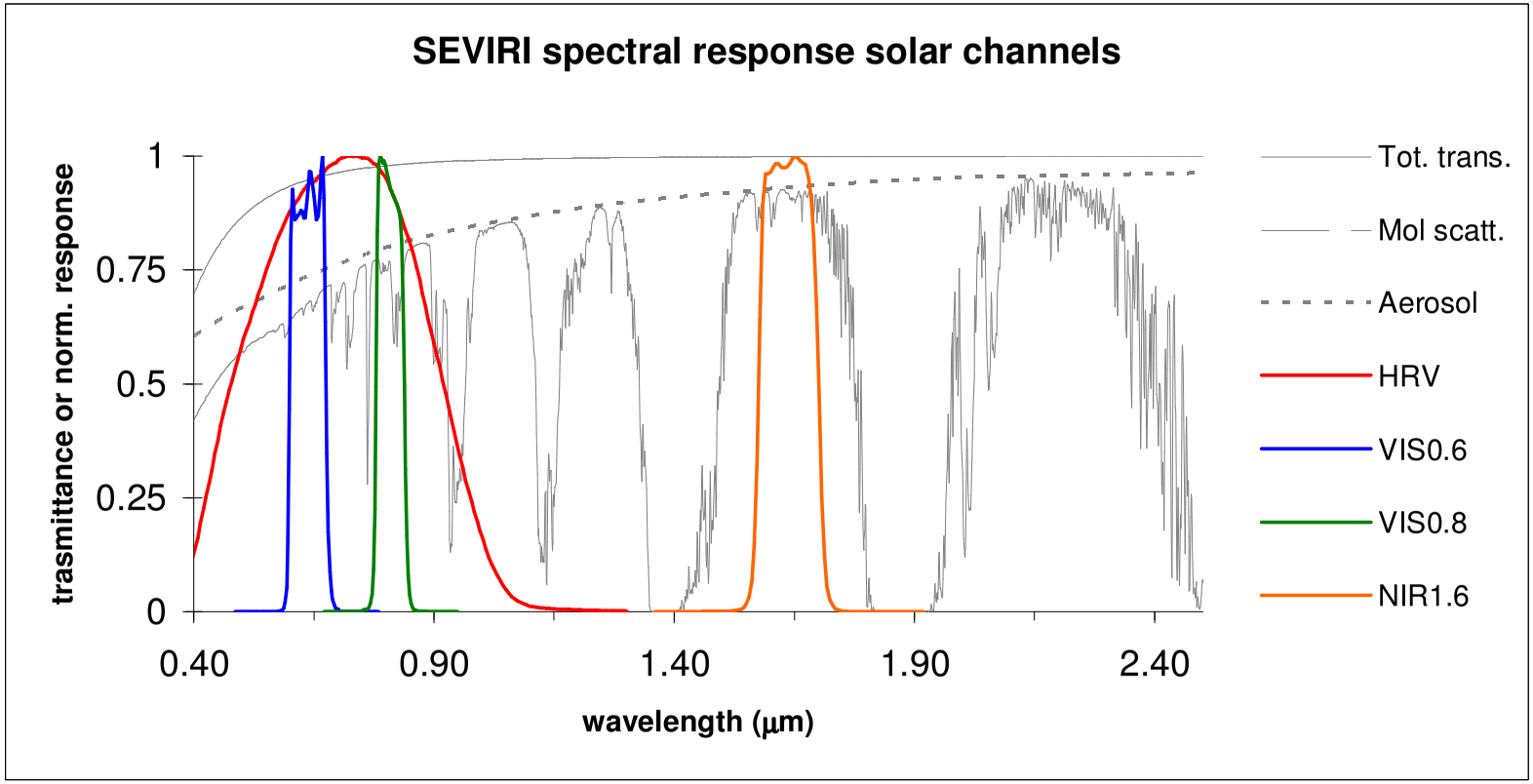

Figure 46: SEVIRI solar channel spectral response, together with atmospheric transmittance spectra. The aerosol, molecular scattering and total transmittance spectra have been generated using MODTRAN data ([3]) with a rural spring-summer aerosol, a mid-latitude summer atmospheric profile, for 20 km of visibility and a relative humidity 70% for a vertical line of sight (data provided by the section "Osservazione del Sistema Terra" of the Applied Physics Institute "Nello Carrara" of Florence, Italy).

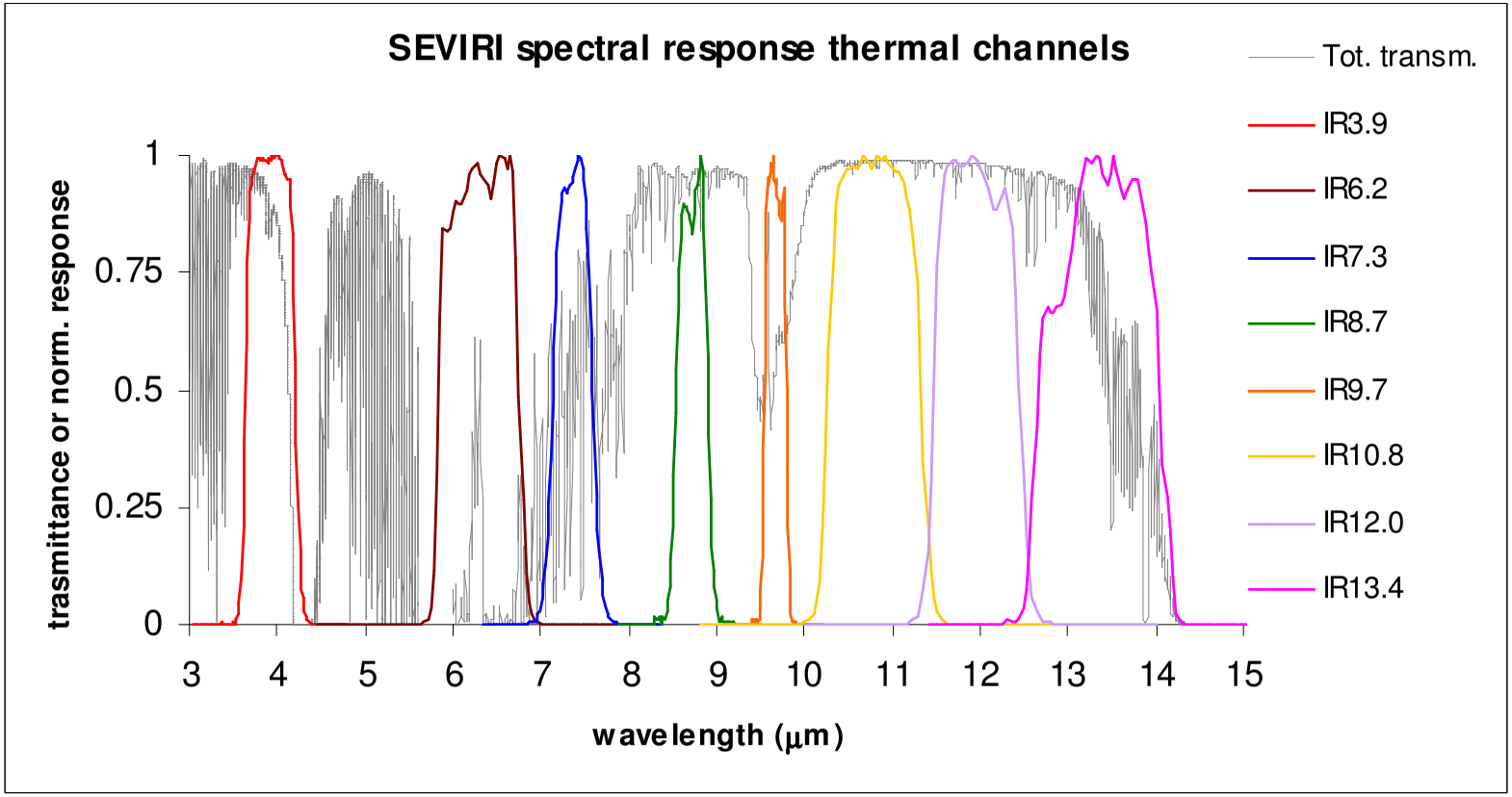

Figure 47: SEVIRI thermal channel spectral response, together with a typical atmospheric transmittance spectrum. MSG data from Eumetsat documentation (www.eumetsat.int). The total transmittance spectrum has been generated considering a standard mid latitude cloudless atmosphere for a vertical line of sight.

- if the measured brightness temperature (determined from observed radiance by the Plank law) in one of SEVIRI's IR window channels is lower than a predefined threshold,

or

- if the measured reflectance (see eq. (14) in paragraph 2.4.3) in one of SEVIRI's visible channels is higher than a predefined threshold,

the pixel is regarded as cloud contaminated. Undetected areas remaining unclassified by these tests could be cold and/or snow covered surfaces misclassified as clouds. The tests applied in the current cloud detection algorithm are listed in table 7.

For the solar channels reflectance tests (Test1A-1C) a climatological reflectance map based on a surface type map is used in addition to clear sky reflectance values extracted from cloud free pixels of mid-day previous images (the clear sky values from the satellite images, if present, replaces the climatological dataset). Threshold are determined from reflectance values $\mathrm{REFL_{ref}}$ for each channel (band) and from channel dependent values (test 1A, 1B and 1C are referred to channels 0.6, 0.8 and 1.6 μm):

$$\begin{aligned} \mathrm{threshold1A\_max} &= \mathrm{REFL_{ref}} + \mathrm{refcld} \\ \mathrm{threshold1A\_min} &= \mathrm{REFL_{ref}} - \mathrm{refclr} \end{aligned} \tag{54}$$

where the refcld and refclr coefficients depend on the channel used. Test 1B and 1C for the other visible (solar) channels use similar equations.

For the reflectance ratio tests in group 2, the maximum and minimum thresholds are determined using constant coefficients:

$$\mathrm{threshold2A} = a + b\,\mathrm{REFL_{channel}} \tag{55}$$

where a, b are different for each test of group 2 and for land/sea conditions, and $\mathrm{REFL_{channel}}$ is the reflectance measured in the reference channel (e.g. 0.6 μm).

For the temperature test (group 3), thresholds are derived by extracting the value for the predicted clear sky temperature T_{PCS} from the average of the neighboring pixel of the previous image. If not enough clear sky pixels are found, clear sky radiance determined near the pixel location and interpolated over the current pixel is converted in the corresponding brightness temperature and used as T_{PCS} (if clear sky pixels are found within a fixed radius around the pixel location). If previous conditions are not satisfied, the value for T_{PCS} is extrapolated from previous images. Two final thresholds are derived for test3C: the first one is used to determine cloud contaminated pixels with high confidence, the second one is used to determine cloud free pixels with high confidence. The thresholds are calculated in the form:

$$\mathrm{threshold3C} = T_{PCS} - d \tag{56}$$

where d is the sum of different correction terms taking into account the presence of non uniform areas (e.g. coastal region, sea/land mixed situation, mountains, snow/ice covered cold surface) and the diurnal temperature cycle (see [19]).

For group 4 tests, the thresholds are determined by using the predicted clear sky brightness temperature of channels IR3.9, WV6.2, WV7.3, IR8.7, IR10.8

Test Id	Test logic	Result
Test1A	R0.6 > threshold1A_max R0.6 < threshold1A_min All other cases	Cloud Clear Unknown
Test1B	R0.8 > threshold1B_max R0.8 < threshold1B_min All other cases	Cloud Clear Unknown
Test1C	R1.6 > threshold1C_max R1.6 < threshold1C_min All other cases	Cloud Clear Unknown
Test2A	R0.8/R0.6 > threshold2A_max1 threshold2A_min2 < R0.8/R0.6 < threshold2A_max2 R0.8/R0.6 < threshold2A_min1 All other cases	Clear land Cloud Clear sea Unknown
Test3C	T10.8 > threshold3C_max T10.8 < threshold3C_min All other cases	Clear Cloud Unknown
Test4A	(T10.8-T3.9) > threshold4A_max1 (T10.8-T3.9) < threshold4A_min1 threshold4A_min2 < (T10.8-T3.9) < threshold4A_max2 All other cases	Cloud Cloud Clear Unknown
Test4B	IF((T10.8-T6.2) < threshold4B_min) All other cases	Cloud Unknown
Test4C	IF((T10.8-T7.3) < threshold4C_min) All other cases	Cloud Unknown

Test4D	(T10.8-T8.7) < threshold4D_min
	For (viewing_angle > threshold4D_angle):
	(T10.8-T8.7) > threshold4D_max1
	For (viewing_angle < threshold4D_angle) and for bare soils :
	(T10.8-T8.7) > threshold4D_max2
	All other cases
		Cloud
		
		Cloud
		
		Clear
		Unknown

Test4F	(T10.8-T13.4) < threshold4F_min All other cases	Cloud Unknown
Test5B	StdDev0.8 > threshold5B All other cases	Cloud Unknown
Test5F	StdDev10.8 > threshold5F All other cases	Cloud Unknown
Snow and ice	R0.6 > ThresholdSnow1) (R0.6-R1.6)/(R0.6+R1.6) > ThresholdSnow2 T10.8 < ThresholdSnow3 T10.8 > ThresholdSnow4 (T10.8-T12.0) < ThresholdSnow5	Snow for land Ice for sea

Table 7: Test applied in cloud detection algorithm for SEVIRI instrument. The symbol Txx represents the brightness temperature in the channel (band) xx; The symbol Rxx represents the reflectance in the channel xx. From Eumetsat documentation "Cloud Detection for MSG - Algorithm Theoretical Basis Document" [19], www.eumetsat.int.

and IR13.4 and coefficients depending on different day/night, land/sea conditions, geometrical conditions and surface type using equations of the form:

$$\text{threshold4} = e + f\,T_{PCS_1} + g\,T_{PCS_2} \tag{57}$$

where T_{PCS1} is the predicted clear sky temperature of channels $10.8\,\mu m$, T_{PCS2} the predicted clear sky temperature of the other IR channels and e, f, g fixed coefficients different for each test of group 4 and for day/night and land/sea conditions.

For tests of Group 5 and 6 (standard deviation tests), thresholds based on fixed coefficients are applied, depending on the pixel location (land/sea) and (only for group 5) time.

6.3.3 Use of cloud mask data in this thesis

In the following paragraphs CLM data will be used for selecting cloudless pixels in a time series of MSG images for generating average clear sky albedo maps to be used as a flat-field for cloudiness determination. A CLM is shown as an example in figure 48.

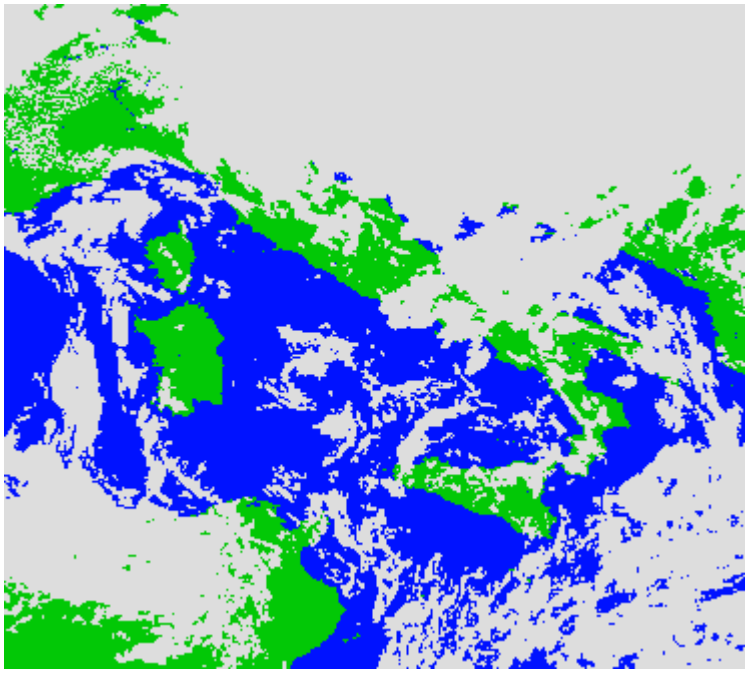

Figure 48: Cloud mask portion from Meteosat Second Generation MPEF CLM for the day January 19, 2008 12:00 UTC. Colors correspond to different values $(0-3)$ of the mask: blue (0): cloud free sea pixels, green (1): cloud free ground pixels, grey (2): cloud covered pixels, black (3, not shown in figure): pixels external to Earth image.

6.4 Cloudiness from satellite image: the cloud index

The HRV Meteosat Second Generation image determines the radiance observed by the satellite for each pixel in the high resolution visible band. Received radiance depends on the radiation entering in the solid angle corresponding to each pixel of the image and is a function of ground reflection (considered Lambertian), scattering by air molecules (Rayleigh scattering, see paragraph 2.4.3, depending on viewing geometry) and scattering by aerosols (including clouds). Thus, for cloud cover characterization, a parameter is needed: the cloud index n, independent by the ground and by the geometry of the observation. The cloud index quantifies the reflective properties of the cloud cover and it is calculated from the apparent albedo of the image. The following procedure for cloud index calculation has been implemented in IDL for processing the HRV channel of MSG for the purposes of this thesis.

Following the definition of albedo (14), the apparent albedo of the satellite image (considered as a Lambertian plane) is[27]:

$$\rho = \frac{\pi L_{band}}{\epsilon \, E_{0\,band} \, cosSZA} \tag{58}$$

where L_{band} is the radiance in the band of interest, $E_{0\,band}$ the extraterrestrial solar irradiance at the mean Sun-Earth distance normal to Sun direction, ϵ the correction for irradiance variation due to Earth-Sun distance, SZA the solar zenith angle. The term π takes into account the Lambertian assumption. ρ is called also the *reflectivity* of the image. Note that the symbol ρ has been used to underline the difference between the albedo of a Lambertian plane (independent by viewing condition, as in (14)) and the apparent reflectivity of the image ρ calculated using (58): in fact ρ depends on the viewing geometry and Sun position.

Using the formulas described by Dagestad *et al.* [12], we look for a *correction* of the definition 58, for obtaining a reflectivity independent by ground effects and molecular scattering.

The cloudiness characterization by Dagestad describes the cloud cover for the Heliosat method [14, 39], an Eumetsat algorithm (www.eumetsat.int) for determining the ground irradiance. In this thesis we use the same definition of cloud index.

Consider a clear sky situation and a planar atmosphere. First, we have to correct the formula (58) for the atmospheric contribution given by single scattering events, so we define a contribution given by a cloudless atmosphere to the received radiance (path radiance):

$$\begin{aligned} R_{atm} = E_0 \tfrac{3}{16\pi} \left(1 + cos^2\psi\right) \tfrac{cosSZA}{cosVZA + cosSZA} \cdot \\ \cdot \left\{1 - \exp\left[-\tau \left(\tfrac{1}{cosSZA} + \tfrac{1}{cosVZA}\right)\right]\right\} \end{aligned} \tag{59}$$

where E_0 is the solar constant[28] at the top of atmosphere normal to Sun direction ($1367\,W\,m^{-2}$), SZA and SVA are the solar and satellite zenith angle

[27] Note that a Lambertian plane is specifically different than sky in its phase function. Aerosols and air molecules are all angle dependent scatterers while the ground is not: impinging irradiance is "reflected" (scattered) isotropically. The albedo depends on $cosSZA$ only for normalization.

[28] The definition of solar constant is bolometric: it is the spectrally integrated Sun irradiance at Earth's mean distance from the Sun (1 astronomical unit).

with respect to the normal to the ground plane, ψ is the scattering angle (phase angle) between Sun and satellite directions and $\tau = 0.0426$ is the optical depth for a wavelength of $0.68\,nm$ (representative of the equivalent wavelength of the Meteosat Second Generation HRV channel) in clear sky conditions (in a cloudy atmosphere the single scattering approximation is no longer well satisfied). Eq. (59) is calculated as shown in figure 49: being $\tau(s)$ the vertical optical depth between the top of atmosphere and altitude s, the radiance reaching the altitude s can be expressed as $E_0 \exp\left(-\frac{\tau(s)}{cosSZA}\right)$. The fraction of radiance scattered at the altitude between s and $s+ds$ (from the definition of scattering coefficient σ_s) is $\sigma_s \frac{ds}{cosSZA}$, and the fraction reaching the satellite in the direction given by ψ after a single scattering event and considering only direct propagation (to avoid the integration over the pixel solid angle) is given by $p(\psi) \exp\left(-\frac{\tau(s)}{cosVZA}\right)$, where $p(\psi) = \frac{3}{16\pi}\left(1 + cos^2\psi\right)$ is the Rayleigh phase function (see e.g. [48]). Integrating along the vertical brings to eq. (59). The assumption of single scattering events is justified by the value of $\tau \ll 1$ (considering τ as the mean number of scattering events occurring along the path).

The angle ψ is determined by Sun and satellite directions (defined by the solar and satellite zenith angles SZA, VZA and azimuth angles SAA, VAA) by the relation:

$$cos\psi = cosVZA\,cosSZA + sinVZA\,sinSZA\,cos(SAA - VAA) \tag{60}$$

The reflectivity of ground and (if present) clouds[29] can be expressed as:

$$\rho = \frac{\pi L_{band}}{\epsilon\, E_{0\,band}\, cosSZA} - \frac{\pi R_{atm}}{E_0 cosSZA} \tag{61}$$

If we consider a cloudless atmosphere, the reflectivity ρ is equal to the ground reflectivity $\rho_g = \rho_g(\psi)$, here named clear sky albedo. Dagestad shows that ρ_g can be written as:

$$\rho_g(\psi) = \rho_{g_0} \rho_{shape}(\psi) \tag{62}$$

where ρ_{g_0} is the reflectance for $\psi = 0$ and ρ_{shape} a shape function for taking into account any non-Lambertian behavior of the ground surface reflection, shading due to the ground structure and contributions of multiple scattering events and molecular and aerosol absorption. ρ_{shape} is empirically modeled as (the coefficients are from [12]):

$$\rho_{shape} = 1 - 0.59\psi + 0.11\psi^2 + 0.05\psi^3 \tag{63}$$

The cloud index is finally defined as the normalized[30] quantity:

$$n = \frac{\rho - \rho_g}{\rho_c - \rho_g} \tag{64}$$

[29] Following Dagestad *et al.* [12], for the calculation of the cloud index, ρ is represented as the reflectivity of the ground and clouds, although this is not strictly physically correct, due to the assumption of single scattering event for the path radiance and to the Rayleigh scattering function used to model the relation between air and back scattered radiance (regardless of the appropriate aerosol scattering function). For most layers of the atmosphere, and for an optically thin atmosphere, this first order assumption is generally sufficient.

[30] The cloud index is only approximately normalized between 0 and 1: there are cases in which $n > 1$ and $n < 0$, due to the algorithm used for determining ρ_{g_0} and to cloudy situations in which $\rho > \rho_c$.

where ρ_c is the reflectivity of the total cloud cover case (fixed at $\rho_c = 0.81$). In the following paragraphs we'll refer to the reflectance and cloud index data obtained from the original MSG radiance image as *reflectance image*, *cloud index image*, etc. The clear sky albedo is a flat-field, so cloudiness is retrieved by a normalized difference between the reflectance image ρ and the clear sky albedo image ρ_g.

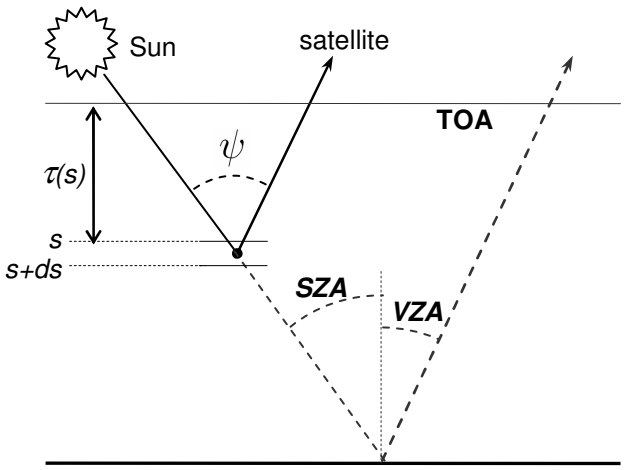

Figure 49: Sun and satellite geometry considered in calculating the path radiance contribution R_{atm}. Note that SZA and VZA are referred to the normal to the ground, and ψ is referred to the angle between Sun and satellite directions, that in general lie in different planes ($\psi \neq VZA+SZA$). The contribution R_{atm} is calculated using single scattering approximation for a cloudless atmosphere (the single scattering hypothesis is non satisfied by a cloudy atmosphere).

6.5 Algorithms for cloud index calculations

The cloud index calculation requires ρ obtained from the image and ρ_g from the cloud-free case. In particular, ρ_g needs to be calculated by considering the geometry of each image.

The calculation of ρ_g is obtained by processing only cloudless pixels and storing a clear sky albedo image scaled to a co-scattering angle $\psi = 0^\circ$ (using eq. (62)). Then, during the processing of a MSG image for cloud index calculation, the observed value of ρ for a generic point comes from the value of the reflectance image in the corresponding pixels and the corresponding value for ρ_g can be determined by the value of ρ_{g_0} stored (ordered by the spatial and temporal coordinates of the point).

The physical meaning of the clear sky albedo as a flat-field, introduced in paragraph 6.4, is pointed out not only by the exclusion of cloudy pixel in ρ_g and ρ_{g_0} calculation, but also by considering eq. (61) as a normalization with respect to lighting condition. In figure 50 the behavior of such a normalization is evidenced by the series of images in different moments of the day with the image corresponding to ρ_{g_0}. The effect of lighting is clearly visible in the MSG image series and disappears (making the image "flat") in the reflectance image

ρ_{g_0}. The reflectance image ρ_{g_0} is created by the IDL code developed for cloud index calculation (see D.4 for a detailed description of the procedure).

6.5.1 Clear sky albedo image

The clear sky albedo image calculation is performed by the `CLEAR_SKY_GENERATOR` IDL procedure (see sec. D.4). The algorithm uses the cloud mask data introduced in 6.3 to identify cloud free pixels. The steps of the `CLEAR_SKY_GENERATOR` procedure are the following:

1. selection of a set of MSG images in HRV band for the desired period (typically 15-20 days);
2. selection of corresponding CLM data for each image of the set;
3. an array $\rho_{g_0}^{cumulative}$, corresponding to the size of the image, is allocated and set to 0 for ground reflectance image calculation (ground reflectance values ρ_{g_0} will be added to $\rho_{g_0}^{cumulative}$ for clear sky pixels only); also a second array n_{pixel} is created for storing the number of clear sky reflectance values processed for each pixel of each image of the set;
4. for each image of the set the following operations are performed:
   - conversion (transformation to radiance units);
   - calculation of the geometrical parameters for the current acquisition (solar and viewing angles, Earth-Sun distance, co-scattering angles, etc.);
   - determination of the reflectance image ρ (in the clear sky pixel $\rho = \rho_g$);
   - calculation of the ground albedo for $\psi = 0$ for each pixel: $\rho_{g_0} = \rho_g / \rho_{shape}(\psi)$;
   - using the CLM mask, only the cloudless pixels are selected and added to $\rho_{g_0}^{cumulative}$; the corresponding pixels are incremented by a single unit in n_{pixel}.
5. at the end of the iteration on each image of the set, ρ_{g_0} is calculated as average value from:

$$\rho_{g_0} = \frac{\rho_{g_0}^{cumulative}}{n_{pixel}} \tag{65}$$

   and saved to disk.

The use of a time series (typically 15 days) ensures the presence of cloudless pixels. Also, using a mean value for ρ_{g_0} allows to average on different aerosol conditions[31] (changing daily respect with wind, local characteristics, etc.).

[31] Any "static" aerosol layer is included in the albedo definition, e.g. an industrialized zone may have a change on such a long term in the lowest atmospheric layer that the albedo is integrated through a thin (unresolved) stratum.

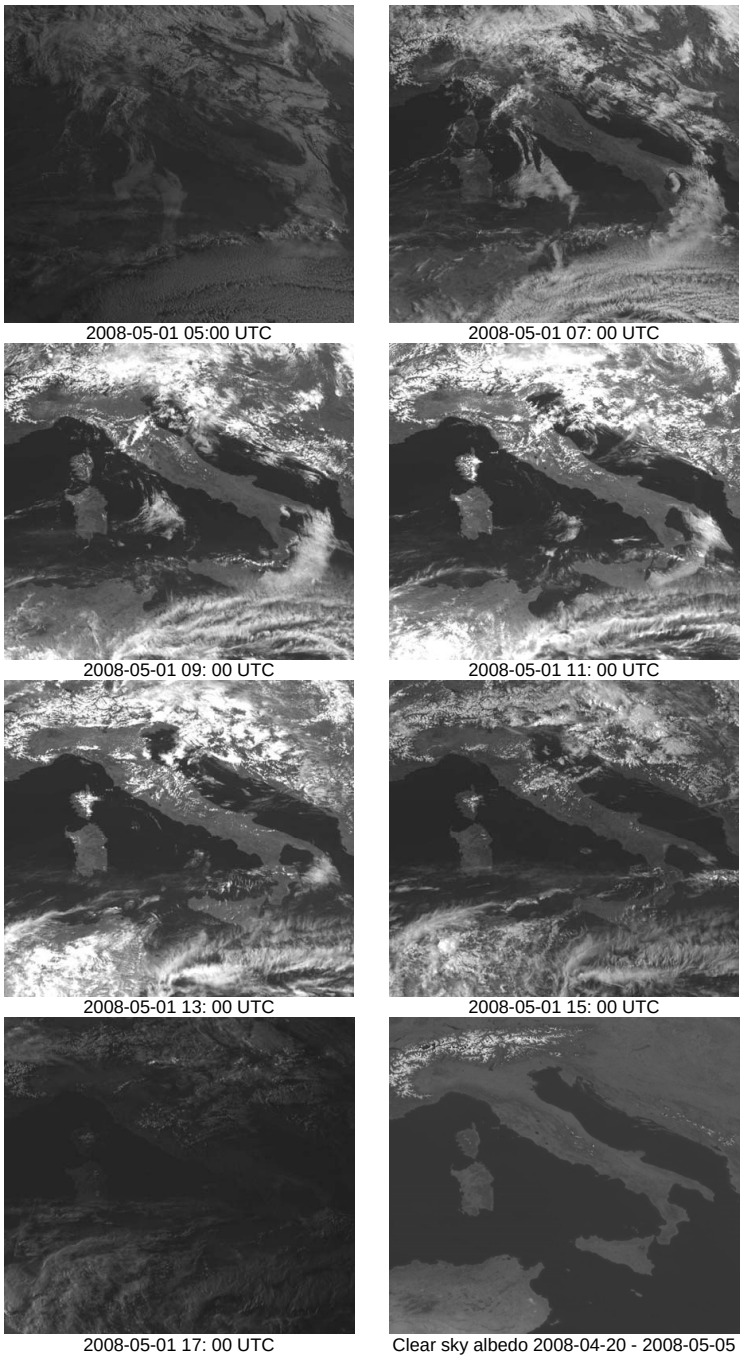

Figure 50: Subsets of MSG images in HRV band in different moments of the day 05 May 2009 (first 7 images from top) compared with the image corresponding to the clear sky albedo ρ_{g_0} obtained from cloudless pixel of the images between 20 April 2008 and 05 May 2008 (at the bottom, on the right). The effect of Sun lighting is clearly visible in the MSG images and disappears (making the image not only cloudless but also "flat") in the ρ_{g_0} image. It becomes evident the meaning of the clear sky albedo as a flat-field. The ρ_{g_0} image is generated by the IDL code written for the purposes of the thesis.

6.5.2 Cloud index image

Knowing ρ_{g_0}, the cloud index image n is calculated by the procedure `CLOUD_INDEX_CALCULATION` (details in sec. D.4). The steps are as follows:

1. selection of the image in HRV band for the desired time;
2. image conversion (from digital number to radiance units);
3. calculation of the geometrical parameters for the current acquisition (solar and viewing angles, Earth-Sun distance, co-scattering angles, etc.);
4. calculation of the reflectance image ρ (in general for cloudy pixels);
5. reading of ρ_{g_0} from the clear sky albedo image stored on disk for the current period and calculating ρ_g for each pixel;
6. calculation of cloud index value.

Because the ground albedo in the visible and infrared bands changes on a seasonal basis (e.g. due to the vegetation life cycle and human activities) cloud index calculation must be performed using a clear sky albedo consistent with the actual situation (that is, recently calculated with respect to the current image). A non-current value of the ground albedo ρ_g causes systematic errors in applying the cloud index definition (formula 64).

6.5.3 Dispersion in ground reflectance values

The precision of the cloud index value depends on the dispersion of the ground albedo ρ_{g_0} (as defined in paragraph 6.5.1) retrieved from cloud free pixel of the satellite image. For example, the histograms of ρ_{g_0} values for different time series of Meteosat Second generation images for a single point are shown in fig. 51 and fig. 52. The values used in the histograms have been extracted from the time series used for clear sky albedo data generation. Average values for ρ_{g_0} for the point of interest (the location of the sensors: 43.506°N, 10.322°E) are listed in table 8. Note that the uncertainty for data set in May is greater, due to the large aerosol contribution in a spring-summer atmosphere respect with a winter. Differences in the mean value take into account the seasonal variability of the ground albedo, probably due to different vegetation cover and different wetness of the soil and surface[32].

Another aspect to be pointed out is the relative uncertainty associated with the data (greater than 35%). The discussion of this result requires the interpretation of the physical meaning of the distribution of ρ_{g_0} in the histograms of figure 51 and 52. The large uncertainty associated with the clear sky value depends in part by the strong assumptions in the clear sky albedo map generation procedure. These assumptions relate to the non-Lambertian nature of the ground, shading due to soil rawness, seasonal and climatic changes in the surface albedo and unmodeled aerosol (there are in fact strong assumption on the aerosol phase function in estimating the path-radiance contribution R_{atm} in eq. (59)), although these effects are, in part, modeled by the quantity ρ_{shape} (eq. (62)). Pixel contamination also contributes to ρ_{g_0} uncertainty: the MSG

[32] This also includes unresolved lakes (for instance in farm fields).

cloud mask data (par. 6.3.1) can't discriminate the presence of clouds at resolution higher than the pixel, thus unresolved clouds can contaminate the pixel, although masked as cloudless. The presence of "residual cloudiness" in the pixels used for calculating ρ_g (and consequently ρ_{g_0}) brings to a systematic error with asymmetrical distribution around the true value of ρ_{g_0}. Therefore, following this interpretation, it is possible to distinguish two different sources of errors for the distribution of measured values of ρ_{g_0}: a pure clear sky pixel distribution (really cloudless, with randomly distributed errors given mainly by the mismatch between the atmospheric contribution R_{atm} and the real aerosol and Rayleigh contribution) plus the asymmetrical error distribution due to cloud contamination in CLM data that generates the right tail of the distribution, contributing to the large uncertain on ρ_{g_0}. Together with unseen clouds, also haze due to condensed layers above the ground (unclassified as clouds by the cloud mask algorithm) brings to fluctuations in the surface albedo value, contributing to the asymmetry of the distribution.

Time series	**Mean**	**St. deviation**	**Rel. uncertainty**
2008-04-20 - 2008 05-05	0.157	0.057	$\sim 36\%$
2008-01-03 - 2008-01-20	0.215	0.046	$\sim 21\%$

Table 8: Average values for ρ_{g_0} in the location of the sensors (43.506°N, 10.322°E) for the time series of May and January 2008. The larger aerosol contribution in a spring-summer atmosphere respect with a winter atmosphere causes the uncertainty for data set in May to be greater. Differences in the mean value take into account the seasonal variability of the ground albedo, due to different vegetation cover and wetness of the soil.

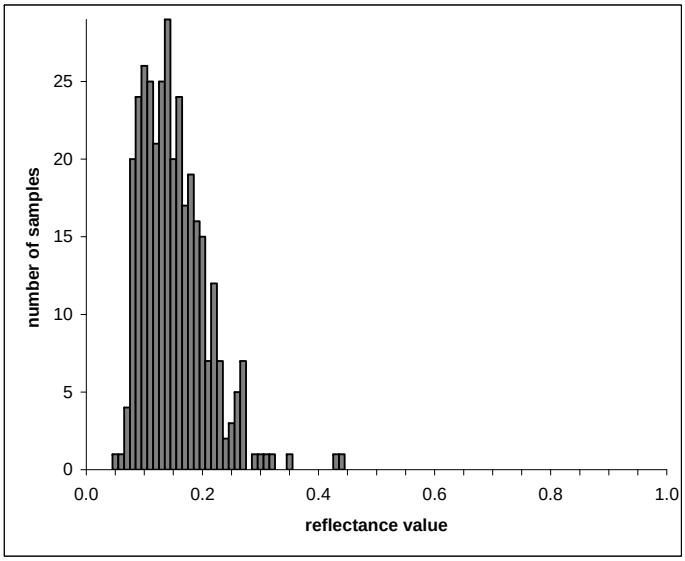

(a)

Figure 51: Histogram of ρ_{g_0} values for a time series of Meteosat Second generation images for the point at coordinates 43.506°N, 10.322°E. Only values for clear sky acquisition have been used, as in the creation of the clear sky albedo image. The time series is obtained from images between 20 April 2008 and 5 May 2008.

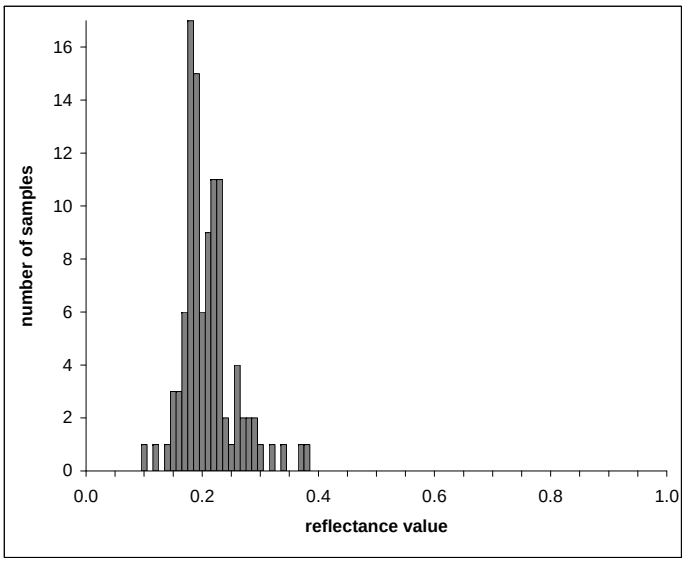

(a)

Figure 52: Histogram of ρ_{g_0} values for a time series of Meteosat Second generation images for the point at coordinates 43.506°N, 10.322°E. Only values for clear sky acquisition have been used, as in the creation of the clear sky albedo image. The time series is obtained from images between 3 and 20 January 2008.

7 Simulation of ground irradiance and satellite observed cloud index using the composite atmosphere model

7.1 Radiative transfer simulation and composite atmosphere

Although the use of an MM5 run as a forecast is an interesting possibility for a future application of the procedure described in this thesis, the MM5 output data, i.e. a grid of atmospheric profiles for each time step of the simulation, is used for obtaining a realistic structure for the atmosphere around the point of interest (Livorno, 43.506°N, 10.322°E). The use of the MM5 simulation allows the construction of the composite profile (par. 2.7). Such a composite profile is used as input for the UVSPEC radiative transfer code (requiring a plane parallel atmosphere model) for calculating both ground irradiances and satellite observed radiances. The results of the simulations are then compared with both the ground measured values performed in Livorno and with the cloud index from Meteosat Second generation data.

We must note that, although the thesis points out various examples of phenomena due to the three-dimensional structure of the atmosphere (see for example par. 2.9 and fig. 12), the composite model is still plane parallel. In fact, the need of a widely used tool for radiative transfer calculations and the computational difficulties in considering truly three-dimensional conditions in solving the radiative transfer equation (that is considering a different composite profile for each propagation direction towards the observer), brings to the use of a plane parallel model. Nevertheless, the composite approach described here takes into account different profiles of the MM5 grid for the creation of the composite profile, in opposition to the traditional "vertical-column only" model that characterizes the atmospheric plane parallel layers using a single profile of the datacube. The composite profile depends by the atmospheric three-dimensional grid as well as by the Sun-observer line of sight at each time step.

To simulate the radiative transfer in a realistic atmosphere, the knowledge of cloud profile as well as the cloud drop radius, aerosol concentration profile, atmosphere and aerosol constituents are needed. Because the MM5 simulated data provides information only about cloud profile[33], the standard atmosphere model (par. 2.6) has been used for providing the complete parameter profile to the radiative transfer model UVSPEC. Details about the software procedures used for this purpose are given in appendix A. The parameters provided by the MM5 simulations doesn't completely describe the optical parameters of the composite atmosphere, thus some parameters remain undetermined. For this reason the simulations are presented using different (constant) cloud drop radius distributions and different amount of non-cloudy aerosol in the boundary layers (that is, different values of the horizontal visibility). The lack of these local parameters prevents the measured irradiance from being fully replicated in its direct and diffuse components, and the trend of the simulated values is discussed and commented.

[33] The cloud radius is not provided by MM5 simulations.

7.2 Ground irradiance simulation

For verifying the application of the composite atmosphere approach, two measured data subsets, representative of midlatitude winter and summer conditions, have been chosen: days January 17 to 19 and May 1 to 3 2008. Sensor data (see sec. 3) provide calibrated measurements of the irradiance in the visible - near infrared ($335\,nm - 2200\,nm$) band (direct, diffuse and total components) and (uncalibrated) total irradiance in UV band ($280\,nm - 360\,nm$). the ground measurements have been compared with simulated data using different values for visibility (to test different aerosol situations of the standard model) and different values of cloud drop radius. Liquid water and ice clouds have been classified using the temperature profile from MM5 data and input separately in the radiative transfer model. Lacking measured data for cloud drop radius profile, we assumed a fixed radius value for all the cloud layers of the dataset. Using constant values for the drop radius distributions implicates that the angular scattering properties (i.e. the scattering function) cannot exactly replicate the measured ratio of diffuse to total as well as direct to total irradiances. The comparison of the measured direct and diffuse irradiance with the simulated data allowing the selection of the nearer value, although the problem of having a realistic profile for the drop size distribution (and, in general, aerosol characteristics) still remain unresolved.

The parameters used for the radiative transfer simulations are summarized in table 9. Ozone data (they have significant impact only on UV band simulation) have been extracted from OMI data [50, 1] (freely downloadable at http://toms.gsfc.nasa.gov).

Figures 53 and 55 show the ratio of direct to total irradiance and of diffuse to total irradiance simulated in the wavelength band of the pyranometers compared with measured values. The corresponding direct and diffuse irradiance measurements are presented in figures 54 and 56 for visible - near infrared and UV bands. The simulations have been launched using different cloud drop radius and different values for the visibility. The January and May data sets are best reproduced for visibility $50\,km$ and drop radius $25\,\mu m$.

An example of disagreement between simulated and measured data is visible in high cloud cover situations, on the contrary, for low cloud cover (as in January 17), the trend is simulated correctly almost always in both January and May data sets. The disagreement between the measured and simulated data for January 19 (figure 54) could be ascribed to the irregular cloud cover (par. 2.9), as confirmed by the corresponding UV sensor data: an amplification of the total irradiance (a typical non-plane parallel effect) can be recognized both in figure 54.a and in 54.b.

The spikes, due to broken clouds, in measured diffuse irradiance for January 17 and May 1 (figures 54.a and 56.a) show the difference between the instantaneous measurements of the sensor and the integrated simulation obtained from MM5. The latter can't reproduce the short spikes because it assumes uniformity on the scale of the grid, while the broken cloud effects are not resolved by the MM5 simulation resolution (1 h). The total irradiance simulation in visible - near infrared fits better the hourly averaged measured data, with an absolute error of $43 Wm^{-2}$ for January and of $105 Wm^{-2}$ for May. The UV data are uncalibrated, thus only a qualitative analysis is possible.

Although the relative error is quite high ($\sim 20\%$), we notice that the simu-

lated (composite) atmosphere has been reconstructed using no direct measurements (apart for ozone, needed for a qualitative analysis of UV data). The simulation uses as input only MM5 simulated data and atmospheric parameters from the standard model.

A comment should be made regarding the use of a$25\mu m$ radius for cloud drops. Although the graphs suggest that increasing the cloud drop radius produces a more faithful simulation of ground irradiance, the study of the aerosol distribution of paragraph 3.3 confirms that setting a single value for drop radius (due to the lack of reliable measurements) is too restrictive an approximation and that the radius distribution for drops in a real atmosphere is wider.

A different source of error is given by the non-spherical shape of ice particles: the calculation of the scattering function is performed by the radiative transfer model using the Mie theory (valid for spherical particles), whereas the hypothesis of spherical drop clouds is not necessary valid for ice clouds (May cloud data contain only ice clouds). The sphericity is certainly not valid for ice in some phases (e.g. amorphous or semi-crystalline), thus the shape of the particles depends on the processing of the ice. Other sources of error are given by the aerosol model and by the low spatial and time resolution of MM5 data (imposed by the long time needed for a single MM5 run).

For a comparison of the composite atmosphere with the traditional "punctual" plane parallel model, the direct, diffuse and total contributions to the ground irradiance have been calculated using both a composite profile for each hour of January and May datasets (the composite atmosphere used for figures 54.a and 56.a) and the single profile corresponding to the sensor position (i.e. a non-composite, plane parallel atmosphere). Fig. 57 shows the irradiance for January and May datasets. In fig. 58 the differences between the components of the ground irradiance are emphasized by the corresponding scatter plot of the direct, diffuse and total irradiance from the composite and from the single profile. When the clouds are not well resolved by the MM5 simulations (days January 17 and May 1) or the cloud cover is uniform (January 19) the two atmospheric models determine the same ground irradiance (i.e. the composite atmospheric profile is well represented by the profile on the vertical of the point of interest). For irregular cloud cover (January 18, May 2 and 3) the differences in the profiles are emphasized by the outliers in the direct contribution scatter plot. We note also differences in the diffuse contribution: a future improvement of the model will provide an equivalent composite profile also for the diffuse contribution.

Parameter	Value
Visibility	20 km - 50 km
Ground albedo	0.1
Ground altitude (ASL): the average altitude of the corresponding MSG image pixel has been considered	0.1 km
Atmosphere and aerosol standard model	MIDLATITUDE WINTER (for January dataset) MIDLATITUDE-SUMMER (for May dataset)
Aerosol type	RURAL
Ozone data	OMI data (from http://toms.gsfc.nasa.gov)
Drop radius	$1\mu m$ to $25\mu m$
Wavelength range visible - near infrared band (simulation of the pyranometers for total and diffuse irradiance measurement)	$335nm$ - $2200nm$
Wavelength range UV band (simulation of the UV sensor)	$280nm$ - $360nm$
Wavelength range MSG HRV channel (MSG received radiance simulation)	$450nm$ - $1050nm$

Table 9: Parameters used for radiative transfer simulations.

Day	Ozone value (DU)
January 17 2008	311
January 18 2008	277
January 19 2008	246
May 1 2008	354
May 2 2008	340
May 3 2008	345

Table 10: Ozone values used for radiative transfer simulations. OMI data for the location of interest (Livorno, 43.506°N, 10.322°E). Relative uncertainty is 5%.

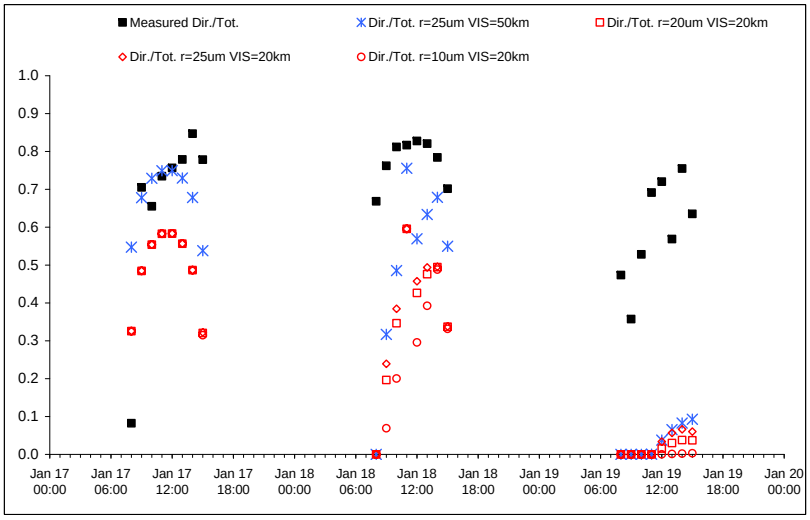

(a)

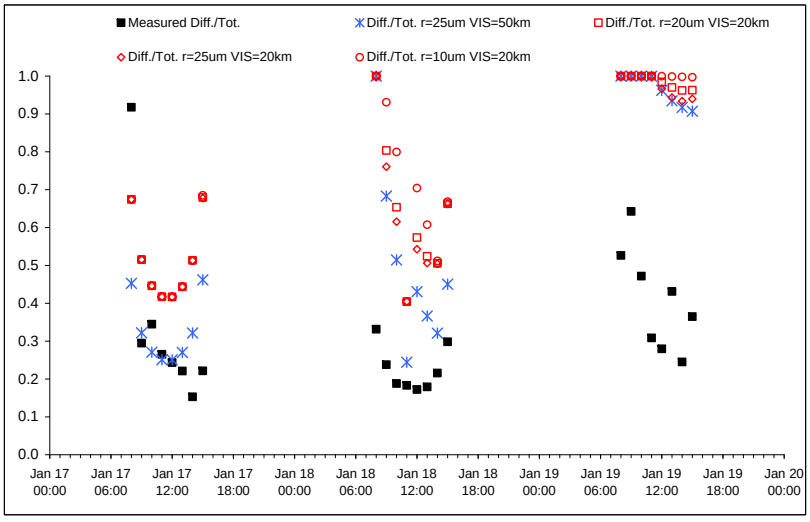

(b)

Figure 53: Ratio of direct to total irradiance (a) and diffuse to total irradiance (b) in the wavelength range $350nm$ - $2200nm$ compared with hourly averaged measured values by pyranometers for days 17-19 January 2008. We note that the trend of the ratio of direct to total and diffuse to total irradiance is reproduced better by the simulation with drop radius $25\mu m$ and visibility $50km$.

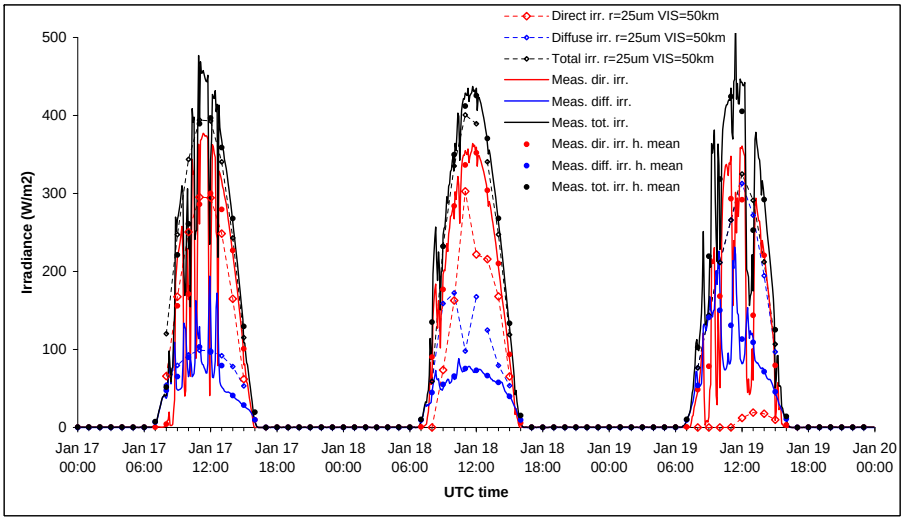

(a)

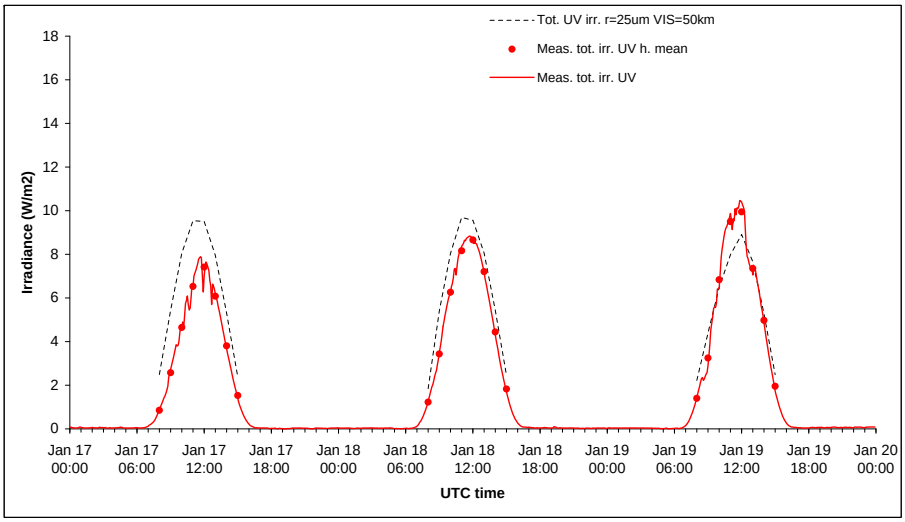

(b)

Figure 54: Irradiance for days 17-19 January 2008 in visible and near infrared band measured by pyranometers (a) and in ultra violet band by the UV sensor (b) in Livorno (43.506°N, 10.322°E) together with the hourly averaged values, compared with estimated irradiance by the composite atmosphere model for different cloud drop radius and visibility. The simulation for UV in figure (b) is shown only for cloud drop radius $25\mu m$ and visibility $50km$. The model shows differences amenable to the irradiance amplification due to broken cloud situations described in par. 2.9 for the day 19 (both in (a) and (b)). The absolute error between simulated and total irradiance in visible - near infrared band for the case with drop radius $25\mu m$ and visibility $50km$ is $43Wm^{-2}$, the relative error $\approx 20\%$ for the general cloud cover situations and solar zenith angles of the January dataset.

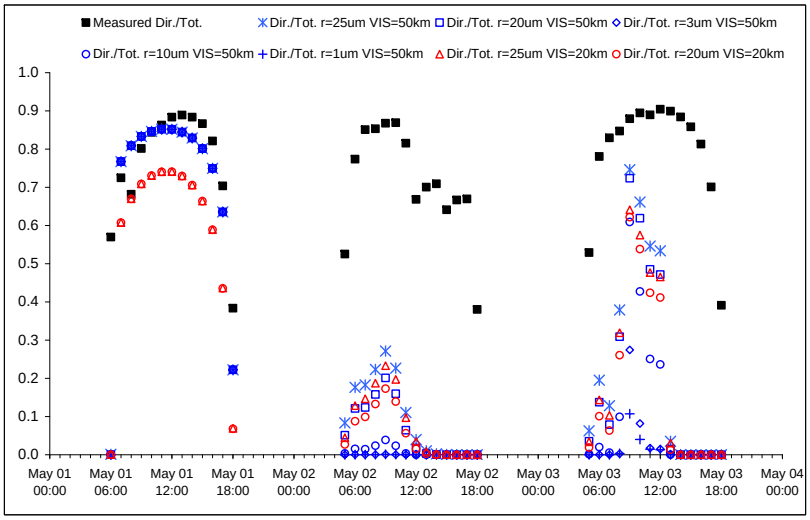

(a)

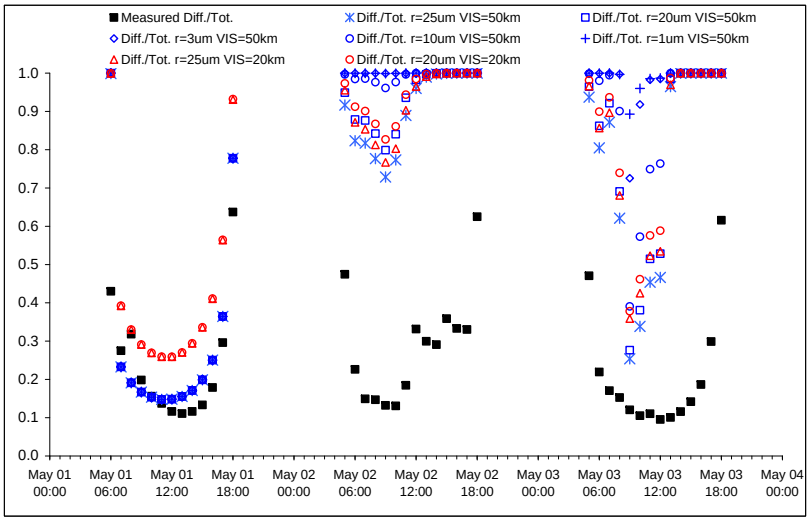

(b)

Figure 55: Ratio of direct to total irradiance (a) and diffuse to total irradiance (b) in the wavelength range $350nm$ - $2200nm$, simulated for different cloud drop radius and visibility, compared with hourly averaged measured values by pyranometers for days 1-3 May 2008. The trend of the ratio of direct to total and diffuse to total irradiance is reproduced better by the simulation with drop radius $25\mu m$ and visibility $50km$. For low cloud cover (May 1) the agreement is excellent. We notice also that, for the simulated values, especially for days May 2 and 3, the diffuse contribution is dominant. Using a radius greater than $25\mu m$ for cloud drops (i.e. a lesser scattering efficiency) the agreement would probably be better. Simulations with bigger radius values have not been performed due to limitations of the radiative transfer model (see libRadtran documentation, www.libradtran. org).

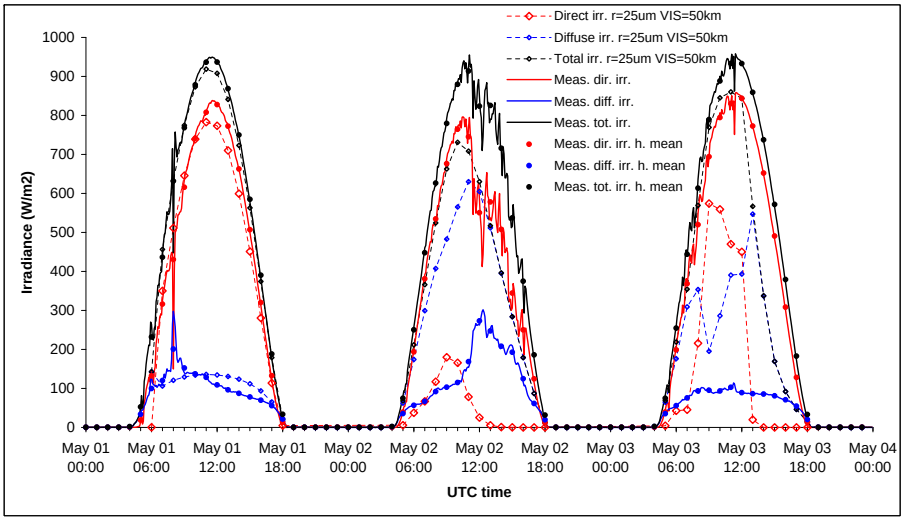

(a)

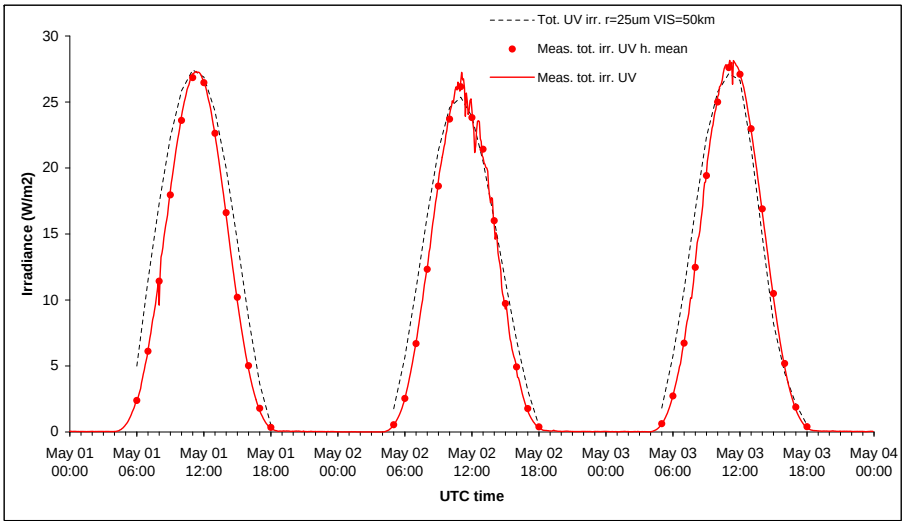

(b)

Figure 56: Irradiance for days 1-3 May 2008 in visible and near infrared band measured by pyranometers (a) and in ultra violet band by the UV sensor (b) in Livorno (43.506°N, 10.322°E) together with the hourly averaged values, compared with estimated irradiance by the composite atmosphere model for different cloud drop radius and visibility. The simulation for UV in figure (b) is shown only for cloud drop radius $25\mu m$ and visibility $50km$. The absolute error between simulated and total irradiance in visible - near infrared band for the case with drop radius $25\mu m$ and visibility $50km$ is $105Wm^{-2}$, the relative error $\approx 23\%$ for the general cloud cover situations and solar zenith angles of the May dataset. For May 3 we notice differences probably due to the spatial resolution of MM5 data.

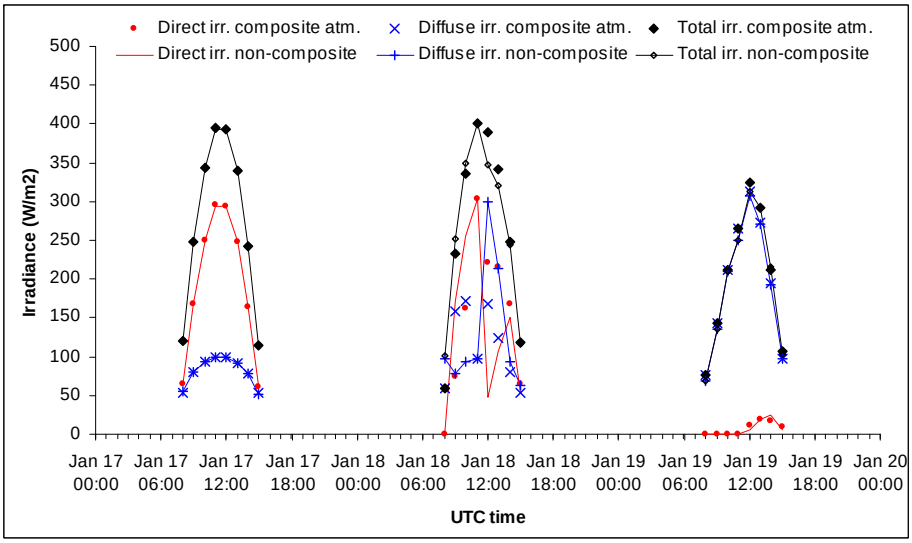

(a)

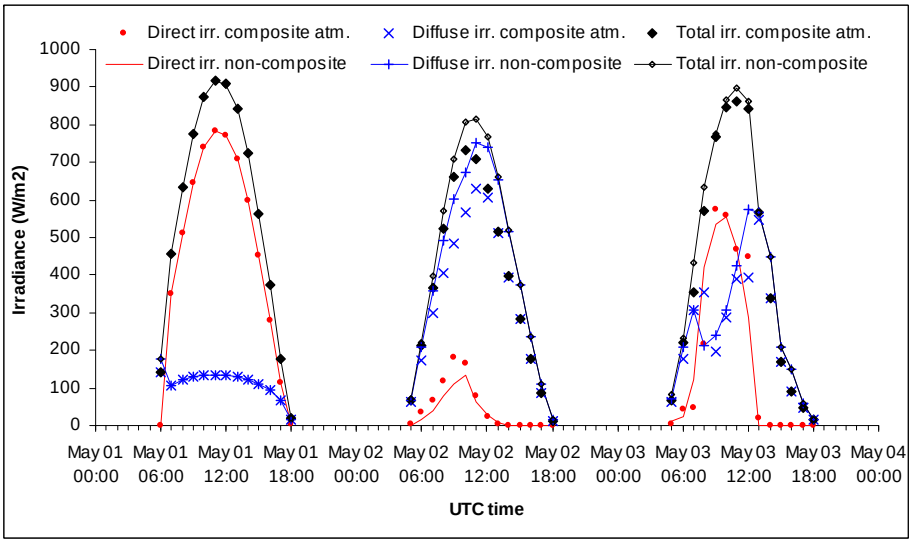

(b)

Figure 57: Ground irradiance for days 17-19 January (a), and 1-3 May 2008 (b) in visible and near infrared band simulated using the atmospheric profiles generated by MM5. The curves have been calculated using both the composite atmosphere model (i.e. "cutting" the atmospheric profiles for generating the composite profile) and the (non-composite) profile corresponding to the sensor location. The parameters of the simulation have been set as in tab. 9 and 10, using a cloud drop radius of $25\mu m$ and a visibility of $50km$. For conditions of unresolved clouds (days January 17 and May 1) or uniform cloud cover (as for day January 19) the composite atmospheric profile is well represented by the profile on the vertical of the point of interest. Differences arise with cases of irregular cloud cover (as for days January 18, May 2 and 3): the differences in the profile correspond with the outliers in the direct irradiance scatter plot of fig. 58.

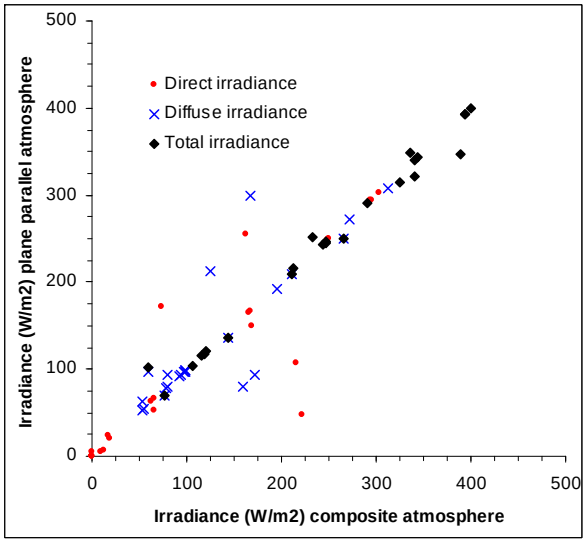

(a)

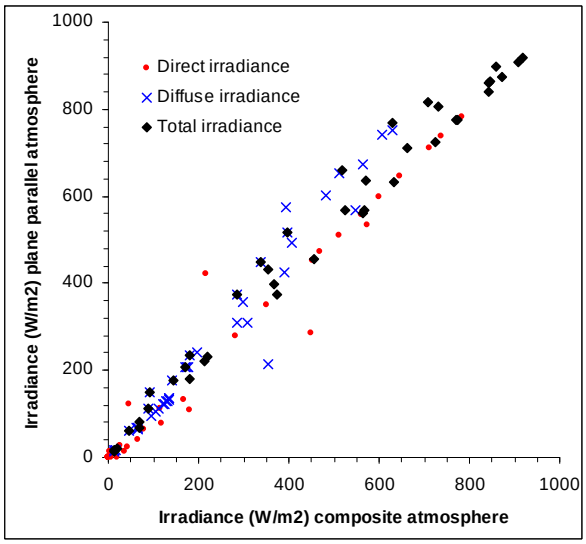

(b)

Figure 58: Scatter plots of the direct, diffuse and total ground irradiance for days 17-19 January (a), and 1-3 May (b), in visible and near infrared band, simulated using the atmospheric profiles generated by MM5. The ground irradiance is calculated using both the composite atmosphere model (i.e. "cutting" the atmospheric profiles for generating the composite profile) and using a single profile corresponding to the sensor location. The scatter plots enhance the differences between the "classic" (non-composite) plane parallel atmosphere (although still based on the meteorological simulation, not a *standard* atmosphere) and the composite one. Differences are evident both for direct irradiance (directly affected by a change in the atmospheric profile) and for diffuse irradiance.

7.3 Satellite observed cloud index simulation

Using a drop radius in the range $10\mu m$ - $25\mu m$ and $50km$ visibility, the satellite received radiance has been simulated for cloud index determination (fig. 59). Simulated cloud index is calculated using the same formula given in par. 6.4 and running the radiative transfer model in the band $450nm$ - $1050nm$ (representative of MSG HRV channel). The agreement with measured data appears to be better than for ground irradiance because of the small aerosol induced effect on satellite observed irradiance (since the aerosol affects light propagation mainly near the ground). This confirms that the cloud profile is well simulated by MM5 and the application of the composite atmosphere model is correct. In figure 59 is presented the comparison of simulated and satellite observed cloud index, together with the spatially averaged values around the point of interest (showing the same trend of the cloud index for the single pixel). We note again a spike of the cloud index observed by MSG and unresolved by the resolution of MM5 data.

It is interesting to note that the simulated cloud index fits best the MSG observed cloud index for a smaller radius relative to the ground irradiance simulation. It probably indicates that the cloud index distribution in high atmospheric layers is given by clouds characterized by a smaller drop radius.

7.4 Summary of the radiative transfer simulations

This section describes the applications of the composite profile approach for ground irradiance and satellite observed radiance simulations using the radiative transfer model UVSPEC and the composite profile approach. For simulating the satellite observations the cloud index has been chosen for characterizing the (generally) cloudy atmosphere independently on other model parameters (mainly the ground albedo and the non-cloud aerosol extinction, although using a strong approximation on aerosol scattering properties). The theory described in par. 6.4 and 6.5, by the use of the IDL procedures developed for this purpose, allows the creation of the clear sky albedo image (par. 6.5.1) used as "flat field" for the cloud index retrieval.

The composite atmosphere produces an atmosphere with "free" parameters, i.e. not provided by the meteorological model. For the simulations shown in this section a range of fixed values has been used for cloud drops and for the visibility value (that is the non-cloudy aerosol in the radiative transfer model). This is somehow unrealistic with respect to a *real* atmosphere, being such particles characterized by different size distributions, i.e. the corresponding optical properties strongly depend on the tuning of such parameters. The lack of measured values for aerosol and cloud drops prevents the simulated irradiance from being fully replicated in its direct and diffuse components. The simulations allow, however, investigating the order of magnitude of the drops by the comparison with the measured or satellite observed values. For example, the agreement of the cloud index simulated and calculated from MSG data is better for particles with small radius, which are expected to be the major contribution to the satellite observed particles.

Other remarks concern the differences between the composite profile and a truly three-dimensional atmosphere. The composite approach considers dif-

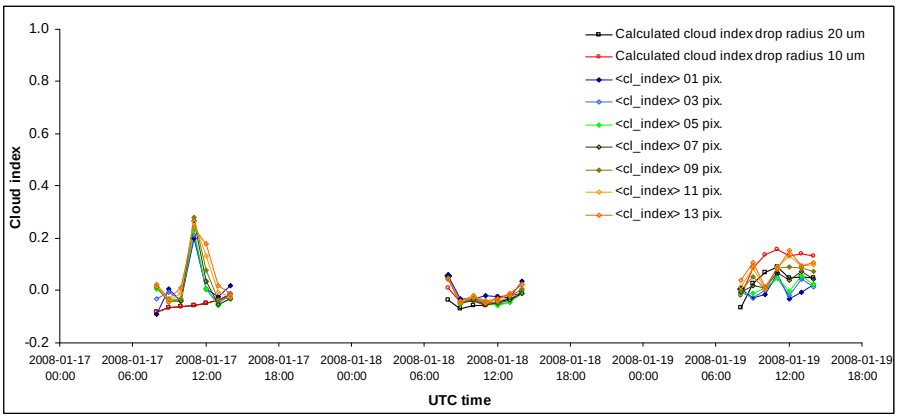

(a)

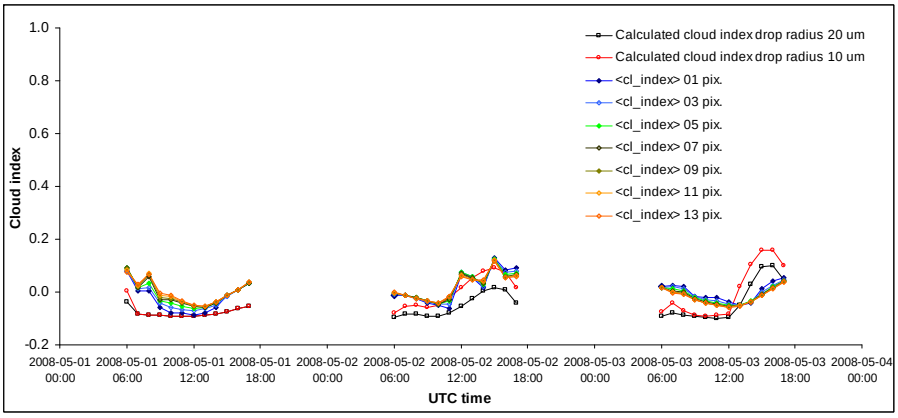

(b)

Figure 59: Cloud index from MSG images for days 17-19 January (a) and 1-3 May 2008 (b) in Livorno (43.506°N, 10.322°E). The cloud index, averaged on a square with side 1 to 13 pixel, is represented together with the cloud index calculated by radiative transfer model using the composite atmosphere, for 20 and $10\mu m$ liquid water and ice cloud drop radius. Calculated and satellite observed data show the same trend. The spikes of satellite estimated cloud index show the need of increasing the time resolution of the MM5 simulated data (evident especially for January 17). Comparing the data for January 1 with the ground measured values of fig. 54 we note that phenomena with a time scale of the order of minutes (e.g. the broken clouds visible for the day January 1 in fig. 54.a) are not seen by the satellite. Note also that a smaller radius provides a better fit for the cloud index distribution.

ferent profiles of the MM5 grid for the creation of the composite profile, in opposition to the traditional plane parallel model using the "on-the-vertical" grid profile, producing both a physically consistent atmosphere (from the meteorological model) and taking into account the entire profile grid for building a composite profile along the Sun-observer line of sight calculated for each time step. This is still different with respect to a truly three-dimensional calculation. In other words it is an assumption valid for the direct contribution only, and the diffuse contributions from other line-of-sight remains unconsidered. Nevertheless it *does* takes into account the spatial (and not only vertical) structure of the atmosphere around the observer allowing the simulations of a part of effects due to irregular cloud cover of the sky. Furthermore, the outliers in the direct contribution shown in the scatter plot of fig. 57 make clear the differences between the composite and the traditional plane parallel "on-the-vertical" model, the latter being unable to consider the clouds (and in general the atmospheric constituent profile) far away from the vertical of the observer location.

8 Conclusions

Although much work must still be done for a complete description of the atmosphere without using direct measurements, the developed method demonstrates to provide a realistic description of the atmosphere using as input a mesoscale model for cloud cover characterization and a standard atmosphere from literature. This work describes the phenomena occurring in a realistic (i.e. truly three-dimensional) atmosphere (non-plane parallel) and presents an innovative approach to radiative transfer calculations by the use of a procedure for determining, from a grid profile in input, a composite profile taking into account the Sun-observer line of sight for a fixed position of the observer and for each time step of a gridded data. Being the composite atmosphere still plane parallel (although depending by the spatial and time coordinates of the point of interest), the procedure is not to be intended as a complete model, providing a complete description of radiative transfer in a three-dimensional atmosphere, but as a first-step approach in which a method is proposed for taking into account part of the phenomena involved by an atmosphere in general horizontally (not only vertically) variable. Such a composite atmosphere approach is therefore the principal result of the work. In section 2 this new model has been introduced for taking into account the horizontal variability of the atmosphere due to the land topography (predicted by the meteorological model as described in par. 5.1.1, 5.1.2 and in particular in fig. 31), to the irregular cloud cover (par. 2.9) and to different atmospheric profiles around the point of interest. The section describes also the radiative transfer phenomena due to irregular cloud cover through a simple model. Section 3 illustrates the measurement campaign and provides the description of the aerosol radial distribution from ground measured data by AERONET stations. The aerosol characteristics are needed as an input for the radiative transfer model UVSPEC, described in detail in section 4. Section 5 describes the use of the meteorological model MM5 for providing the atmospheric profiles in the form of gridded data, used for the creation of the composite atmosphere. MM5 determines the presence of condensed layers, thus providing the cloud cover structure for the radiative transfer model. A corresponding measurement of the cloud cover is carried out by the Meteosat Second Generation images, used for providing the cloud index as an estimator of the atmospheric transmittance (by estimating the cloud reflectance), as described in section 6. Finally, in section 7, the simulations of the ground irradiance and of the satellite observed radiance using the composite atmosphere model is presented using a reasonable range of aerosol and drop radius parameters and they are compared with the ground measured and the satellite observed data.

Practical applications of the developed procedure are useful in both radiative transfer calculation for atmospheric effects correction on satellite images (especially when a corresponding ground measurement is not possible), in radiative budget calculations for irradiation predictions (i.e. in solar plans production monitoring), heating rate calculation (in meteorology and biology applications) and automation of satellite data acquisition procedures (cloud classification, data quality, etc.). Disadvantages of this approach are given by the long time needed for the meteorological simulation to be performed and, consequently, by the poor time and spatial resolution of the output data.

Objections arise about the use of the meteorological model MM5 as a tool for providing the atmosphere structure and about the use of a transport model

for providing a high spatial and time resolution profile grid. In fact, there are situations in which the model may inaccurately reproduce the correct evolution of atmospheric phenomena, especially on the small scale, so that the use of MM5 for determining broken cloud situations could lead to systematic errors in the entire procedure. The problem has been faced in the thesis by carefully selecting the days to be used as the validation dataset, both for avoiding misleading results in the meteorological simulations and for having a dataset that is representative of a wide variability of the cloud cover. Nevertheless, the method presented here provides a first approach to the more extensive treatment of a particular radiative transfer problem for realistic atmospheric models. In this sense, the use of MM5 has to be regarded as a tool for providing both a realistic and spatially gridded atmospheric structure for the composite profile creation, thus the approach itself is not disqualified by hypothetical systematic errors introduced by the atmospheric transport model.

The large amount of code developed for calculating the composite atmosphere profiles and for processing and converting the data between the different models used in this thesis allows the fast implementation of the future evolution of this approach. The first step in the future development of the research will be the improvement of the radiative transfer model described in par. 2.8 for a more accurate description of the radiative transfer processes in a real atmosphere. Such a new model is currently in development: it will take into account not only the structure of the atmosphere in the direction of the Sun (as in the composite atmosphere model), but also the contribution given to the observed radiation by the atmosphere along the direction of observation. The new model will also consider the angular effects due to aerosols (especially in cloudy and lower layers), by taking into account the contribution of the scattering function. Such a model will avoid the long computation time requested for the current radiative transfer model, thus allowing the application of the model also to spectrally resolved calculation. The assumption is that the atmospheric layer in which the first order scattering occurs depends on the Sun angle, and the received radiance depends on both Sun and observing directions. Thus it is needed a characterization of the scattering function depending both on the spatial position with respect to the observer and on the altitude. Other steps for improving the algorithm will be a second order approximation for diffuse scattering based on the reflectance and transmittance model introduced in par. 2.8, a change in the microphysics for a better prediction of aerosol properties (composition and size distribution) and the use of *in situ* lidar or absolute measurements for characterizing the atmospheric column with particular focus on the aerosol profile both in the boundary layer and in cloudy layers, by associating to liquid water and ice clouds the corresponding drop radius distribution.

A IDL procedures for composite atmosphere model

This section details the IDL software written for creating the composite atmosphere model (see paragraph 2.7). The procedures and functions discussed here have been written for generating the atmosphere profiles from MM5 output data (see sec. 5), creating the composite profiles for atmosphere and cloud liquid water and ice content using Sun direction and coordinates of a user defined location. These profiles are then used as input for the UVSPEC program (see sec. 4 and in particular paragraphs 4.4 and 4.5). The UVSPEC output is generated as ASCII files that can be tabulated in any spreadsheet.

A.1 Composite atmosphere model creation and launching (JOIN_PROFILES procedure)

The algorithm shown in figure 60 is executed by the `JOIN_PROFILES` procedure for calculating the profile for atmosphere and clouds to be used by the radiative transfer model. The composite atmosphere model requires the atmosphere and cloud profiles observed in the Sun direction. These profiles are determined by calculating the intersection of the Sun-observer direction with the MM5 grid boundaries (the pixel of the grid containing the vertical profiles for each MM5 pixel).

Given the time and the observer position at ground and the MM5 grid in terms of latitude and longitude table, the `FIND_COORD_CROSSED_PIXELS` procedure finds the altitude of each intersection. The `LAUNCH_GRADS` procedure (see paragraph A.2) is then launched for determining the vertical profile of each pixel and the composite profile along the Sun direction is built by "cutting" each vertical profile at the intersection points with the grid. The radiative transfer model is then launched for calculating one of the following:

- the irradiance observed at ground (see paragraph A.3);
- the radiance observed by the satellite in the corresponding position (see paragraph A.4).

The simulated satellite-observed radiance is used for determining the corresponding simulated cloud index for the comparison with the measured cloud index. The results of the simulations for each time step (corresponding to the time step of the MM5 data) are then written in an ASCII output file, and can be graphed using a spreadsheet.

A.2 Atmosphere profile extraction from MM5 data (LAUNCH_GRADS procedure)

The procedure for extracting atmospheric profile data from GrADS files and converting them for using with the UVSPEC radiative transfer model (see UVSPEC description in paragraph 4 and in www.libRadtran.org) is performed by the `LAUNCH_GRADS` IDL procedure. GrADS is the tool used for reading, plotting and saving 2D, 3D or 4D data sets by the use of a command line interface (see

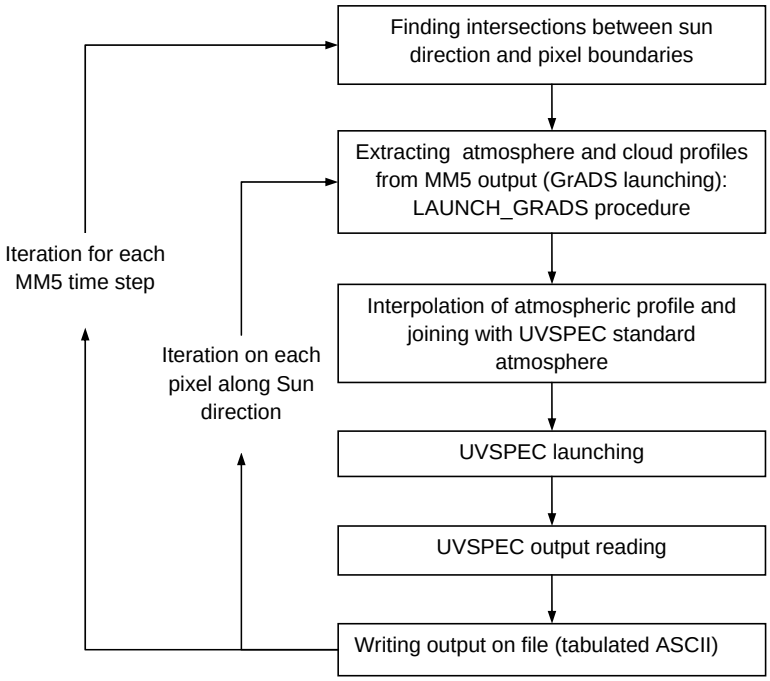

Figure 60: Composite atmosphere creation and ground irradiance simulation algorithm

GrADS description in paragraph 5.3). The GrADS files considered in this thesis are generated by MM5 (see MM5 description in paragraph 5.1) and contain 4D atmospheric data (the result of an MM5 atmospheric simulation) converted to GrADS format using the **MM5toGrADS** tool in MM5 package (see paragraph 5.1.8). The IDL procedure `LAUNCH_GRADS` launches the GrADS program for extracting the atmospheric vertical profile in a point of the MM5 grid for a user-specified time range.

`LAUNCH_GRADS` then generates:

- an output ASCII file with a summary of the variables contained in the MM5 file:
  - low cloud fraction;
  - mid cloud fraction;
  - high cloud fraction;
  - temperature;
  - pressure;
  - H2O mixing ratio;
  - relative humidity;
  - dew point temp;
  - cloud water;

  - rain water;
  - ice water;
  - geopotential height;
  - sea level pressure;
  - terrain elevation;
  - 2 m temperature;
  - 2 m H2O mixing ratio;

- an UVSPEC atmosphere file with:
  - pressure profile as a function of the geopotential height;
  - temperature profile as a function of the geopotential height;
  - water mixing ratio profile as a function of the geopotential height;
  - other gas profiles and pressure and temperature profiles in the range not covered by the MM5 simulation (they are scaled from an atmosphere standard file, as described in paragraph A.2.1);
- an UVSPEC cloud water content file with the cloud water mixing ratio as a function of the geopotential height (paragraph A.2.2);
- an UVSPEC ice water content file with the ice water mixing ratio as a function of the geopotential height (paragraph A.2.2).

These data are generated for user-specified coordinates and for each time step of the MM5 simulation. `LAUNCH_GRADS` program uses the GrADS program script language for generating a script file for GrADS and launching the GrADS program itself to execute it. The script contains instructions for:

- setting the point of interest on the space data grid for a time interval covered by the MM5 run file;
- extracting the variables of interest (variables can be referred to a single value or to an entire array, i.e. vertical profiles) for the time interval;
- writing the variables in binary format on disk.

Then the `LAUNCH_GRADS` procedure reads the variables in binary format and writes them in ASCII format in a log file. `LAUNCH_GRADS` uses the `CREATE_UVSPEC_PROFILES` procedure to generate also the atmospheric profiles in the format needed for UVSPEC, as described in paragraph A.2.1.

A.2.1 LAUNCH_GRADS atmosphere file creation

The MM5 simulation provides only the atmosphere structure from the ground to approximately 16 km. The atmosphere model used by UVSPEC considers a higher atmospheric layer (from the ground to 120 km). For linking the two different atmospheres, a standard atmosphere profile is used to describe the layers from the top to the higher altitude of the MM5 data (the user is prompted to choose a standard atmosphere file), then, from the MM5 higher altitude to the ground, the altitude steps, pressure, temperature and water vapor mixing ratio

are taken from MM5 file. Profiles of O2, CO2, O3, NO2 gases (not provided by MM5) are scaled proportionally to the ratio between the standard air density profile and the MM5 air density profile. The new profiles are also re-interpolated at MM5 altitude steps. An example of the syntax of an atmosphere profile for UVSPEC is given in table 11.

# z(km)	p(mb)	T(K)	air(cm-3)	o3(cm-3)	o2(cm-3)	h2o(cm-3)	co2(cm-3)	no2(cm-3)
120.00	0.00004	333.00	7.83E+11	3.92E+02	5.68E+10	1.57E+05	2.74E+07	1.18E+02
115.00	0.00006	293.00	1.48E+12	7.40E+03	1.39E+11	3.55E+05	5.92E+07	2.29E+02
110.00	0.00011	259.50	2.95E+12	1.48E+05	3.54E+11	8.27E+05	1.77E+08	4.69E+02
105.00	0.00020	237.10	6.11E+12	1.22E+06	8.56E+11	2.08E+06	6.73E+08	1.00E+03
...	...	...	...	...	...	...	...	...
0.912	900.000	277.25	2.35E+19	6.98E+11	4.92E+18	5.87E+16	7.76E+15	5.41E+08
0.470	950.000	279.28	2.46E+19	7.93E+11	5.15E+18	6.78E+16	8.14E+15	5.67E+08
0.033	1001.00	281.78	2.57E+19	9.25E+11	5.38E+18	7.41E+16	8.50E+15	5.92E+08
0.019	1000.00	281.93	2.57E+19	9.28E+11	5.37E+18	7.41E+16	8.49E+15	5.91E+08

Table 11: Example of an atmosphere profile file for UVSPEC

Conversions are needed to properly convert MM5 data for UVSPEC. The conversion formulas between UVSPEC and MM5 units are described here. Given the mixing ratio of water vapor from MM5, expressed as the ratio of water in kg for $1kg$ of dry air, we have:

$$r_{H2O}\left(\frac{kg}{kg}\right) = \frac{M_{H2O}N_{H2O}}{M_{dry\,air}N_{dry\,air}} \tag{66}$$

with:

$N_{dry\,air}$**:** number of particles in $1\,kg$ of dry air (considering dry air a perfect gas);

N_{H2O}**:** number of molecules of water vapor;

$N_{H2O} = 0.018015\,kg\,mol^{-1}$**:** molar mass ($kg\,mol^{-1}$) of water;

$N_{dry\,air} = 0.02896\,kg\,mol^{-1}$**:** molar mass ($kg\,mol^{-1}$) of dry air;

And using the perfect gas equation:

$$PV = N_{dry\,air}kT \tag{67}$$

with:

T**:** temperature (K);

P**:** pressure (Pa);

$k = 1.3806504 \cdot 10^{-23} Pa\,m^3\,K^{-1}$**:** Boltzmann constant;

it follows that:

$$r_{H2O}\left(\frac{kg}{kg}\right) = \frac{M_{H_2O}\,N_{H2O}}{\left(\frac{PV}{kT}\right)M_{dry\,air}} \tag{68}$$

Being δ the density of the water vapor expressed in number of molecules for m^3, it follows that:

$$\delta(m^{-3}) = \frac{M_{dry\,air}\left(kg\,mol^{-1}\right)}{M_{H_2O}\left(kg\,mol^{-1}\right)} \frac{P(Pa)}{kT(K)} r_{H_2O} \left(\frac{kg}{kg}\right) \tag{69}$$

or:

$$\delta(cm^{-3}) = 10^{-4} \frac{M_{dry\,air}\left(kg\,mol^{-1}\right)}{M_{H_2O}\left(kg\,mol^{-1}\right)} \frac{P(hPa)}{kT(K)} r_{H_2O} \left(\frac{kg}{kg}\right) \tag{70}$$

Profiles are also re-distributed from the highest to the ground level, following the convention of UVSPEC.

A.2.2 LAUNCH_GRADS cloud and ice water content files creation

Cloud and ice water content profiles are used by UVSPEC to model the presence of clouds. For defining cloud water content and ice water content profiles, a file with three columns is needed:

- altitude ASL in km,
- cloud (or ice) water content (CWC, IWC) in $g\,m^{-3}$,
- effective droplet radius (in μm), as in table 12:

# z(km)	(g/m^3)	(um)
5.00	0.00	0.00
4.00	0.20	12.00
3.00	0.10	10.00

Table 12: Example of a cloud or ice water content profile file for UVSPEC

Cloud and ice water content values (CWC, IWC) are interpolated by UVSPEC between altitude values in the first column for non-zero value of CWC, IWC. Given the mixing ratio of cloud and ice water content from MM5, expressed as the ratio of $1kg$ cloud/ice water in for $1kg$ of dry air, the unit conversion formula for each level of the profile is described below. For CWC:

$$\delta_{CWC}(cm^{-3}) = 10^{-4} \frac{M_{dry\,air}\left(kg\,mol^{-1}\right)}{M_{H_2O}\left(kg\,mol^{-1}\right)} \frac{P(hPa)}{kT(K)} r_{CWC} \left(\frac{kg}{kg}\right) \tag{71}$$

$$CWC(g\,m^3) = 10^9 \delta_{CWC}(cm^{-3}) \frac{M_{H_2O}\left(kg\,mol^{-1}\right)}{N_A(mol^{-1})} \tag{72}$$

and for IWC:

$$\delta_{IWC}(cm^{-3}) = 10^{-4} \frac{M_{dry\,air}\left(kg\,mol^{-1}\right)}{M_{H_2O}\left(kg\,mol^{-1}\right)} \frac{P(hPa)}{kT(K)} r_{IWC} \left(\frac{kg}{kg}\right) \tag{73}$$

$$IWC(g\,m^3) = 10^9 \delta_{IWC}(cm^{-3}) \frac{M_{H_2O}\left(kg\,mol^{-1}\right)}{N_A(mol^{-1})} \tag{74}$$

where N_A is the Avogadro's number, $r_{CWC,IWC}\left(\frac{kg}{kg}\right)$ is the mixing ratio of cloud or ice water content, $\delta_{CWC,IWC}(cm^{-3})$ is the number of particles of cloud water or ice as a function of the mixing ratio.

At the end of data extraction and files generation, UVSPEC program can be launched using the IDL procedures `LAUNCH_UVSPEC_WITH_DATETIME_AND_ATM_PROFILES` (for ground irradiance calculation) or `LAUNCH_UVSPEC_WITH_RADIANCES_ATM_PROFILES_AND_SZA` (for radiance distribution calculation, used for simulating the radiance observed by a satellite sensor, see also `A.3` and `A.4`).

The `LAUNCH_GRADS` procedure data flow is represented in figure 61.

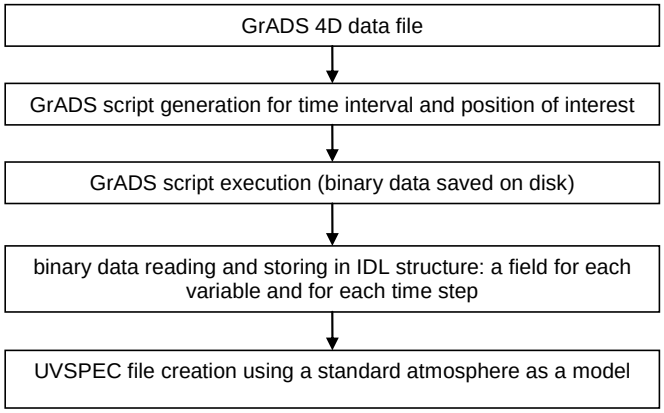

Figure 61: `LAUNCH_GRADS` procedure data flow

A.2.3 File names conventions

The atmosphere file generated by the `LAUNCH_GRADS` procedure for UVSPEC has the name syntax:

- *atm_<standard. atm. file>_<YYYYMMDDHH>.dat*, with:
  - *<standard. atm. file>* name of the standard UVSPEC atmosphere file used as a model,
  - *<YYYYMMDDHH>* year (YYYY), month (MM), day (DD) and UTC hour (HH) of the MM5 simulation step.

The cloud and ice water file names for UVSPEC have the form:

- *wc_<YYYYMMDDHH>.dat*,
- *ic_<YYYYMMDDHH>.dat*, with:
  - *<standard. atm. file>* name of the standard UVSPEC atmosphere file used as a model,
  - *<YYYYMMDDHH>* year (YYYY), month (MM), day (DD) and UTC hour (HH) of each MM5 simulation step.

Atmosphere and cloud/ice water content files are generated by the procedure `CREATE_UVSPEC_PROFILES` called by `LAUNCH_GRADS`. It is important that name syntax is not changed for the use of these files with the IDL procedures `LAUNCH_UVSPEC_WITH_DATETIME_AND_ATM_PROFILES` or `LAUNCH_UVSPEC_WITH_RADIANCES_ATM_PROFILES_AND_SZA`.

A.3 Ground irradiance simulation (LAUNCH_UVSPEC_WITH_DATETIME_AND_ATM_PROFILES procedure)

The simulation of ground irradiance in the band of interest is obtained by launching the UVSPEC radiative transfer model using the IDL procedure `LAUNCH_UVSPEC_WITH_DATETIME_AND_ATM_PROFILES`. This procedure performs the simulation of ground irradiance, at given coordinates latitude and longitude, given:

- a set of date and UTC time values (for determining the solar zenith angle);
- an atmosphere file (generated by `LAUNCH_GRADS`, see paragraph A.2.1, a window allows file selection);
- cloud and ice water content (generated by `LAUNCH_GRADS`, see paragraph A.2.2) as a function of the geopotential height;
- terrain altitude;
- atmospheric parameters: visibility, ground albedo, integrated ozone content on the atmospheric column, atmosphere and aerosol model (for constituents not defined in the provided atmospheric profiles);
- wavelength range of interest.

The procedure creates an input file for UVSPEC and executes it, writing the result of the simulation in an ASCII output file.

A.4 Simulation of the satellite observed radiance (LAUNCH_UVSPEC_WITH_RADIANCES_ATM_PROFILES_AND_SZA procedure)

The radiance observed by the MSG satellite is simulated by the IDL procedure `LAUNCH_UVSPEC_WITH_RADIANCES_ATM_PROFILES_AND_SZA`. Such a code calculates the upwelling radiance distribution at fixed altitude for given coordinates latitude, longitude and for:

- a set of solar zenith angle (SZA) values;
- a set of atmosphere files (generated by `LAUNCH_GRADS`, see paragraph A.2.1, a window allows files selection);
- cloud and ice water content (generated by `LAUNCH_GRADS`, see paragraph A.2.2) as a function of the geopotential height;
- terrain altitude;

- atmospheric parameters: visibility, ground albedo, integrated ozone content on the atmospheric column, atmosphere and aerosol model (for constituents not defined in the provided atmospheric profiles). SZA can be calculated from the filename of the atmosphere files (i.e. '$atm\_afglmw\_<YYYYMMDDHH>.dat$', where YYYY, MM, DD, HH are the year, month, day and UTC hour) or UVSPEC can be launched in a "nested loop" for each atmosphere file and for each SZA. Cloud liquid water and ice content file names are determined from the name of each atmosphere file (both the atmosphere files and the cloud/ice water content files are created by the `LAUNCH_GRADS` procedure and their filenames must maintain the syntax given by `LAUNCH_GRADS`). The procedure creates an input file for UVSPEC and executes it, writing the result of the simulation in an ASCII output file.

A.5 READ_SOUNDING_FOR_MM5

The `READ_SOUNDING_FOR_MM5` procedure reads atmospheric soundings from http://weather.uwyo.edu/upperair/sounding.html (the HTML page of results must be simply saved as a normal ASCII file) and generates the customized FORTRAN code for the **LITTLE_R** program (see **LITTLE_R** description in paragraph 5.1.7).
The program uses an original file ASCII (from MM5 distribution) written in FORTRAN as template, adding the lines with values from the sounding profile.

A.6 IDL procedure and functions developed for MM5 data reading, composite atmosphere model data creation and radiative transfer calculations

`CALCULATE_PRESSURE`
: Given two altitude values and the respective temperatures and water vapor mixing ratio, the procedure determines pressure and temperature value at sea level. The calculation is performed in the general case for wet air (considering the virtual temperature definition, see paragraph 5.1.6).

`CALCULATE_PRESSURE_DRY`
: The same calculation of `CALCULATE_PRESSURE`, in the particular case of dry air (this procedure has been used also for development and debug purposes).

`CALCULATE_REFLECTANCE`
: Calculates the reflectance along the Sun-satellite line of view. Used for generating charts for reflectance and transmittance model described in paragraph 2.8, together with the `CALCULATE_TRANSMITTANCE` procedure.

`CALCULATE_TRANSMITTANCE`
: Calculates the transmittance seen by an observer at ground in direction of the Sun. Used for generating charts for reflectance and transmittance model described in paragraph 2.8, together with the `CALCULATE_REFLECTANCE` procedure.

`CREATE_GRADS_SCRIPT`

Creates a script file for launching GrADS (see paragraph 5.3) for MM5 variables extraction. The procedure (launched by the `LAUNCH_GRADS` procedure) allows the extraction of MM5 profiles by launching GrADS: the variables of each atmospheric profile are written on disk in binary format and then read by the `READ_GRADS_BINARYFILE` procedure.

`CREATE_INPUTFILE_UVSPEC`

Given the values of:

- solar zenith angle,
- visibility,
- ground albedo,
- altitude of the ground,
- ozone content,
- atmosphere type,
- aerosol type,
- cloud water content (both for liquid water and ice) profile,
- pressure and temperature profile,
- atmosphere gas content profile,
- wavelength range,

the procedure creates an UVSPEC input file for irradiance or radiance distribution calculations.
The user can specify an output altitude (otherwise the output is generated for the ground altitude value) and a visual zenith and azimuth angles distribution: in this case UVSPEC calculates a radiance distribution (for simulating the radiance reaching the satellite sensor. See also A.3 and A.4 for a detailed description of UVSPEC launching by IDL procedures.
The atmosphere can be described also using radiosonde profiles and water density profiles (see UVSPEC manual at www.libradtran.org), although this feature has been used in development phase only, thus are to be considered obsolete.

`CREATE_UVSPEC_PROFILES`

This procedure creates an atmosphere file for each time step of a custom point of the MM5 output file grid. A structure containing the variables describing the profile is passed to `CREATE_UVSPEC_PROFILE` by the `LAUNCH_GRADS` procedure.
A further description of the atmosphere and cloud profiles generation by `CREATE_UVSPEC_PROFILES` inside the `LAUNCH_GRADS` procedure is given in A.2.1 and A.2.2.

`DATA_TO_SZA_SAA`
: Given an array of UTC date and time in ASCII format and fixed geographical coordinates, the procedure calculates the corresponding solar zenith and azimuth angles. Useful for reporting the Sun position in a spreadsheet for comparison with ground measurements. In the "standalone" use of the procedure by command prompt, arrays can be directly cut and copied into the command line. The `DATA_TO_SZA_SAA` procedure has been largely used for creating charts and analyzing ground sensor data during this thesis. Surprisingly I didn't find similar freeware IDL tools to do this in such a simple way.

`FIND_COORD_CROSSED_PIXELS`
: Finds the position and the altitude of the intersections between the MM5 data grid and the Sun-observer line of view, as described in A.1.

`HHZDDMMMYYYY_TO_INTEGERS`
: Simple ASCII string converter to hour, day, month, year integer values. Used to generate file names for MM5 binary data generated by GrADS (see also `CREATE_GRADS_SCRIPT` procedure).

`JOIN_PROFILES`
: Main procedure for composite atmosphere model creation described in A.1.

`LAUNCH_GRADS`
: Procedure for atmospheric profiles extraction from MM5 data, described in A.2.

`LAUNCH_UVSPEC_UVINDEX`
: Stand-alone launcher for UVSPEC radiative transfer model (see sec. 4). The procedure allows setting of atmospheric parameters, standard atmosphere model and cloud water profiles. It uses the `CREATE_INPUTFILE_UVSPEC` and the `READ_UVSPEC_DATA IDL` procedures. Despite the name, it manages custom wavelength intervals

`LAUNCH_UVSPEC_WITH_DATETIME_AND_ATM_PROFILES`
: Procedure for UVSPEC launching for ground irradiance calculation using user-defined atmosphere and cloud profiles. The procedure is fully described in A.3.

`LAUNCH_UVSPEC_WITH_RADIANCES_ATM_PROFILES_AND_SZA`
: Procedure for UVSPEC launching for satellite received radiance calculation using user-defined atmosphere and cloud profiles. The procedure is fully described in A.4.

`PATHWIN_TO_CYGWIN`
: Converter for Windows-like file paths to Linux/UNIX pathname syntax. Used for script creation for Cygwin-compiled code. For a description of Cygwin, a Linux environment emulator and compiler for Windows based systems, see www.cygwin.com and appendix E.

`READ_GRADS_BINARYFILE`
: The function reads the binary files created by GrADS in reading MM5 output data. See `LAUNCH_GRADS` and `CREATE_GRADS_SCRIPT` procedures description.

`READ_STRINGARRAY_FROM_ASCII`
: Reads an ASCII file returning the corresponding string array. Empty and commented lines can be ignored. This procedure has been used for reading the setting files for various procedures and functions.

`READ_UVSPEC_DATA`
: This procedure executes UVSPEC (see sec. 4) and creates an ASCII output file with columns:

  - filename_input_UVSPEC,
  - wavelength range,
  - solar zenith angle,
  - visibility,
  - ground albedo,
  - ground altitude,
  - ozone content,
  - atmosphere and aerosol type,
  - Direct ground irradiance in the wavelength range,
  - Diffuse (*downwelling*) irradiance in the wavelength range,
  - Diffuse *upwelling* irradiance in the wavelength range,
  - Radiance distribution (if user-specified).

  Input files for UVSPEC are created by the `CREATE_INPUTFILE_UVSPEC` procedure. Geometrical and atmospheric parameters are not directly used but needed to be written in the output file. See also the `CREATE_INPUTFILE_UVSPEC` procedure description.

`STR_REPLACE, STR_SOSTITUTE`
: As the name says, these functions substitute characters in strings. Useful for string arrays.

`STRING_TO_DATE_ELEMENTS`
: Simple ASCII date and UTC time string converter to the corresponding integer values. Widely used in this work, it works efficiently with large string arrays (i.e. for processing large ASCII files containing sensor data).

`TRANSM_UVSPEC`
: This function launches UVSPEC for transmittance calculation in each layer of the atmosphere defined by a UVSPEC input file (any file created by the `CREATE_INPUTFILE_UVSPEC` procedure). The function returns an array with the values of transmittance at user defined altitude values.

The following list describes the external software and IDL code used by the procedures and functions in this section:

- DAY_OF_YEAR: IDL function for calculating the day of year. Freely downloaded from:

www.fz-juelich.de/icg/icg-1/idl_icglib/idl_source/idl_lib/MartinSchultz3/day_of_year.pro. Written by Bob Yantosca, 1997, Harvard University.

- ZENSUN: IDL procedure for calculating solar position information as a function of geographic coordinates, date and time. Freely downloaded from: 132.248.1.102/~morisset/idl_cours/IDL/index_local.htm. Written by P. Ricchiazzi, 1992, Earth Space Research Group.
- **Cygwin**: Linux-like environment for Windows. Used to compile UNIX and Linux code in Microsoft Windows environment[34]. Freely downloaded from www.cygwin.com.
- **GrADS**: Freely downloadable software for accessing and extracting profiles of atmospheric constituents for a selected pixel of the MM5 output data (see paragraph 5.3 and www.iges.org/grads).

[34]ZENSUN, DAY_OF_YEAR and Cygwin have been used also in MSG data elaboration, see paragraph D.5.

B The leapfrog algorithm

As described in par. 5.1.4 and 5.1.6, the resolution of MM5 equation is performed by a leapfrog algorithm, that is the tendencies at time n are used to step the variables from time $n-1$ to $n+1$. However, for certain terms, the model time step is too long for stability: these terms have to be calculated with a shorter time step, therefore the algorithm resolves "fast" terms (pressure gradients, divergence terms and u, v, w, p') by updating more frequently these variables when the time step is split., as shown from figure 62 to figure 64.

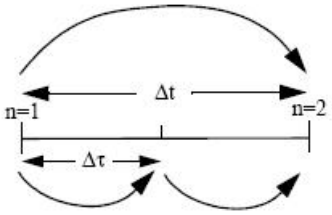

Figure 62: First time step of leapfrog algorithm. Figure from MM5 documentation (www.mmm.ucar.edu/mm5).

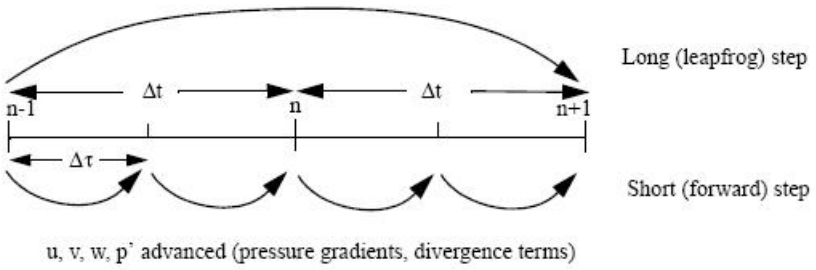

Figure 63: Time step n of leapfrog algorithm. Variables at time n are used to step the variables from time $n-1$ to $n+1$. Since pressure gradients, divergence terms, u, v, w, p' are "fast" terms, they are updated more frequently. Figure from MM5 documentation (www.mmm.ucar.edu/mm5).

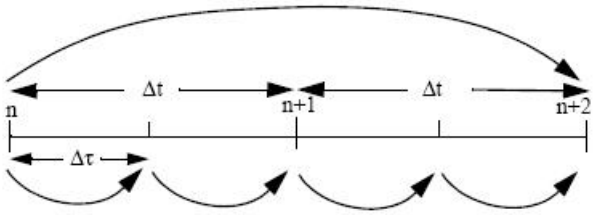

Figure 64: Time step $n + 1$. From MM5 documentation (www.mmm.ucar.edu/mm5).

C The MM5 model customization

MM5 schematic diagram shown in figure 65 shows the order of the programs, the flow of the data, and describes the primary functions.

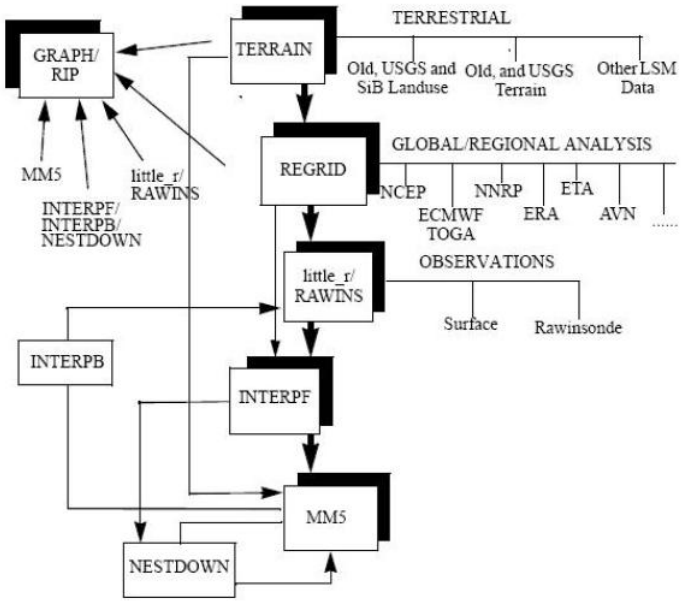

Figure 65: MM5 modeling system flow chart (from www.mmm.ucar.edu/mm5).

As described in paragraph 5.1.7, MM5 is a regional model, so it requires initial conditions and boundary condition to run, with gridded data covering the entire time period. Terrestrial and isobaric meteorological data are horizontally interpolated by the programs **TERRAIN** and **REGRID** from a latitude-longitude grid to a variable high-resolution domain. The code needs to be edited and recompiled for setting custom domain and parameters. The changes needed for customizing the code are now described.

In the *TERRAIN/terrain.deck* file the following parameters need to be specified:

- latitude and longitude extension range and spatial resolution step (we chose a 5 km grid centered on the position of the ground sensors in Livorno, at coordinates 43.50°N, 10.32°E);
- projection type (Mercator projection has been used);
- dominion type (one or two way nested).

The last option allows the user to set nesting between domains (see paragraph 5.1.3). For using this option, the position of any domain needs to be specified with respect to the position of the mother domain, although only runs using a single domain have been needed for this work. It is possible to ask the code for the creation of an output file containing the coordinates of each point of the grid: the edges of this grid have been used to download meteorological data from stations inside the grid boundaries, for setting further starting conditions for MM5 to run. Meteorological data have been downloaded from N.O.M.A.D.S. servers [41] in GRIB data format (http://nomads.ncdc.noaa.gov); then they are checked and interpolated by the REGRID program.

The REGRID program is made up of two modules:

- Pregrid: for reading meteorological data;
- Regridder: for grid interpolation of the data.

The file *REGRID/pregrid/pregrid.csh* needs to be modified for setting:

- data type and files names for Pregrid;
- path for sea surface temperature, snow cover and soil type files, generated from GRIB data;
- pre-defined template for GRIB data reading;
- date, time and time step of the data.

Pregrid will read the GRIB data files for generating the sea surface temperature, snow cover and soil type data as input for the **Regridder** program. Setting the same data and time interval in the file *REGRID/regridder/namelist.input* allows the interpolation of the atmospheric profiles by **Regridder** using the **Pregrid** generated data.

Since the interpolation does not provide mesoscale details, the interpolated data may be enhanced with station data (ground measured data and vertical profiles by atmospheric sounding). The programs **RAWINS** or **LITTLE_R** allow generating data with a structure similar to the ones generated by **Regridder**. This technique (objective analysis) uses a typical algorithm (Cressman scheme) for calculating a new grid corrected for station provided data. In the Cressman scheme, several successive scans nudge a first-guess field toward the neighboring observed values. For each observation (from stations or radiosonde) an influence area can be defined. Usually the area is a circle around the point, but the user can define the shape of this area differently (i.e. an ellipse in the direction of the wind). The gridded data are the first-guess field: each grid point

is then adjusted by taking into account all the observations whose area of influence contains the point. The differences between the first-guess field and the observations are added to the value of the first-guess using a distance weighted average. When all grid points have been adjusted, the new field is used as first guess for another adjustment. The scheme is then iterated using a smaller radius of influence. Using objective analysis allows the program to improve the quality of the low resolution gridded data, thus increasing the accuracy of the simulation between two consecutive observations from stations. Input variables used by MM5 are:

- pressure;
- altitude;
- temperature;
- dew point temperature;
- wind direction;
- wind speed;
- sea level pressure;
- station position;
- observation UTC time.

An example of input data for objective analysis is shown in table 14.

16144 S. Pietro Capofiume Observations at 00Z 17 Jan 2008

PRES	HGHT	TEMP	DWPT	RELH	MIXR	DRCT	SKNT	THTA	THTE	THTV
hPa	m	C	C	%	g/kg	deg	knot	K	K	K
1007	11	6.8	6.2	96	5.94	270	9	279.4	295.8	280.4
1000	67	6.2	6.2	100	5.98	280	8	279.4	295.8	280.4
990	150	5.8	5.8	100	5.87	269	6	279.8	296	280.7
...	...	...	...	...	...	...	...	...	...	...
36.1	22027	-66.5	-86.6	4	0.01	265	85	533.7	533.8	533.7
36	22044	-66.5	-86.6	4	0.01	265	85	534.2	534.2	534.2
35.9	22061	-66.5	-86.5	5	0.01	534.6	534.7	534.6		

Station information and sounding indices

Station number: 16144
Observation time: 080117/0000
Station latitude: 44.65
Station longitude: 11.61
Station elevation: 11.0
...
...
Precipitable water [mm] for entire sounding: 21.54

Table 14: Example of radiosonde data from University of Wyoming (http://weather.uwyo.edu/upperair/sounding.html)

The IDL procedure `READ_SOUNDING_FOR_MM5` (see IDL procedures description, paragraph A.5) has been written for generating, from downloaded station data, the customized FORTRAN code for **LITTLE_R**.

The output of Regridder is the file *REGRID_DOMAIN*$< i >$ (where i is the domain index: $i = 1$ if a single domain has been used, $i = 1, 2, ...$ in case of nested domains), that will be merged with station or ground measured data (if present) by the **INTERPF** module. The output of **Regridder** and **LITTLE_**R needs to be redirect to **INTERPF** input by modifying the *INTERPF/namelist.input file*, setting:

- date, time and time interval of input data (the same specified for the preceding blocks);
- sigma level (usually the standard levels don't need to be modified: it's the case of this work);
- top pressure (to "cut" the atmosphere at the top).

The Program **INTERPF** performs the vertical interpolation from pressure levels to the sigma coordinate system of MM5 (as explained in paragraph 5.1.2). **INTERPF** creates three files:

- *BDYOUT_DOMAIN1*: boundary condition;
- *LOWBDY_DOMAIN1*: low layer conditions;
- *MMINPUT_DOMAIN1*: input data. These files contain the starting conditions as input for the MM5 program (together with the files generated by the **TERRAIN** module).

To start MM5 the input files need to be copied in the *MM5/run/* folder and the file *MM5/configure.user* needs to be changed for MM5 recompiling. The *MM5/configure.user* file needs the same parameters of the other module to be replicated (number of dominions, dominion dimensions, number of sigma levels) and allows the user to choose the type of the parametrization for taking into account the seasonal and local characteristics. Cumulus cloud models are needed for taking into account sub-grid phenomena such as convection and precipitations. Possible parametrization for cumulus cloud are listed below.

None: uses no cumulus parametrization at grid sizes smaller than 5-10 km.

Anthes-Kuo: applicable to larger grid sizes greater than 30 km, it predicts low resolution precipitations [30].

Grell: simple single-cloud scheme [24] with updraft and downdraft fluxes and compensating motion determining heating/moistening profile; scheme used for 10-30 km grid sizes.

Arakawa-Schubert: multi-cloud scheme similar to Grell scheme. Suitable for scales larger than 30 km [2].

Fritsch-Chappell: suitable for 20-30 km scales due to single-cloud assumption [22].

Kain-Fritsch: similar to Fritsch-Chappell, but using a more sophisticated cloud-mixing scheme; this scheme predicts both updraft and downdraft properties and also predicts clouds and precipitations [27].

Betts-Miller: based on a reference thermodynamic profile over a given period [5, 6, 7, 26]. This scheme is suitable for scales greater than 30 km.

Kain-Fritsch 2: A new version of Kain-Fritsch model [28] including shallow convection.

Shallow Cumulus: handles non-precipitating clouds. Assumed having a strong entrainment and small radius, no downdrafts, and uniform clouds. Based on Grell and Arakawa-Schubert schemes.

Also for moisture schemes the user has to set the proper parametrization. The following parametrization takes into account the microphysical processes for cloud and precipitation prediction. Possible models are:

- Dry: no moisture prediction; no water vapor;
- Stable precip: non convective precipitation: large scale saturation removed and rained out immediately; no rain evaporation or explicit cloud prediction;
- Warm rain: cloud and rain water fields predicted explicitly with microphysical processes but no ice phase process;
- Simple ice: adds ice phase processes to warm rain parametrization; no supercooled water and immediate melting of snow below freezing level;
- Mixed-phase: adds supercooled water to simple ice model [37] and allows for slow melting of snow but no graupel processes;
- Goddard microphysics: it includes additional equations for prediction of graupel so it's suitable for cloud-resolving models [31, 46, 47];
- Reisner graupel: based on mixed-phase scheme but adding graupel and ice concentration prediction; also suitable for cloud-resolving models;
- Schultz microphysics: a highly efficient and simplified scheme [42] designed for fast computation time; it represents water phase change and precipitation processes; it considers ice and graupel processes and well describes mesoscale convection.

MM5 documentation suggests the correct parametrization for the selected grid step and the desired output (in this thesis the Kain-Fritsch 2 parametrization for cumulus scheme and the Schultz parametrization for moisture scheme have been chosen).

D MSG data description

D.1 Description of MSG xRIT image file

Level 1.5 image data are obtained from the processing of satellite raw data (named Level 1.0 data) and they are the main product of the Meteosat Second Generation system. Level 1.5 data are corrected for radiometric and geometric distortions and geolocated using a standardized projection. Images are disseminated as HRIT (High Rate Information Transmission) or LRIT (Low Rate Information Transmission) files together with ancillary meteorological data derived from the analysis of all MSG bands. The so called xRIT format contains coefficients for extracting, calibrating and georeferencing the radiance image and the meteorological products. xRIT files can be received using a common parabola and a decrypting key on the dissemination channel of Eumetsat, by requesting appropriate authorization to Eumetsat.

The single acquisition (every 15 minutes) or the corresponding products (i.e. CLM, see paragraph 6.3) are divided into a series of xRIT format files (HRIT or LRIT).

Each group of files starts with a prologue (PRO) file (in case of radiance images it contains the parameters for image georeferencing and calibrating) and a fixed number of segment files (24 segments for an HRV image, 6 segments for CLM files).

The code identifies the files of the same group by the file name syntax (examples of fields for the generic xRIT file are summarized in table 15).

As anticipated in paragraph 6.2, all segment files need to be decompressed, image data have to be extracted from each segment and joined to obtain the final image. Decompression of the xRIT file is performed by calling (through the IDL code) the command line tool for decompression of HRIT/LRIT files xRITDecompress (distributed by Eumetsat: www.eumetsat.int). The reading of the data contained in the decompressed file and the joining of each data segment is performed by the IDL procedure `read_HRIT` (see paragraph D.5), allowing image reconstruction (units are at this stage expressed in digital numbers). Parameters for passing to radiance physical units are read from the PRO file (see paragraph D.3). Figures 66 and 67 show the division of the data in segments.

D.2 Image georeferencing

MSG images are referred to a fixed grid (in the following lines named MSG grid). Data acquired from SEVIRI instrument (Level 1.0 data) are corrected and referenced (Level 1.5 data) with respect to this grid, thus each pixel of the MSG grid can be associated to the corresponding latitude and longitude ground coordinates[35]. The pixel of the image read from the xRIT file must be positioned on the grid for overlapping the corresponding point on the ground, that is, the image needs to be positioned on the MSG grid.

For all bands but HRV (see figure 68) the data have already the form of an array with the same dimension of the MSG grid[36], and no further positioning

[35] Routines for passing from grid coordinates to geographic coordinates are freely distributed from Eumetsat website (www.eumetsat.int) and have been re-adapted for the use in this work.

[36] The grid for higher resolution data (i.e. HRV band) has pixel dimension multiple with respect to low resolution grids (i.e. other MSG channels or MPEF data grid), so that different

File name description	File name example							
file HRIT PRO	H - 0 -	MSG2__	-MSG2_____	- _____	-PRO_____	-	200811191545	- __
file HRIT band HRV segm. 20	H - 0 -	MSG2__	-MSG2_____	-HRV_____	- 000020___	-	200810290615	- C_
file LRIT MPEF CLM segm. 6	L - 0 -	MSG2__	-MPEF_____	-CLM_____	- 000006___	-	200811101045	- __
file LRIT MPEF CLM PRO	L - 0 -	MSG2__	-MPEF_____	-CLM_____	-PRO_____	-	200811191530	- __
Field description	*Channel ID*	*Version*	*Dissemination*	*Product ID1*	*Product ID2 (band / product name)*	*Product ID3 (PRO or segment number)*	*Product ID4 (acquisition date YYYYMMDDhhmm)*	*Flags compressed and/or encrypted*
n. of characters	1	3	6	12	9	9	12	2

Table 15: MSG file name syntax: the file name fields describe the acquisition starting time and the file content. Examples are provided for different file types.

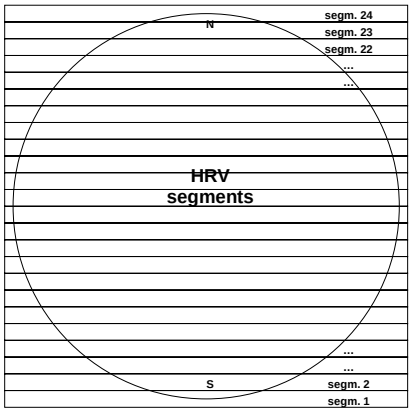

Figure 66: HRV image segmentation: a full image of the Earth is made up of 24 segments.

is needed. For HRV images, due to the higher resolution, only a portion of all the image (corresponding to half of the grid) is acquired, using the alternative coverage, with the upper part of the image positioned on Europe and the lower part moving, following the Sun apparent path during the day on Indian Ocean, Africa and Atlantic Ocean (see figure 68, case b).

For image positioning on the MSG grid, offsets for each portion of the image are provided in the prologue segment of the HRIT file for each acquisition (figure 69). IDL functions for calculating geographical coordinates from pixel coordinates are provided by Eumetsat (www.eumetsat.int). A further development of these functions is used in the chain.

grids can be scaled of an integer factor for overlapping.

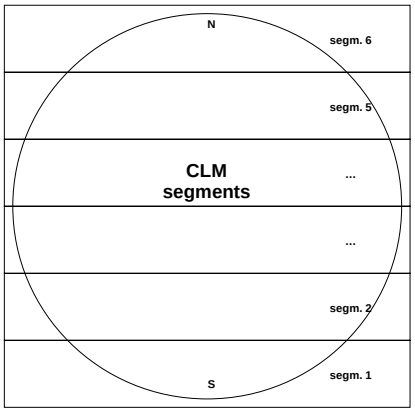

Figure 67: CLM segmentation: the full CLM data is made up of 6 segments (at lower resolution with respect to radiance images).

D.3 MSG HRV image calibrating

This radiometric scale for passing from digital numbers to physical units is provided via two parameters (CAL_slope and CAL_offset) in the image file header. Thus, the radiance L_i in the $i-th$ band can be calculated from digital number value DN as:

$$\begin{aligned} L\left(\frac{mW}{m^2\ sr\ cm^{-1}}\right) = \mathsf{CAL\_offset}\ \left(\frac{mW}{m^2\ sr\ cm^{-1}}\right) + \\ +\mathsf{CAL\_slope}\ \left(\frac{mW}{m^2\ sr\ cm^{-1}}\ counts^{-1}\right) \cdot DN\ (counts) \end{aligned} \tag{75}$$

The calibration parameters are read from the PRO file using the IDL procedure `READ_CALIBR_COEFF` (see paragraph D.5).

D.4 The MSG data processing chain

The so-called MSG processing chain is an IDL procedure used in this work to select, read and calibrate MSG images in HRV band for determining the cloud index using clear sky albedo data (generated by a separate chain, as introduced in paragraph 6.5).

The program performs a selection of the user-defined MSG PRO files (by defining in input the time range of the data to be processed or by direct selection of the files of interest) and checks for the existence of all the segments corresponding to each PRO file.

The entire procedure works in an array-oriented environment (taking advantage of the flexibility of the IDL language in operating with large data arrays): images and ancillary data are maintained and processed as 2D matrices).

Although the algorithm could process the entire image of the Earth acquired by MSG, only a cutout of the image has been used in this work (the data used lay in the segments 20 to 23 of the entire acquisition, in practice Italy only[37])

[37] In fact considering an even smaller zone (tens of km) around the point of interest (where ground sensors are placed) would have been sufficient because the cloud index has been calculated only around a single point. Computation time is sufficiently short, anyway, to allow the processing of the whole of Italy for having visual control of mesoscale cloud distribution:

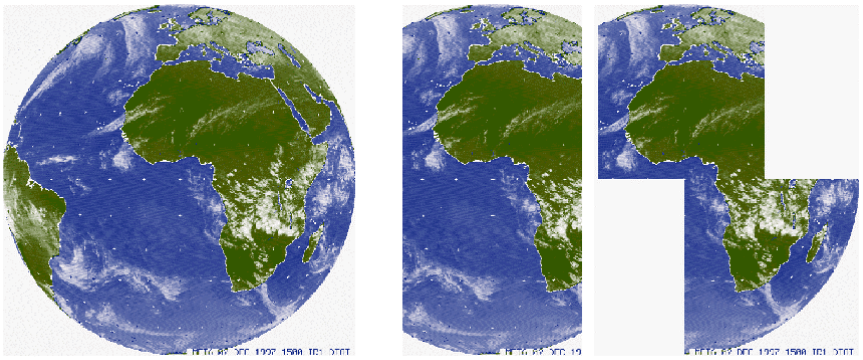

(a) (b)

Figure 68: Earth coverage for MSG channels for all bands except HRV (a) and nominal and alternative coverage for HRV band. At the moment HRV images are acquired using alternative coverage, with a southern and a northern part of the HRV image having different positions in East-West direction. From Eumetsat documentation [20].

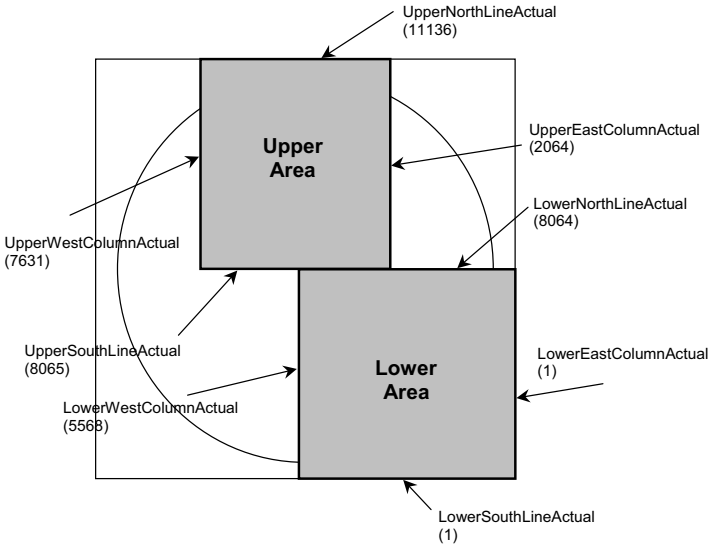

Figure 69: Example of alignment and numbering of the HRV image offset with respect to the HRV reference grid. The image in the segments of interest has to be positioned on the reference MSG grid. From Eumetsat documentation [20].

As introduced in paragraph 6.5, the processing chain needs the pre-calculated clear sky albedo data, stored on disk and read for calculating the cloud index. Thus, the dimension of the clear sky albedo data fix the dimension of any other array data: latitude, longitude, solar zenith and azimuth angles, visual (satellite) zenith and azimuth angles are matrices corresponding to the cutout used during clear sky albedo image generation. This way of processing satellite and geometrical and geographical ancillary data, although requiring a large usage of memory, allows fast calculations. Moreover, fixed data can be calculated once and stored on disk (i.e. latitude and longitude, visual angles, acquisition delay for each pixel, clear sky albedo, etc.). Image-dependent parameters (i.e. solar azimuth and zenith angles for each pixel) are calculated at runtime, since they depend on the acquisition time of each image. The algorithm flow is shown in figure 70.

For generating a clear sky albedo image, a different algorithm has been implemented in IDL. A single image of clear sky albedo is the average of cloud free pixels of a time series of approximately 15 days. The clear sky albedo image is stored on disk and can be used to process a data set of multiple days of acquisition. A limit of the usage of the clear sky albedo data is given by the change of the ground albedo (due to vegetation cover change, presence of burned or ploughed soil, etc.).

A considerable limitation to the use of the clear sky albedo file is given by snow covered soil. Such a terrain is characterized by a fast change in ground albedo. Thus the clear sky albedo for a snow covered pixel cannot be representative of ground albedo when the cloud index is calculated (snow contribution can drastically change the ground albedo in timescales of hours), bringing to unpredictable results for the cloud index value of cloud covered pixels. During this work, datasets have been selected taking only snow-free pixel for the period of interest.

The algorithm for clear sky albedo calculation is shown in figure 71. The list of the procedures/functions written in IDL is provided in the following paragraph.

D.5 IDL procedures and functions developed for MSG data processing

`CALCULATE_RO_DAGESTAD`
: Calculates the apparent albedo for the current MSG HRV image.

`CALCULATE_RO_GO_DAGESTAD`
: Calculates the ground albedo normalized to a co-scattering angle zero.

`CALIBRA_IMAGE`
: Converts an MSG radiance image applying gain and offset values for passing from digital numbers to physical units (radiance).

`CARICA_LAT_LON`
: Cuts the latitude and longitude 2D arrays corresponding to the MSG reference grid at fixed coordinates (corresponding to the clear sky albedo data).

computational bottlenecks are primarily in the xRIT file decompressing and reading, not in data processing.

`CARICA_VIEWANGLE`
: Calculates the 2D array containing the solar zenith and azimuth angle values corresponding to a 2D array of longitude and latitude values in input. Data are calculated once and stored on disk.

`CHECK_PRO_AND_SEGMENTS`
: Given an array of PRO filenames, the procedure verifies the presence of all segments (used to process only PRO files having all segments, both for HRV band and CLM data).

`CLEAR_SKY_GENERATOR`
: Main procedure for clear sky albedo calculation.

`CLOUD_INDEX`
: Calculates the cloud index from the apparent albedo and the clear sky albedo 2D arrays.

`CLOUD_INDEX_FROM_MSG`
: Main procedure for cloud index calculation.

`CONVERT_ROGO_TO_RO`
: Calculates the apparent reflectance (albedo) for the current co-scattering angle from the normalized ground albedo. The normalized ground albedo is calculated for a co-scattering angle zero during the clear sky albedo data generation.

`CREA_MSG_SCANTIME_MATRIX`
: Creates a 2D array corresponding to the latitude and longitude 2D arrays containing the acquisition delay for each pixel of the MSG image in HRV band.

`CROSS_MSG_CHECK`
: Compares two string arrays with xRIT file names and returns an arrays containing the name of the corresponding elements (optionally chronologically ordered). Used to process MSG files having a corresponding CLM file.

`GEOREFER_GRID_MSG`
: Creates 2D arrays of latitude and longitude corresponding to the HRV MSG reference grid 11136 x 11136 pixels.

`MSGFILENAME_TO_ORA_DATA`
: Extracts acquisition date and time from a xRIT file.

`MSGNAME_TO_SINGLE_FIELDS`
: Extracts single fields and acquisition time from a xRIT file.

`READ_CALIBR_COEFF`
: Reads the Calibration Coefficients Record and the Image Description Record of the HRIT PRO file[38]. Calibration coefficients are used to convert the MSG HRV image from digital numbers to physical units (radiance).

`READ_CLM`
: Extracts the CLM data in GRIB2 format from each CLM segments. Data are converted from GRIB2 to binary by launching the executable **WGRIB2**. Finally the CLM mask is read from binary.

[38] See p. 85-86 and 88 in 'Level 1.5 data description 2005 - ICD_105_30.pdf' from www.eumetsat.int for the complete file records description.

`READ_HRIT`
: Reads a MSG HRV image in HRIT compressed format segment by segment. It uses the Wavelet decompression tool xRITDecompress.

`READ_HRIT_UNCOMPRESSED`
: Reads an uncompressed HRIT segment file and returns the corresponding MSG HRV image as a 2D array.

`READ_STRINGARRAY_FROM_ASCII`
: Reads an ASCII file returning a string array with an element for each line of the ASCII file. Optionally it ignores the lines starting with a custom comment symbol and the empty lines.

`SELECTFILES_HRIT`
: This function selects one or more HRIT PRO files given a time range. It is used to select xRIT files to be processed.

`ZENITH_MSG`
: Calculates the 2D array containing the solar zenith and azimuth angle values corresponding to a 2D array of longitude and latitude values in input.

The following list describes the external software and IDL code used in IDL procedures/functions during the development of this work :

- **xRITDecompress**: Tool from the Public Wavelet Transform Decompression Library from www.eumetsat.int, freely downloadable for Windows, Linux and Solaris operative systems.
- **SEVIRI Pre-processing Toolbox**: IDL code (modified for the purposes of this work) from www.eumetsat.int. Used for HRV grid georeferencing and MSG visual zenith and azimuth angles calculation for each pixel of the MSG reference grid.
- **WGRIB2**: GRIB2 file reader from: www.cpc.noaa.gov/products/wesley/wgrib2.
- DAY_OF_YEAR: IDL function for calculating the day of year. Freely downloaded from: www.fz-juelich.de/icg/icg-1/idl_icglib/idl_source/idl_lib/MartinSchultz3/day_of_year.pro. Written by Bob Yantosca, 1997, Harvard University.
- ZENSUN: IDL procedure for calculating solar position information as a function of geographic coordinates, date and time. Freely downloaded from: 132.248.1.102/~morisset/idl_cours/IDL/index_local.htm. Written by P. Ricchiazzi, 1992, Earth Space Research Group.
- **Cygwin**: Linux-like environment for Windows. Used to compile UNIX and Linux code in Microsoft Windows environment. Freely downloaded from www.cygwin.com.

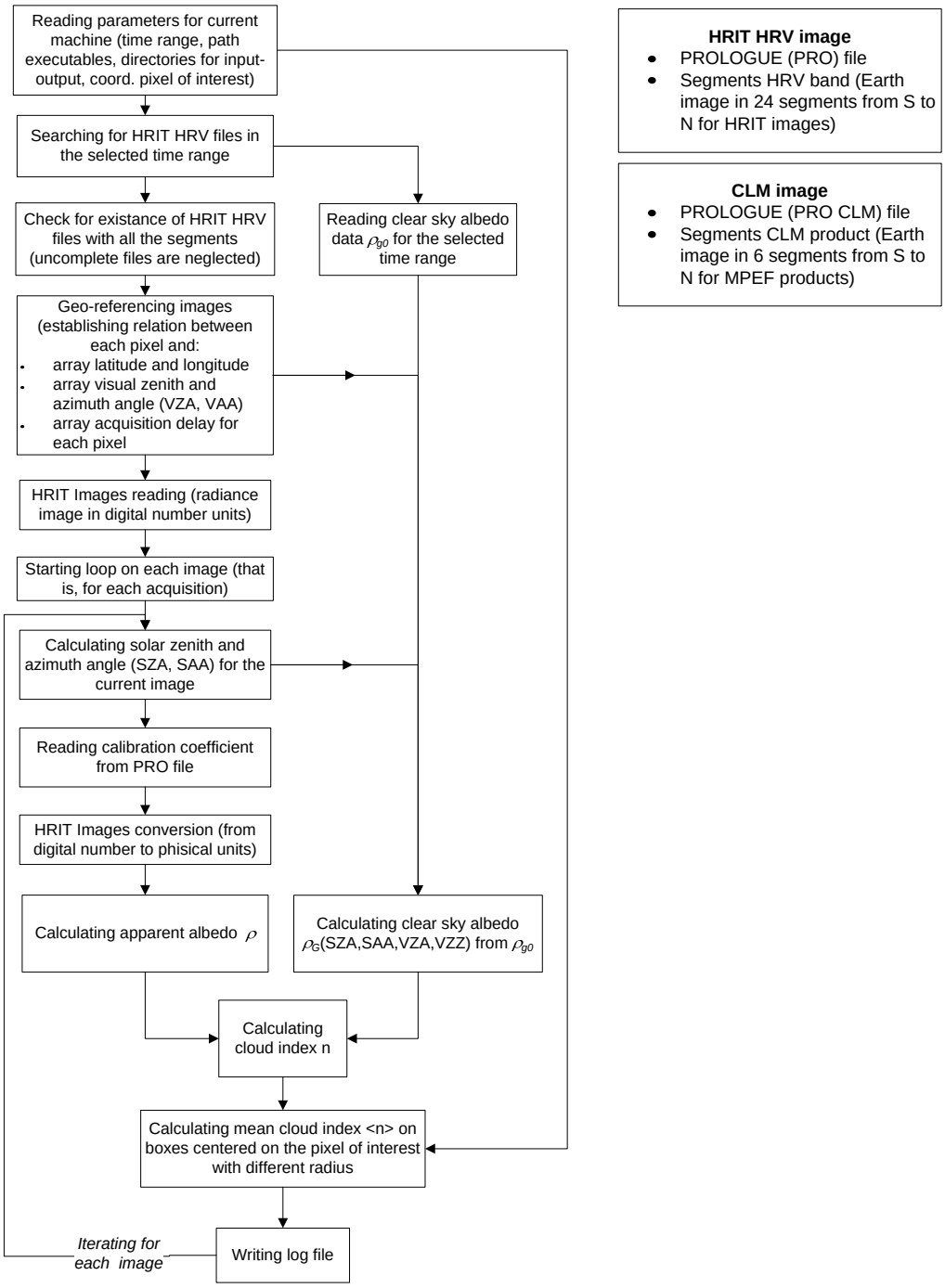

Figure 70: `CLOUD_INDEX_CALCULATOR` IDL procedure scheme. The procedure decompresses, reads and calibrates the MSG image in HRV band and, using the clear sky albedo data, calculates the cloud index.

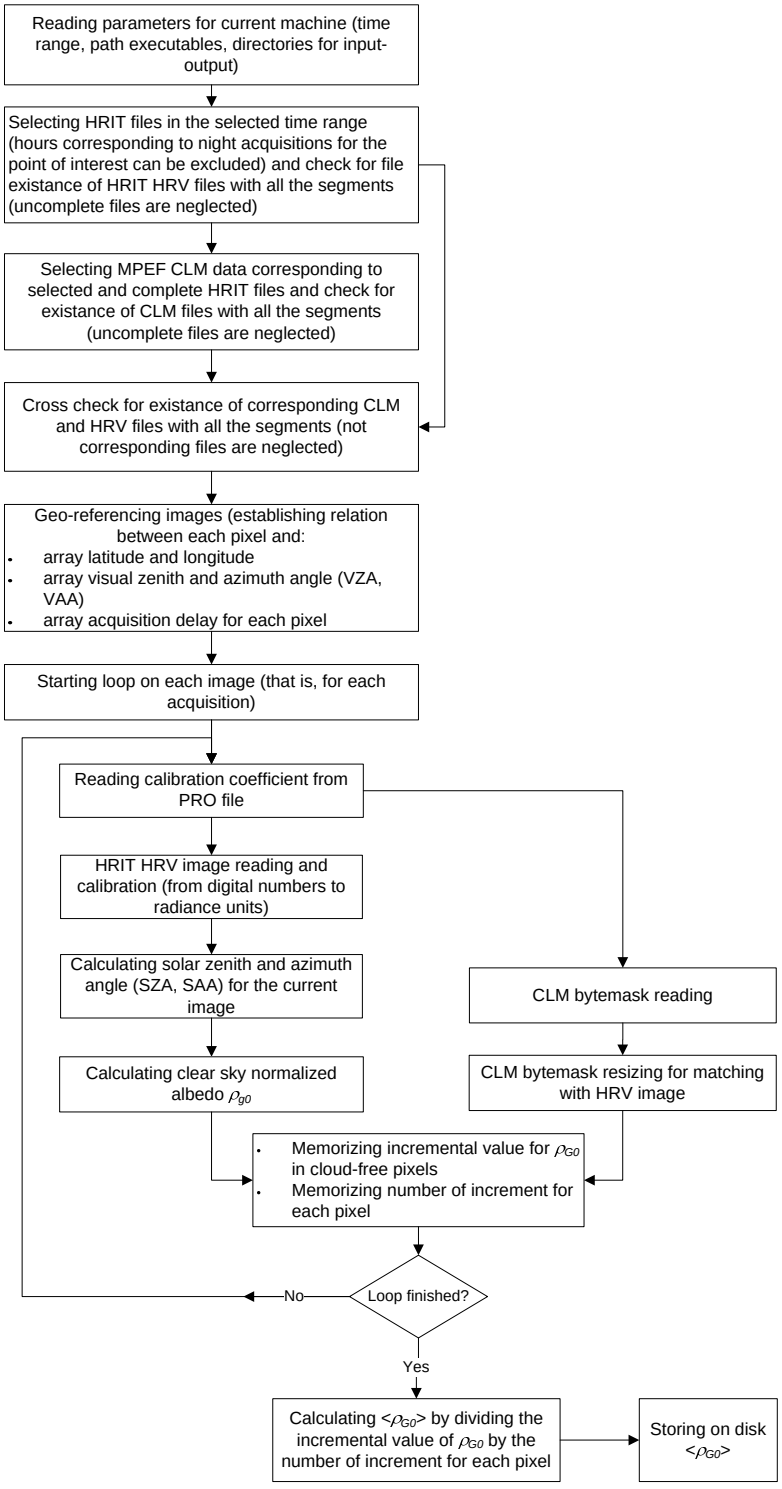

Figure 71: `CLEAR_SKY_GENERATOR` IDL procedure scheme. The clear sky image is calculated by averaging on cloud free pixels of a time series of MSG images and it is stored on disk.

E Notes on the software environment

The software written for the purposes of this work has been developed using IDL Version 6.2 for Microsoft Windows, © 2005, Research Systems, Inc. IDL codes can be freely executed on different operative systems (Windows, Macintosh, UNIX, Linux) by the use of the IDL Virtual Machine, a runtime version of IDL that allows execution of IDL programs without needing a license. Procedure and functions described in this work have been developed on a PC with Microsoft Windows XP and Vista operative systems.

External software released for Linux/UNIX environment has been compiled using the freely downloadable application Cygwin (www.cygwin.com), a Linux environment emulator and compiler for Windows based systems.

All the software has been tested on different machines. Minimum requirements for running the IDL code described in this work are:

- RAM: 512 Mb;
- Processor: Intel Pentium 4 2.66 GHz
- OS: Microsoft Windows XP or Vista

References

[1] Ahmad Z., Bhartia P.K., Krotkov N., 2004: Spectral properties of backscattered UV radiation in cloudy atmospheres. J. Geophys. Res., 109, D01201.

[2] Arakawa, A., and W.H. Schubert, 1974: Interaction of a cumulus cloud ensemble with the large-scale environment; Part I. J. Atmos. Sci., 31, 674-701.

[3] Berck A., Bernsten L.S., and Robertson D.C., 1989: MODTRAN: A Moderate Resolution Model for LOWTRAN7. Air Force Geophysics Laboratory, Hanscom AFB, MA, GL-TR-89-0122, pp.38.

[4] Berk A., Anderson G.P., Acharya P.K., Chetwynd J.H., Bernstein L.S., Shettle E.P., Matthew M.W., and Adler-Golden S. M., 1999: Modtran4 User's Manual. Air Force Research Laboratory.

[5] Betts, A.K., 1986: A new convective adjustment scheme. Part I: Observational and theoretical basis. Quart. J. Roy. Meteor. Soc., 112, pp. 677-692.

[6] Betts, A.K., and Miller M.J., 1986: A new convective adjustment scheme. Part II: Single column tests using GATE wave, BOMEX, ATEX and Arctic air-mass data sets. Quart. J. Roy. Meteor. Soc., Vol. 112, Issue 473, pp. 693 - 709.

[7] Betts, A.K., and Miller M.J., 1993: The Betts-Miller scheme. Chapter in The representation of cumulus convection in numerical models of the atmosphere. Eds. Emanuel K.A. and Raymond D.J., American Meteorological Society.

[8] Beyer H.G., Costanzo C., Heinemann D., 1996: Modifications of the Heliosat procedure for irradiance estimates from satellite images. Solar Energy Vol. 56, Issue 3, pp. 207-212.

[9] Bovensmann H., Burrows J.P., Buchwitz M., Frerick J., Noël S., and Rozanov V.V., 1999: SCIAMACHY: Mission Objectives and Measurement Modes. J. Atm. Sci., Vol. 56, pp. 127-150.

[10] Cano D., Monget J.M., Albuisson M., Guillard H., Regas N., and Wald L., 1986: A method for the determination of the global solar radiation from meteorological satellite data, Solar Energy 37, pp. 31-39.

[11] Courant R., Friedrichs K., and Lewy H., 1928: Über die partiellen Differenzengleichungen der mathematischen Physik. Mathematische Annalen, Vol. 100, No. 1, pp. 32–74.

[12] Dagestad K.F., and Seth J.A., 2007: A modified algorithm for calculating the cloud index, Solar Energy, Vol. 81, No. 2, pp. 280-289.

[13] Dahlback A., and Stamnes K., 1991: A new spherical model for computing the radiation field available for photolysis and heating at twilight. Planet. Space Sci., Vol. 39, pp. 671-683.

[14] Diabaté L., Mossou G., Wald L., 1989: Description of an operational tool for determining global solar radiation at ground using geostationary satellite images. Solar Energy, Vol. 42, pp. 201-207.

[15] Dubovik O., Smirnov A., Holben B.N., King M.D., Kaufman Y.J., Eck T.F., and Slutsker I., 2000: Accuracy assessments of aerosol optical properties retrieved from AERONET Sun and sky-radiance measurements. J. Geophys. Res., Vol. 105, pp. 9791-9806.

[16] Engelsen O. and Kylling A., 2005: Fast simulation tool for ultraviolet radiation at the Earth's surface. Optical Engineering, 44 (4), 041012.

[17] Eumetsat documentation, 1999: LRIT/HRIT Global Specification - Coordination Group for Meteorological Satellites. CGMS 03, Issue 2.6.

[18] Eumetsat documentation, 2005: MSG Ground Segment LRIT/HRIT Mission Specific Implementation. EUM/MSG/SPE/057.

[19] Eumetsat documentation, 2007: Cloud Detection for MSG - Algorithm Theoretical Basis Document. EUM/MET/REP/07/0132.

[20] Eumetsat documentation, 2007: MSG Level 1.5 Image Data Format Description. EUM/MSG/ICD/105.

[21] Evans, K. F., 1998: The spherical harmonic discrete ordinate method for three-dimensional atmospheric radiative transfer. J. Atmos. Sci., 55, pp. 429-446.

[22] Fritsch J.M., and Chappell C.F., 1980: Numerical prediction of convectively driven mesoscale pressure systems. Part I: Convective parameterization. J. Atmos. Sci., Vol. 37, pp. 1722-1733.

[23] Goody R.M. and Young Y.L., 1989: Atmospheric Radiation (Theoretical Basis). 2nd ed., Oxford University Press.

[24] Grell G., 1993: Prognostic evaluation of assumptions used by cumulus parameterizations. Mon. Wea. Rev., Vol. 121, pp. 764-787.

[25] Holben B.N., Eck T.F., Slutsker I., Tanre D., Buis J.P., Setzer A., Vermote E., Reagan J.A., Kaufman Y., Nakajima T., Lavenu F., Jankowiak I., and Smirnov A., 1998: AERONET - A federated instrument network and data archive for aerosol characterization. Rem. Sens. Environ., Vol. 66, pp. 1-16.

[26] Janjic Z.I., 1994: The step-mountain eta coordinate model: Further development of the convection, viscous sublayer, and turbulent closure schemes. Mon. Wea. Rev., Vol. 122, pp. 927-945.

[27] Kain J.S., and Fritsch J.M., 1993: Convective parameterization for mesoscale models: The Kain-Fritsch scheme. The representation of cumulus convection in numerical models. Meteor. Monogr., No. 24, Amer. Meteor. Soc., pp. 165-170.

[28] Kain J.S., 2004: The Kain-Fritsch convective parameterization: An update. J. Appl. Meteor., Vol. 43, pp. 170-181.

[29] Kato S., Ackerman T.P., Mather J.H., and Clothiaux E.E., 1999: The k-distribution method and correlated-k approximation for a shortwave radiative transfer model. J. Quant. Spectrosc. Radiat. Transfer, Vol. 62, pp. 109-121.

[30] Kuo Y.H., and Anthes R.A., 1984: Semiprognostic Tests of Kuo–Type Cumulus Parameterization Schemes in an Extratropical Convective System. Mon. Wea. Rev., Vol. 112, pp. 1498–1509.

[31] Lin Y.-L., Farley R.D., Orville H.D., 1983: Bulk parameterization of the snow field in a cloud model. J. Clim. Appl. Meteor., Vol. 22, pp. 1065-1092.

[32] Mayer B. and Kylling A., 2005: Technical note: The libRadtran software package for radiative transfer calculations - description and examples of use. Atmos. Chem. Phys., Vol. 5, pp. 1855-1877.

[33] McKinlay A.F., Diffey B.L., 1987: A reference action spectrum for ultraviolet induced erythema in human skin. CIE Research Note, CIE-Journal, Vol. 6, No.1, pp.17-22.

[34] Nardino V., Martelli F., Bruscaglioni P., Zaccanti G., Del Bianco S., Guzzi D., Marcoionni P., Pippi I., 2008: McCART: Monte Carlo Code for Atmospheric Radiative Transfer. Geoscience and Remote Sensing, IEEE Transactions on, Vol. 46, Issue 6, pp. 1740 - 1752.

[35] National Oceanic and Atmospheric Administration, National Aeronautics and Space Administration, United States Air Force, 1976: U.S. Standard Atmosphere, U.S. Government Printing Office, Washington, D.C.

[36] O'Neill N.T., Ignatov A., Holben B.N., and Eck T.F., 2000: The lognormal distribution as a reference for reporting aerosol optical depth statistics; Empirical tests using multi-year, multi-site AERONET sunphotometer data. J. Geophys. Lett., Vol. 27, Issue 20, pp. 3333-3336.

[37] Reisner J., Rasmussen R.M., and Bruintjes R.T., 1998: Explicit forecasting of supercooled liquid water in winter stroms using the MM5 mesoscale model. Quart. J. Roy. Meteor. Soc., Vol. 124, Issue 548, pp. 1071-1107.

[38] Ricchiazzi P., Yang S., Gautier C., and Sowle D., 1998: SBDART: A research and teaching software tool for plane-parallel radiative transfer in the Earth's atmosphere. Bull. Am. Met. Soc. Vol. 79, pp. 2101-2114.

[39] Rigollier C., Lefèvre M., Cros S., Wald L., 2003: Heliosat 2: An improved method for the mapping of the solar radiation from Meteosat imagery. Groupe Télédétection et Modélization, Ecole des mines de Paris, France.

[40] Rothman L.S., Jacquemart D., Barbe A., Chris Benner D., Birk M., Brown L.R., Carleer M.R., Chackerian Jr. C., Chance K., Coudert L.H., Dana V., Devi V.M., Flaud J.-M., Gamache R.R., Goldman A., Hartmann J.-M., Jucks K.W., Maki A.G., Mandin J.-Y., Massie S.T., Orphal J., Perrin A., Rinsland C.P., Smith M.A.H., Tennyson J., Tolchenov R.N., Toth R.A., Vander Auwera J., Varanasi P., Wagner G., 2005: The HITRAN 2004 molecular spectroscopic database. Journal of Quantitative Spectroscopy and Radiative Transfer, Vol. 96, Issue 2, pp. 139-204.

[41] Rutledge, G.K., Alpert J., and Ebisuzaki W., 2006: NOMADS, a climate and weather model archive at the National Oceanic and Atmospheric Administration. Bulletin of the American Meteorological Society, Vol. 87, Issue 3, pp. 327-341.

[42] Schultz P., 1995: An explicit cloud physics parameterization for operational numerical weather prediction. Mon. Wea. Rev., Vol. 123, pp. 3331-3343.

[43] Shettle E.P., 1989: Models of aerosols, clouds and precipitation for atmospheric propagation studies. AGARD, Atmospheric Propagation in the UV, Visible, IR, and MM-Wave Region and Related Systems Aspects, Conf. Proc., SEE N90-21907 15-32.

[44] Smirnov A., Holben B.N., Eck T.F., Dubovik O., and Slutsker I., 2000: Cloud screening and quality control algorithms for the AERONET database, Rem.Sens.Env., Vol. 73, pp. 337-349.

[45] Stamnes K., Tsay S.C., Wiscombe W., Jayaweera K., 1988: A numerically stable algorithm for discrete ordinate method radiative transfer in multiple scattering and emitting layered media. Applied Optics, Vol. 27, pp. 2502-2509.

[46] Tao, W.-K., Simpson J., and McCumber M., 1989: Ice-water saturation adjustment. Mon. Wea. Rev., Vol. 117, pp. 231-235.

[47] Tao W.-K. and Simpson J., 1993: Goddard Cumulus Ensemble Model. Part I: Model Description. Terrestrial, Atmospheric and Oceanic Sciences, Vol. 4, pp. 35-72.

[48] Van de Hulst H.C., 1957: Light scattering by small particles. Eds. Wiley & Sons.

[49] Vardavas I.M., and Taylor F.W., 2007: Radiation and Climate. Oxford University Press.

[50] Vasilkov A.P., Joiner J., Spurr R.J.D., Bhartia P.K., Levelt P., and Stephens G., 2008: Evaluation of the OMI Cloud Pressures Derived from Rotational Raman Scattering by Comparisons with Other Satellite Data and Radiative Transfer Simulations. Geophys. Res., 113, D15S19.

[51] Zangl G., 2003: A generalized sigma coordinate system for the MM5. Mon. Wea. Rev., 131, pp. 2875-2884.